MINISTRY OF EDUCATION, RESEARCH, YOUTH AND SPORT

THE ANNALS OF "DUNAREA DE JOS" UNIVERSITY OF GALATI

Fascicle IX
METALLURGY AND MATERIALS SCIENCE

YEAR XXX (XXXV),
June 2012, no.2

ISSN 1453-083X

2012
GALATI UNIVERSITY PRESS

THE ANNALS OF "DUNAREA DE JOS" UNIVERSITY OF GALATI.
FASCICLE IX. METALLURGY AND MATERIALS SCIENCE
N^0. 2 – 2012, ISSN 1453 – 083X

Table of Content

THE ANNALS OF "DUNAREA DE JOS" UNIVERSITY OF GALATI.
FASCICLE IX. METALLURGY AND MATERIALS SCIENCE
N^0. 2 – 2012, ISSN 1453 – 083X

PROPERTIES OF SLAGS IN THE SYSTEM CaO-MgO-Al_2O_3-SiO_2, IMPORTANT IN DEOXIDIZATION AND DESULPHURIZATION OF LOW CARBON ALUMINIUM KILLED STEELS

Petre Stelian NITA
Faculty of Metallurgy, Materials Science and Environment,
"Dunarea de Jos" University of Galati
email: pnita@ugal.ro

ABSTRACT

Properties of refing slags belonging to the system CaO-MgO-Al_2O_3-SiO_2 are important in simultaneous or succesive refinig treatment processes in the ladle and other refing metalurgical reactors. The efficiency of treatments depends upon the values of physicochemical properties of treatment slags which become important technological parameters. Surface tension of slags and interfacial tension in teh system slag steel also, viscosity and density are important in managing refining processes which must be correctly evaluated as values and influence exerted by modification of slag composition, mainly by sulphur content.

KEYWORDS: CaO-MgO-Al_2O_3-SiO_2 system, surface tension, interfacial tension, viscosity, density, sulphur solubility

1. Introduction

In the analysis of the dynamical effects at steel-slag interface during the desulphurization process, usually only the surface tension of steel, the interfacial tension steel-slag effects and the steel side of the interface are taken into account. It is a reality that the influences due to the contribution of solutal effects in slag, seems to be un-approached and sometimes even neglected. Many special characteristics appear from the particularities of the slags used in deoxidization and desulphurization of the low carbon and/or low alloyed steels. Possible contributions of slags to the dynamic effects are due to special nature and properties of refining desulphurizing slags and sometimes to the properties of the steel, which form the interface. For sustaining, besides the criteria classically used to appreciate the possibility that certain dynamic effects as the Marangoni convection occur, it must be supplementary considered the lower solubility of sulphur in slags, taken into account as thermodynamically homogeneous liquid solutions, coupled with the fact that, at industrial scale, the amounts of desulphurizing slags are usually between 8-14kg/tone of steel [1]. While in steel the desulphurization under slags leads to a suphur content decreasing by about 0.01-0.02% mass, in the same time, in the desulphurization slag, the sulphur content increases about one hundred times faster up to contents of 1-2%mass [1]. When desulphurization reaction takes place in a non uniform manner on the whole interface, due to different conditions, higher concentrations of sulphur in slag locally appear, overcoming the limits corresponding to the existence of the thermodynamically and physically homogeneous liquid solutions and the whole panel of conditions are changed. Therefore an extended analysis of such properties as surface and interfacial tension, viscosity and density of slags in the mentioned system could contribute to obtaining an improved image and perception of the conditions leading to performances.

2. Influence of the sulphur content on the surface and interfacial tension in CaO-Al_2O_3-CaS slags at 1873K

The only available experimental reported data, covering a wider range of compositions, are those reported in the ref.[2][3] for surface tension in the system CaO-Al_2O_3-CaS and interface tension between the same slags and a liquid steel of a specified grade. It must be mentioned that the paper [2] is focused on the influence of sulphur in the system CaO-Al_2O_3-CaF_2, but this research includes points without CaF_2. From them, two sets of data have been extracted as selected points from the

graphical representation given in ref. [3], mainly taking into consideration their coincidence with the chemical compositions of slags used in practical activities of steel desulphurization and refining. They have been used to generate different statistical dependence relations, finally being selected those having the highest value of the determination coefficient R^2.

The regression equations serve to study the comparative behavioral trends of the respective quantities using computed values, not only the impression due to visual aspects, but especially as their values. This procedure will be very useful for the purpose of the present paper. In the legend of figures presented in the present paper, both the regresion relations and determination coefficients are given. As it is shown, in each case R^2=1 or it is closed to this value.

According to the initial composition of the slags, in % mass, they will be nominated as slag A (or C/A=1.5) at initial composition of 60% CaO-40%Al_2O_3 and slag B (or C/A=1) at initial composition of 50%CaO-50%Al_2O_3. They are presented in the form of dependences upon the concentration of sulphur, and the sulphur content is calculated in the sense of the procedure used during the reported experiments, consisting in additions of different percentages of CaS to such slags.

In fig.1 are presented the dependences of the surface tension of both mentioned slags upon the sulphur content (in % mass) at 1873K. In fig.2 are presented the dependences of the interfacial tension between the two mentioned slags and a steel grade H52-3 at a fixed composition of the steel (0.11%C; 0.44%Si; 1.32%Mn; 0.022%P; 0.035%S; 0.0045%O; 0.0115%N) [2].

It is evident a similar influence exerted by sulphur content up to 2.5%mass, on surface tension dependences (fig.1) and the ratio K(fig.3) in the case of both slags, A and B.

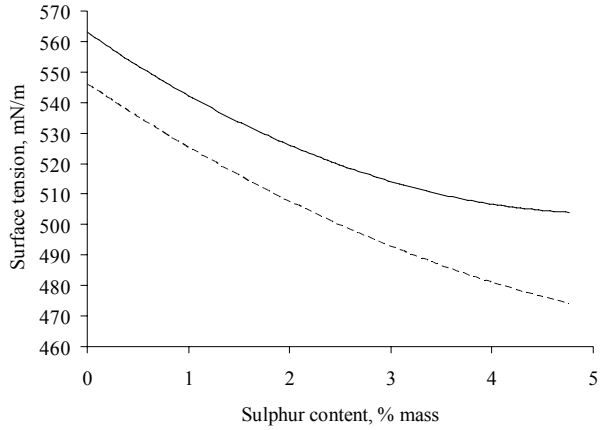

Fig. 1. *Dependence of the surface tension upon the sulphur content in CaO-Al_2O_3- CaS slags at 1873K.*
—— C/A=1.5 σ_A=2.1217(%S)^2-22.922(%S)+563 (R^2=1);
– – – C/A=1 σ_B=1.4781(%S)^2-22.159(%S)+546 (R^2=1)

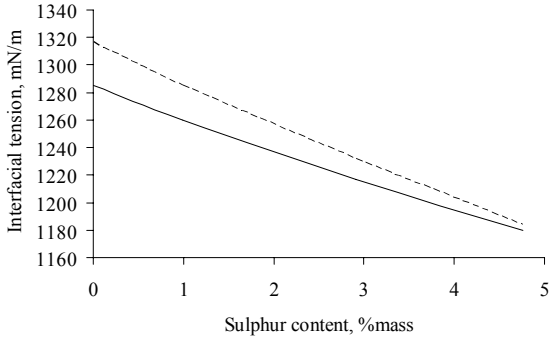

Fig. 2. *Influence of the sulphur content in slag on the interfacial tension between CaO-Al_2O_3-CaS slags and a low carbon steel (H52-3 grade) at temperature of 1873K;*
—— C/A=1.5, ($\sigma_{interf.A}$=0.7353(%S)^2-25.504(%S)+1284.8);
– – – C/A=1, ($\sigma_{interf.B}$ =0.7928(%S)^2-31.548(%S)+1316.5)

In fig.4 are represented dependences of the surface tension variations of the slags A and B obtained based on the partial molar surface tension of each slag upon the mole fraction of sulphur in slags, compared to the predictions made using the general statistic relation deduced and presented in ref. [4] based on the relation given in ref. [5]. In the fig.4, besides the similarity of the trends, consisting in a parabolic type dependence and therefore in the existence of a minimal value at a specific sulphur concentration, on each curve, it is obvious the difference between the predicted values in the cases of the slags A and B, belonging to CaO-Al_2O_3-CaS, and the predicted values using the general statistic relation.

This means that all effects connected to this quantity are less intensively influenced in the particular cases of slags A and B than those obtained with the general statistical averaged relation. It can be noticed also that the dependences of the products $X_S\partial\sigma/\partial X_S$ for slags A and B are practically superposed in the range of sulphur concentration

lower than $X_S \leq 0{,}015$.The value of the interfacial tension at 1873K, between CaO-Al_2O_3 slag and iron decreases from 1238mN/m for a ratio C/A=1 decreases to 1200mN/m at C/A=1.5[6]. A slight increasing to the value 1250mN/m results from the ref. [7] at C/A=1.5 and iron containing 0.1%C. At 1843K from the ref. [8] it results, at 0.1%mass carbon content in iron, an interfacial tension about 1300mN/m, between this alloy and a slag of 50% CaO-50%Al_2O_3.

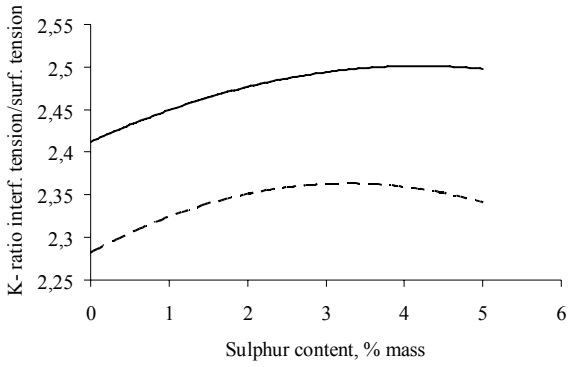

Fig. 3. *Ratio(K) between the interfacial tension and the surface tension in the system CaO-Al_2O_3- CaS at 1873K, upon the sulphur content in slags;*
—— C/A=1.5($K_{1.5}$= -0.0051(%S)^2+ +0.0425(%S)+2.412);
– – – C/A=1(K_1= -0.0076(%S)^2+ +0.0489(%S)+2.282)

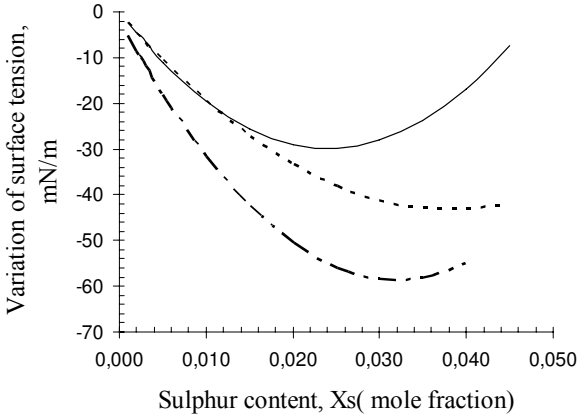

Fig.4*. Dependence of the surface tension decreasing ($X_s\partial\sigma/\partial X_S$) upon the sulphur content (X_S) in CaO-Al_2O_3- CaS at temperature of 1873K.*
—— C/A=1.5($X_S\partial\sigma/\partial X_S$= 55778$X_S^2$- -2498$X_S$+0.2919);
····· C/A=1($X_S\partial\sigma/\partial X_S$ =28894X_S^2- -2226.3X_S+0.3045);
— · — · according to ref. [3]

Many difficulties are due to the atypical behaviour of the system CaO-Al_2O_3, which is proven to be in a way "out of rules" in many respects, making difficult the including of the system in a general model of establishing the quantities contributing to viscosity, density, and even to the surface tension.

3. Viscosities in CaO-Al_2O_3-CaS slags, at 1873K

Despite the presumed simplicity due to the number of components, the viscosity values in the system CaO-Al_2O_3 are not accurate enough as the experimental or predicted values using models. Some trials to establish the general trend of the viscosities in the CaO-Al_2O_3 system, have led to finding a decreasing one and another one, of increasing value with the increasing of the CaO content.

In ref.[9], in a systematic experimental research, at a slag composition of 50% CaO-50%Al_2O_3 it was obtained the value 0.23Pa.s.

From the relations established in the [10], it results the value η=0.1956Pa.s at a close composition of 51.5%CaO+ 48.5%Al_2O_3 and the value η=0.199Pa.s at a composition of 49.5% CaO +50.5% Al_2O_3. Using Urbain model, a value 0.4396Pa.s is obtained.

In slag 60%CaO-40%Al_2O_3 a value η=0.1184Pa.s is obtained by extrapolating at 1873K a statistic relation (lgη=23.10^{-7}T^2-0.010556T+ 10.776, R^2=1), established in the present study, based on data obtained in ref.[1], on the interval 1973-2073K. From ref.[10], at a relatively close composition (55.5% CaO-43.5%Al_2O_3-1% SiO_2) a value η=0.162Pa.s is obtained. Using Urbain model, a value η=0.2735 Pa.s is obtained. The values obtained using the Riboud model are much lower than the lower experimental value, in case of both compositions of slags.

There are not data concerning the influence of the sulphur content on the viscosity in slags based on the simple CaO-Al_2O_3 system. Some trends of influence result from data in other systems. In the system CaO-CaS-SiO_2, at 1873K and ratios of mole fractions representing (X_{CaO}+ X_{CaS})/ X_{SiO2}=1.5-2, at contents of X_{CaS}=0.02-0.1, there are not sensible influences of the sulphur content [11][12]. At 1773K, in a complex system CaO-SiO_2-Al_2O_3-MgO-MnO-CaS, at basicity index b=%massCaO/%massSiO_2=1.3, the replacing of about 3%CaO by CaS leads to increasing of the viscosity by about 10% (from 0.3 to 0.33Pa.s) and at

b=1.43, the replacing of about 6%CaO by CaS leads to decreasing of the viscosity with about 16% (from 0.38 to 0.32Pa.s)[13]. The presented data lead, by a certain similitude, to the acceptance of a low influence of the sulphur content on the viscosity, in the system CaO-Al_2O_3-CaS at 1873K, up to 6% CaS.

Densities in CaO-Al_2O_3 system, at 1873K

In slags 50% CaO-50%Al_2O_3, values 2710kg.m^{-3}[14], 2750kg.m^{-3} [15][16] and 2870kg.m^{-3} [17] have been found as points in diagrams[12]; in ref.[18], a value of 2710kg.m^{-3} is given also. For slag 60% CaO-40%Al_2O_3, a value 2685kg.m^{-3} is given [11][19].

Sulphur solubility in slags and its influence

From data presented before it results that the major effect, during the desulphurizatin of the steels using slags based on the oxydic system CaO-Al_2O_3, is the decreasing of the surface tension of the slag and of the interfacial tension between the slag and the mentioned low carbon steel, due to the increasing of the sulphur content of the slag. In the industrial practice only rarely the final sulpur content is higher than 2%mass. At each temperature in the range of interest, a certain value of the sulphur capacity C_S' corresponds to each chemical composition of the slag, at equilibrium with metallic bath and therefore, there is a limit of solubility of sulphur; up to this limit the sulphur forms with the other components of slag fully liquid slags. The content of sulphur overcoming the solubility limit will precipitate in slag as CaS, which will float in the slag as cristals, as it was observed experimentally [20].

The limits of CaS solubility in CaO-Al_2O_3 slags are given by the relation in fig.5 and can be transformed in the corresponding limits of sulphur solubility. For the considered CaO-Al_2O_3 slags, the limit of sulphur solubility is 2.092 % mass at C/A=1.5 and 1.46% mass at C/A=1.

It follows that all effects taking into consideration the chemical composition of the slag must be analyzed under the consideration of the effects due to CaS precipitation as crystals in the slag. In ref.[20] it is mentioned that the CaS precipitation inhibits the generation of interfacial convection.

Using the effects of the chemical composition shown in fig.3 and fig.5 this could be explained by the strong lowering of the sulphur content in the liquid surrounding the CaS precipitated crystals and the corresponding lowering of the product $X_S\partial\sigma/\partial X_S$ which gives a measure of the maximal surface tension decreasing which could contribute to the interfacial convection evaluated as Marangoni effect.

This can be seen also in fig 4. where at lower sulphur contents the decrease of the surface tension is more important than at higher sulphur contents.

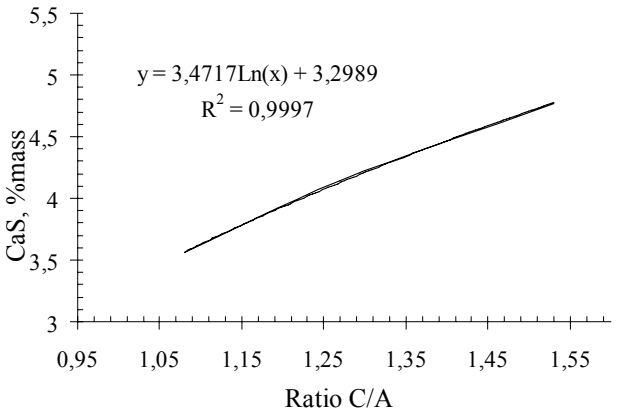

Fig. 5. *Solubility limit of CaS in slags CaO- Al_2O_3 at 1873K, as function of the ratio C/A =(%mass CaO)/(%mass Al_2O_3), according to experimental values of sulphur solubility from ref.[2]. The equivalent relation of the solubility of sulphur in slag is (%S)=1.5428Ln(C/A)+1.466*

4. Conclusions

The present values of physico-chemical properties of slags in the system CaO-MgO-Al_2O_3-SiO_2 are important by their values and influence exerted by sulphur content in refining processes of deoxidization and desulphurization which occur simultaneously and subsequantly during steel treatment in ladle reactors and other refining reactors. Based on several values of important quantities and parameters influenced by these properties, the processing route and parameters of treatment could be better established to obtain an optimized maximal efficiency in steel refing processes at industrial scale. All these are possible only based on correct evaluations of the properties presented. Because of some important differences of values found in the literature, it is necessary to improve and to establish a standard procedure for measurements of slag properties and not only.

References

[1]. P. S. Nita, I. Butnariu, N. Constantin - Revista de metalurgia (Madrid), vol.46. No 1, (2010), pp.5-14.
[2]. B,van Muu, H.W., Fenzke - Freib. Forschungsh. B, Metall. Werkstofftech. Vol. B252, pp. 40-50, (1985).
[3]. *** Slag Atlas, 2nd Edition, Verlag Stahleisen GmbH, D-Düsseldorf, (1995).
[4]. P. S. Nita - Materials Science and Engineering A 495 (2008), 320-325
[5]. Mills, K. C., Keene, B.J. - International Materials Research vol.32, no1-2, (1987), 107.
[6]. J. L. Bretonnet, L.D.Lucas, M.Olette - Circ. Inf. Techn., Cent. Doc. Sider. 33, (1976), 105-108.
[7]. J. L. Bretonnet, L. D. Lucas, M. Olette - C.R. Hebd. Seances Acad. Sci. Vol. 285C, no. 2,. 11 July, (1977), 45-47.
[8]. Mukai, K., Kato, Sakao, H. - Tetsu-to-Hagane, 59(1) (1973), 55.
[9]. Elyutin, V.P., Kostikov, V.I., Mitin, B.S., Nagibin, Yu.A. - Russian Journal of Physical Chemistry, 43(3) (1969), p.316-319.
[10]. Shalimov, A.G. - *The establishing of optimal parameters of the steel refining process with liquid sinthetical slags in the pouring ladle.* Thesis for Ph. Dr. in Technical Science, Moskow, 1957, cited in: Bornatskii, I.I. Desul'furatsiia metalla, 1970, Moskva, Metallurgiia, romanian translation- Desulfurarea fontelor si otelurilor, ed.tehnica, Bucuresti, (1972), tab.117, p334.
[11]. Panov, A.S., Kulikov, I.S., Selev, L.M. - Isv.Akad.Nauk SSSR, otdel Teckn.nauk, Metallurgiia I toplivo (1961) (3), 25-30.
[12]. Slag Atlas, 2nd Edition, Verlag Stahleisen GmbH, D-Düsseldorf, 1995, fig.9.61.b., tab.9.15, 8.13, 8.14, 8.17.
[13]. Kozakevich, P. - Rev. Metall 51 (1954), 571-573.
[14]. Zhmoidin G.I., Sokolov L.N., Podgornov G.V., Smirnov G.S. - Teoriia Metallurgicheskih Protsesov, (3) (1975), p150.
[15]. Zelinski M., Sikora B. - Pr.Inst.Metall, Zelaza im St.Stasgira, 29(3-4), (1977), p157.
[16]. El Gammal T., Müllenberg R.-D. - Arch. Eisenhüttenw. 51(6), (1980), p 221.
[17]. Sikora, B., Zelinski, M, - Hutnik 41(9) (1974), p433.
[18]. Hara, S., Ogino, K. - Can.Met.Quaterly, 20 (1981), 113.
[19]. Dymov,V.V., Baidov,V.V. - Sb.Tr.Tsent.Nauch-Issled Inst. Chem. Met. 619 (1968), 78.
[20]. Deng, J., Oeters, F. - Steel Research 61**,** (1990), 443-448.
[21]. Özturk,B., Turkdogan, E.T. - Metal Science, vol.15. june 1984, 299-305.

THE ANNALS OF "DUNAREA DE JOS" UNIVERSITY OF GALATI.
FASCICLE IX. METALLURGY AND MATERIALS SCIENCE
N^0. 2 – 2012, ISSN 1453 – 083X

MICROSTRUCTURAL EVOLUTION OF AL 1100 ALUMINUM SUBJECTED TO SEVERE PLASTIC DEFORMATION

Gheorghe GURAU, Carmela GURAU
"Dunarea de Jos" University of Galati
email: ggurau@ugal.ro

ABSTRACT

The goal of this document is to promote a sequence of bulk-deformation processes able to produce ultrafine grain and also nanostructured wires with adequate length to be interesting for processing in metallurgical industry. Samples of aluminum Al 1100alloy (98.41 % Al) were subjected to repetitive Equal Channel Angular Pressing at room temperature in 1 to 4 passes. Severe deformed specimens were cold classical plastic deformed in wires. Microstructural evolution and mechanical properties were investigated. Optical microscopy progression is evaluated through a sequential interrupted process on each separate ECAP pass. The XRD studies reveal the influence of SPD on grain refinement of samples. A simply and new technology for obtaining intermediary products UFG and nanocristalline wires was developed.

KEYWORDS: SPD, ECAP, UFG, in bulk nanomaterials cold extrusion, aluminum alloys, microstructural evolution

1. Introduction

On October 18, 2011 the European Commission adopted the following definition of a nanomaterial: a natural material, made accidentally or manufactured, containing particles in the free, the aggregate or the agglomerate states and where 50% or more of the particles have size distribution, one or more dimensions, the size range 1 nm - 100 nm [1]. Under certain conditions described by the legislator, the percentage may drop below 50%.

In bulk nanostructures have all three dimensions at the nanometric scale (3-D). These categories of massive solids are nanometer-scale grains.

Severe plastic deformation are an important approach for manufactured metallic material in bulk, whose crystalline grain size varies from less then 100 nm or up to 200 nm for ultra-fine grained massive. The use of severe plastic deformation (SPD) for the processing of bulk ultrafine-grained and nanostructured materials is now extensive [2, 3, 4].

One of the successful top-down methods producing massive material with three dimensions at the nanoscale is ECAP (Equal Channel Angular Pressing). ECAP was first implemented in the 80s in the Soviet Union. ECAP uses a die where two channels are cut, equal in cross-section, intersecting at an inner angle denoted in literature with Φ, which is generally close to 90^0.

The sample is pressed around a sharp corner. ECAP introduces large plastic strains in metals and their alloys to reduce grain size, using repetitive pressing. The final ECAP products have nanometric grains or ultrafine grains, but keep the cross section and shape of the initial sample. ECAP is based on increasing the free energy of polycrystalline alloy initial coarse grain, through introduction of high density of defects, especially dislocations [5].

The properties of bulk nanostructured or UFG alloys differ very much from the polycrystalline ones with the same average chemical composition, massive with micrometer scale. Properties of nanomaterials depend on two very important factors: grain size and the number of atoms on the surface or in close proximity to the surface. In the case of ECAP, the grain size of the final product can be varied by controlling: die designed angles (Φ the inner angle and ψ the outer angle), pressure, number of successive passes, processing route. All factors described are impact in microstructure and homogeneity developments during process.

The properties of bulk nanomaterials depend on grain size distribution, boundary thickness and local chemical composition.

In the present work we studied an aluminum alloy, which especially displays the size and distribution influence of intermetallic compounds.

ECAP is a feasible process for bulk nanostructure or ultrafine grain materials. A major limit of method is represented by dimensions of deformed material. This paper has the major objective of promoting of technology capable to produce long wires with ultrafine structure and function on true deformation degree, nanometric bulk structure, in order to be implemented in industry. Therefore, the present work was targeted at employing two combined plastic deformation methods, ECAP plus direct extrusion, a desirable severe plastic deformation technology to perform in bulk nanostructured aluminum alloy wires.

2. Experimental procedure

This study was carried out on a commercial A 6061 aluminum alloy (composition of 0.87 % Si, 0.05%Mn, 0.05%Cu, 0.007%Zn, balance aluminum) supplied with rolled billets 10 mm x10 mm and cut at 10mmx10mm x50mm.

The billets were pressed in ECAP die with channel section 10mm x10 mm.

The specific die angles, inner Φ 90^0 and outer Υ 13^0 determine effective strain 1.07 in one pass [6].

$$\varepsilon_{total} = \frac{1}{\sqrt{3}}\left[2\mathrm{ctg}\left(\frac{\Phi+\Psi}{2}\right)+\Psi\,\mathrm{cosec}\left(\frac{\Phi}{2}+\frac{\Psi}{2}\right)\right] \qquad (1)$$

Replacing the values given in the above previous equation we will find:

$$\varepsilon_{total} = \frac{1}{\sqrt{3}}\left[2\mathrm{ctg}\left(\frac{90+13}{2}\right)+0.226\frac{1}{\sin\left(\frac{90}{2}+\frac{13}{2}\right)}\right]=1.07 \qquad (2)$$

Specimens were pressed via route A at room temperature. Before pressing the samples were lubricated with a suspension of graphite in mineral oil to reduce friction. The constant pressing speed 17.3 mm/s was employed using a 20 tf press. After pressing, the die was rotated at 90^0 and the specimen was pressed back in the vertical channel.

Then another specimen pushes out the first one. Similarly, the ECAP process was conducted to obtain specimens with 1, 2, 3, and 4 passes, equivalent strain: 1.07, 2.14, 3.21, respectively 4.28. Following the ECAP procedure, eight samples were obtained, two with the same equivalent strain.

Four samples were used for investigations after severe plastic deformation and other four were deformed by direct cold extrusion. The direct extrusion die parameters are shown in Table 1.

The prismatic ECAP billets were pressed in the cylindrical die to obtain long UFG wires 4 mm in diameter.

Table 1

Diameter of container *D[mm]*	Diameter of calibrated zone *d [mm]*	Strain $\varepsilon=\frac{D^2-d^2}{D^2}\times100$	Equivalent strain $\varphi = \ln\frac{A_0}{A_1}$
15	4	92.88	2.64

The force variation in both processes, ECAP and direct extrusion, respectively, was monitored with Hottinger Spider 8 system and force-stroke data has been recorded. Micro-Vickers hardness measurements were made on ECAP and ECAP plus cold extrusion samples using a load of 0.9807 N and reported as mean of the three readings. The XRD characterization of the samples has been obtained with a RigakuDmax III-C system.

The optical microscopy study has been carried out using a microscope Olimpus BX45 with digital image resolution at higher magnifications. The scanning electron microscopy study has been carried out using a portable microscope SEM type Hitachi. Metallographic samples were processed in longitudinal section for ECAP deformed samples and cross sections for extruded samples and attacked to specific reagent: 0.5 ml HF, 1.5 ml HCl, 2.5 ml HNO3, 95.5 ml water.

3. Result and discussion

3.1. Pressures in ECAP and cold extrusion processes

In the ECAP process, the pressure increased continuously with stroke until the maximum is achieved, and then a decreasing variation take places. Toward the end of the ECAP process, pressure is almost constant. Figure 1 presents pressure versus stroke plot for effective plastic strain 4.28 respectively four ECAP passes. The maximum pressure, 446.94 MPa is also the maximum value reached in the ECAP process as shown in Table 2.

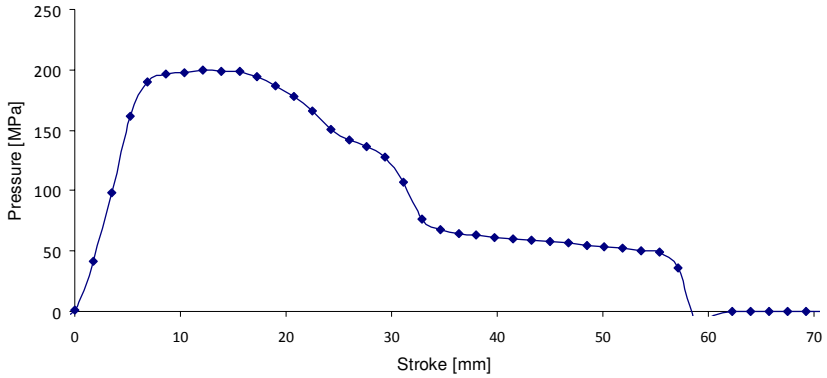

Fig. 1. *Pressure versus stroke on fourth pass of ECAP – effective plastic strain 4.28*

Pressure in the cold direct extrusion process sowed different variation of pressure with stroke but specific for direct extrusion. At the start, a slow increase in pressure occurs suggesting cold pressing from prismatic shape to cylindrical shape, then the pressure increases rapidly to maximum.

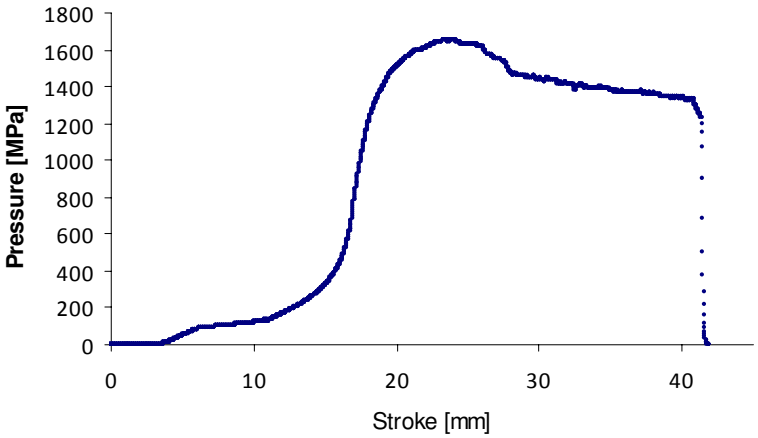

Fig. 2. *Pressure versus stroke in cold direct extrusion process o ECAP billet after four passes- effective plastic strain 6.92*

In Figure 2, pressure versus stroke was plot for the cold extrusion process from four ECAP passes billet (effective plastic strain 6.92). The pressure increase up to 1.6 GPa almost four time higher than simply ECAP. When the maximum is reached, the pressure drops to lower values because the volume of the sample decreases in the container, the same as the friction forces.

Table 2 shows the maximum pressure values for different stages of ECAP and cold extrusion. It can be observed that the ECAP pressure increases from one pass to another and so does the conventional extrusion also. The values for ECAP + CE are higher than simply ECAP because of the accumulated strain and structure distortion.

Table 2

Processing route	**Maximum pressing pressure**
	[MPa]
Pass 1 ECAP	140.74
Pass 2 ECAP	231.75
Pass 3 ECAP	344.49
Pass 4 ECAP	446.94
Pass 1 ECAP + CE	1068.845
Pass 2 ECAP + CE	1220.434
Pass 3 ECAP + CE	1538.592
Pass 4 ECAP + CE	1650.242

3.2. Microhardness

At low temperatures, the increasing of grain boundaries behave as slip barriers, their area being far increased than in coarse grains bulk alloys. Therefore, nanocrystalline bulk metallic alloys are expected to have got value for mechanical resistance consistently higher than polycrystalline material with the same composition. Indeed at low temperatures, nanocrystalline materials were noted to become harder as the grains size is reduced [2, 5].

At elevated temperatures sliding grain boundaries and diffusion processes become meaningful. In the case of nanomaterials, a high density of imperfections and dislocations with different settlement at grain boundaries are specific. That affects significantly mechanical properties.

Due to their reduced grain size, and the increased number of atoms on surface, nanomaterials are expected to become more ductile at the same temperature then coarse grained polycrystalline alloys with the same composition.

In an up to date review on the mechanical behavior of UFG and nanocristalline materials [5] data is showed on normalized yield strength versus percentage elongation in tension for metals with grain sizes in the nanocrystalline range in comparison with UFG in cooper, titanium and aluminum alloys. Ultrafine grained materials (100–500 nm) exhibit increased yield strength along with good ductility in comparison to nanograined materials.

The plastic deformation of nanocrystalline materials is known to change as the grain size decreases into the ultrafine regime. This has been correlated to changes in strain hardening behavior at those grain sizes.

Ultrafine grain size can be described by a core-and-mantle model (grain-boundary limits with spacing of 10–100 nm). As the grain size is reduced, the ratio between volume fractions of the ''mantle'' and ''core'' increases, providing an increase in yield stress [5]. Microhardness values are presented in Figure 3. The values of severely plastically deformed ECAE samples with different degrees of deformation and measured values after extrusion in 4 mm wires were taken into account. Note that all samples ECAE plus extrusion the increase value of microhardness. The hardness value of the initial samples doubled from 337.6MPa to 678.8MPa. Severe plastic deformation leads to an advanced finishing structure.

As a consequence, hardness increases with the increase of deformation. Note the true deformation degree threshold value 3.21, above which plastic deformation by ECAP have no effect on mechanical properties. This correlates with the claims in literature that reveal that the mechanical behavior better marks ultrafine grain size than the nanometric structure.

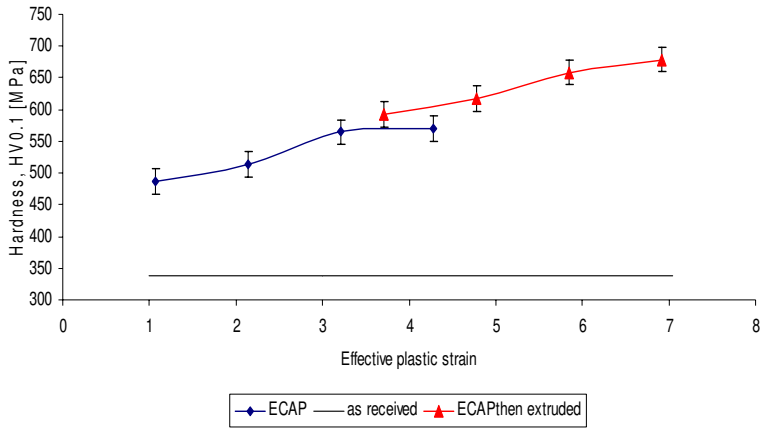

Fig. 3. *Variation of microhardness with the number of ECAP passes and ECAP+CE*

3.3. Microstructure evolution of Al 1100 alloy during the ECAP process

Samples of aluminum were investigated by optical microscopy, in as received state and after severe plastic deformation by the ECAP process with 1, 2, 3 and 4. The structure was analyzed after severe plastic deformation and ECAP plus subsequent direct extrusion 1 to 4 passes. Optical microscopy (OM) in as received sample of Al 1100 reveals a structure consisting of a coarse-grained solid solution and intermetallic compounds precipitated fine (Fig. 4). The solid solution presents polyhedral grain structure straight edges specific to fcc metals.

The microstructure highlighted slight unevenness grain size. Inside the crystalline grains of solid solution and on grain boundaries are observe several precipitates. Dark areas are insoluble phase Mg_2Si particles and Mg_2Al_3.

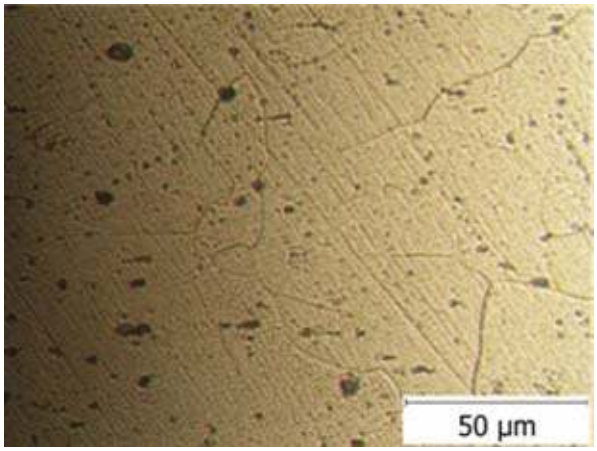

Fig. 4. *Microstructures of Al 1100 magnesium alloy in initial state*

Optical microscopy progression after severe deformation is evaluated through a sequential interrupted process on each separate ECAP pass. Evaluation was performed in 4 distinct regions of the samples severely deformed by ECAP for each 1 to 4 passes.

The four areas of microstructures billets outlining:

- input of the billet before deformation at entry in the die for next pass;
- plastic deformation zone, containing in the shear plane;
- deformed area after leaving the progressive shear zone;
- output end of the billet after current pass at leaving the die

The mode definition of these regions for samples severely deformed by the ECAP process are outlined in Figure 5.

The microstructural observation focused on characterization of the grain structure evolution with increasing number of passes, comparative in all the specific ECAP regions previous described.

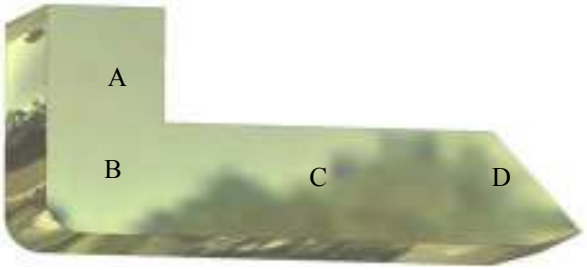

Fig. 5. *Regions of ECAP specimen observed by OM*

Optical images prevailed of the areas defined in Figure 5 for each of the four stages of processing by ECAP, using route A, are shown in Figures 5 - 8.

The deformation produced by ECAE is sequential, the shearing not being distributed in the entire billet simultaneously [7]. More than that, at every reinstatement of the sample in the die for a new deformation, the billet starts with a different texture, discontinuous in volume. But we can consider that deformation appears almost monotonically in a tight region around the shear plan defined by the die intersection plane [ec8]. This region, named plastic deformation zone, is not symmetric around the shear plan, and depends on all the ECAP process parameters.

3.3.1. Microstructure in region A

In the metallographic region A are shown the input of the billet before deformation, at entry in the die for next pass.

In the first ECAP pass, although in this region the material is not yet deformed, the microstructure displays a slightly deformed texture. The image in Fig. 6a is taken before the samples get in touch with the plastic deformation zone.

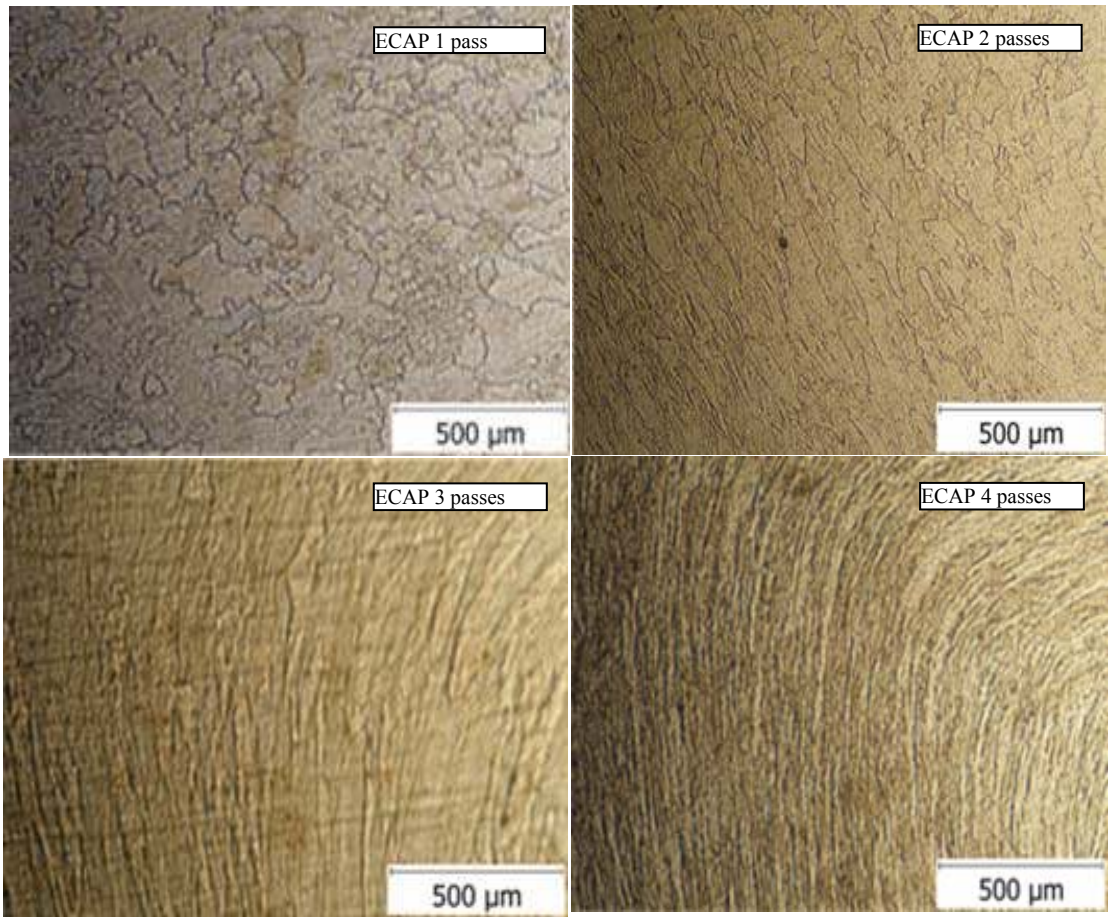

Fig. 6. *OM of ECAP billets after: one pass (a), 2 passes (b), 3 passes (c), 4 passes (d), Region A*

There is a solid solution rich in aluminum that shall grains easily elongated in the direction of application of force, in longitudinal section, on the outer surface of the sample which is in contact with the mold. The grains slightly flattened have dark particles of intermetallic compounds inside and at boundaries. The texture is only due to the contact of the sample with the mold walls. The billet was introduced initially lubricated all over the longitudinal contact with the mold. One possible reason is the effect of friction texture appearance can not be completely excluded. After two ECAP passes, the micrographic aspect reveals significant refinement of microstructure. Extended fine structure is formed then in the zone obtained after the first pass. Limits have parallel leaf appearance due to increased density of dislocations. After three ECAP passes grains, have an increasingly elongated and thin form. After four ECAP passes, just flow lines are observed. Crystalline grains are not OM observed, merely fibrous structure.

3.3.2. Microstructure in region B

Area noted with B is the plastic deformation zone that contain shear plane where plastic deformation occurs almost monotonously at the intersection of the two channels of the mold. At the first ECAP pass the crystalline grains of solid solution support a sinusoidal crimping process to shredding (Fig.7a).

In the following ECAP passes, the successive shearing of the grains already finished during the previous passages takes place. It forms a band structure aligned and finished growing, highlighting fiber flow lines. For all smaller grain sizes (d < 300 nm) shear band development is often observed to occur immediately after the onset of plastic deformation [9, 17].

The mechanism of grain-boundary rotation is one of several mechanisms that try to explain the modality of plastic deformation for ultrafine grains size metallic alloys [19, 11, 12]. The equiaxed grain structure is replaced by elongated grains through plastic deformation inside the shear band. Between two neighboring the barrier of boundary is eliminated by rotation so their orientation became closer together.

Similar mechanisms of grain boundary rotation and also based on dislocation generation at grain boundaries and in the limitrophe area for ultrafine

grained size can explain how plastic deformation takes place.

TEM observation in Ti [13,14], Cu [15], Al–Li [16,18], and brass [19] in case of severe deformation grains, suggests applying mechanism of multiply dislocation that creating a work hardened layer close to the grain boundaries and in the same time grain boundary rotation.

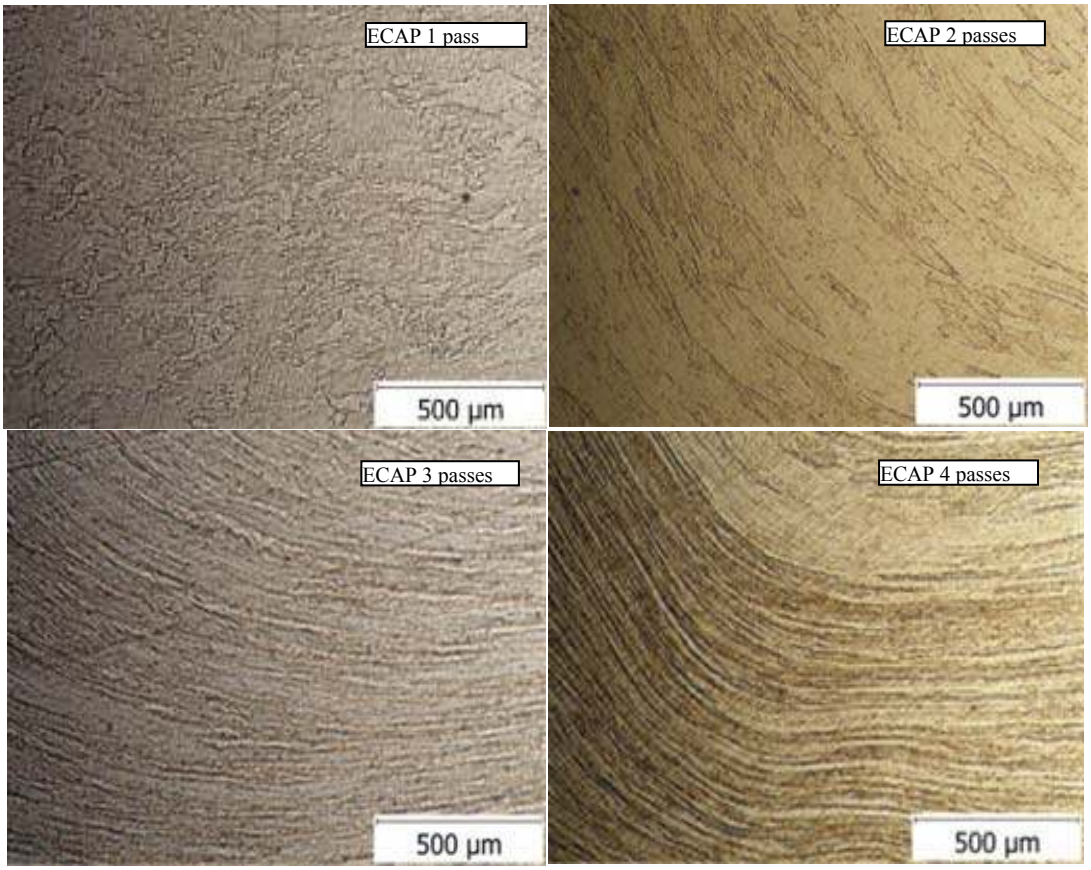

Fig. 7. *OM of ECAP billets Region B after one pass (a), 2 passes (b), 3 passes (c), 4 passes (d),*

3.3.3. Microstructure in region C

The output limit of the plastic zone area is defined in region C. The optical microstructure of the sample after each ECAP pass is presented in Figure 8. After one pass grains are elongated in the direction of deformation and strings as brittle intermetallic compound fine particles arranged along the slide can also be observed.

Increasing strain induces occurring significant microstructures differences.

Structure is becoming more elongated, finer and ultra finer grains size.

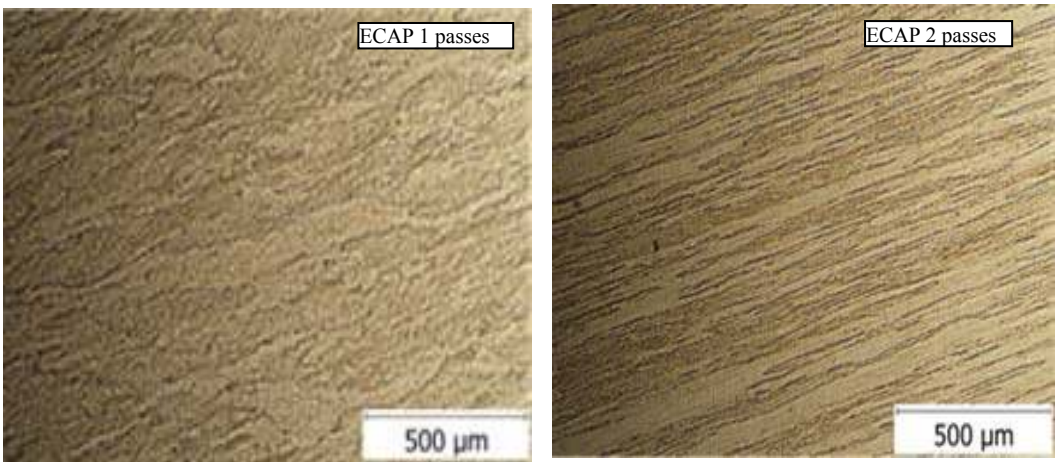

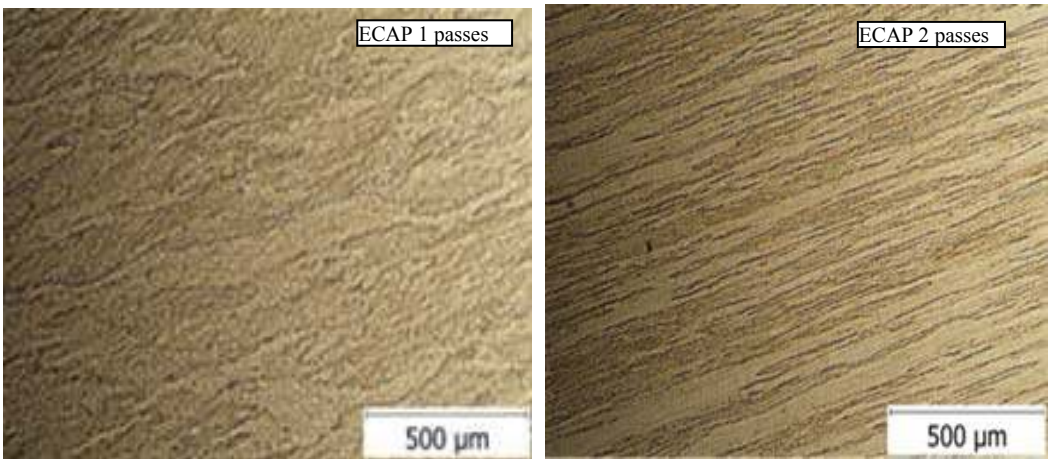

Fig. 8. *OM of ECAP billets after: one pass (a), 2 passes (b), 3 passes (c), 4 passes (d), Region C*

The original grain boundaries disappear and are evident only fiber lines flow. As the deformation increases the fiber structure is compressed in transverse space, becoming more uniform and rotates to the direction of extrusion. The central area of the sample, defined by position in region C, have parallel fiber lines that lie at an angle of 65^0 from the vertical direction of extrusion.

The structure is consistent with the substructure quartz strip aligned with the shear plane direction.

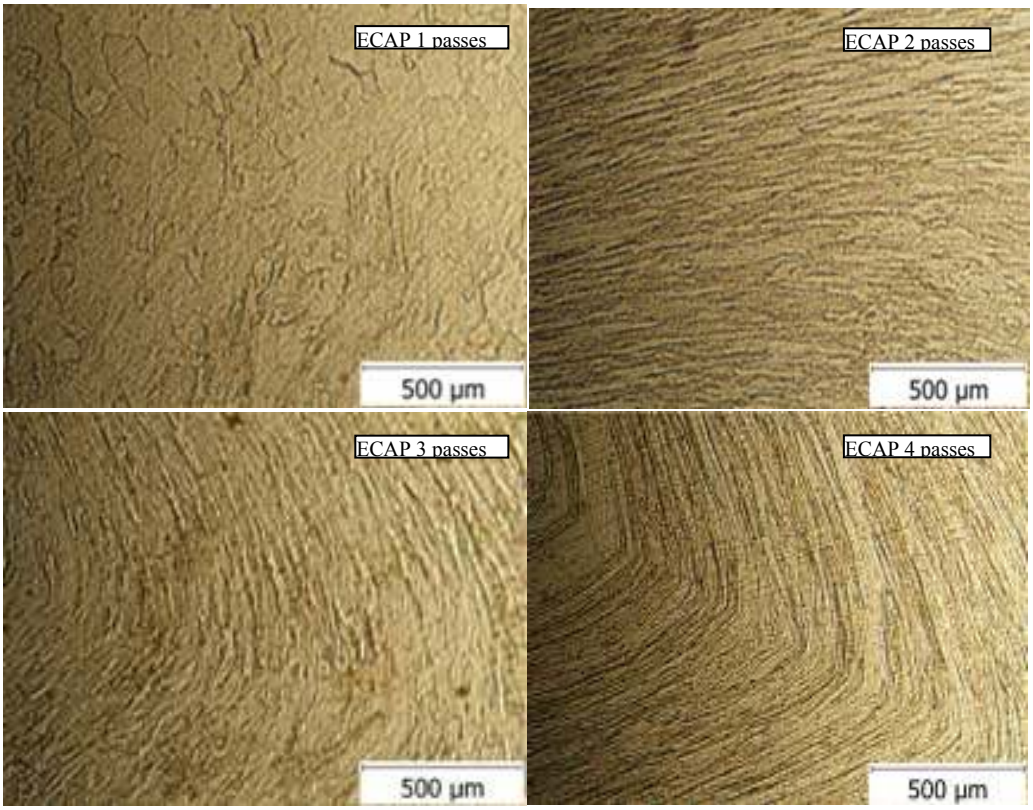

Fig. 9. *OM of ECAP billets, Region D after: one pass (a), 2 passes (b), 3 passes (c), 4 passes (d)*

3.3.4. Microstructure in region D

With increasing plastic deformation in all areas observed by optical microscopy, regions A to D, the finishing of insoluble solid particles dark and gray colored (silicon, magnesium compounds and so on) occurs. Some authors believe that some of them dissolve in solid solution due to the thermal effect of ECAP severe plastic deformation.

In region D, the output end of the billet after current pass at leaving the die is revealed in Figure 8. After more than two ECAP passes, circular fibrous turns the deformation zone appear, a consequence of the uniformity deformation in the ECAP process.

3.3.5. SEM images in region C

SEM images reveal the same ultra dense material aspects after four ECAP passes. The microstructure has got fibrous appearance. Only flow lines and some coagulated precipitates can be seen (Fig 10).

The yield stress and tensile ductility are simultaneously adversely affected by porosity. The restriction, diminishing pores, in the ECAP deformed billet, provide a good behavior in terms of fracture, because of densification.

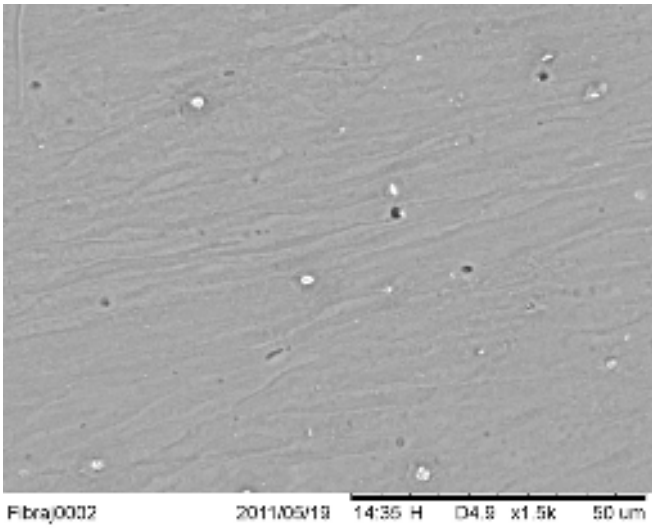

Fig. 10. *SEM micrograph ECAP four passes*

3.4. Microstructure evolution of Al 1100 alloy subjected to combined ECAP and direct extrusion

Samples severely plastically deformed by the ECAP method in one to four passes were subsequently plastic deformed by cold direct extrusion. Wires obtained after extrusion were studied by light microscopy in cross section. Figure 10 shows representative images obtained by OM after extrusion in one pass of the severely deformed semifinished ECAP samples, in one to four passes.

After extrusion of ECAP samples with 1.07 true deformation degrees, materials show the fine grain structure with corrugated and spiral shape (Fig 11 a).

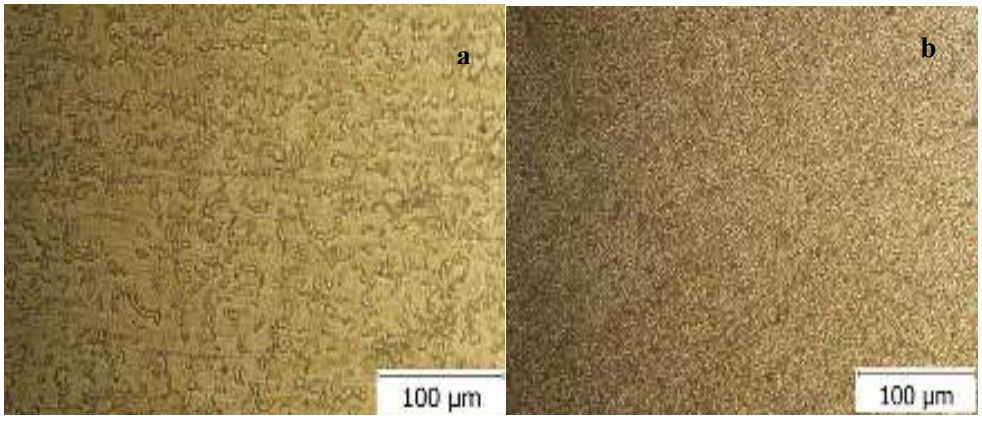

Fig. 11. *OM cold extruded wire one ECAP pass-a and 4 ECAP passes - b*

The increasing deformation degree by the ECAP process followed by classical extrusion in a single pass determine grain size finishing and also fibrous texture. Extruded samples after four ECAP deformations have only fiber lines (Fig.11b). The microstructure in Al1100 wires subjected to high strains ECAP plus Extrusion exhibited grain sizes in the 100–200 nm range.

4. Conclusions

A round-section wire start to square section samples severely deformed by ECAP can be produced, having ultrafine grain size after four ECAP passes and single cold extrusion.

A large increase in hardness for the nanocrystalline aluminum alloy samples made by the ECAP plus classical extrusion as compared to the annealed coarse-grained initial samples.

With the increment of true deformation degree from 1.07 to 4.28, the shape of the particle is changed firstly to become elongated and also corrugated, then it is reduced gradually until it simply becomes flow lines.

Pressing pass has a decisive influence on the microstructure evolution of aluminum alloy. With each increase of ECAP pass, the microstructure aspect is more dense and fibrous and finer. Subsequently, after leaving the plastic deformation zone, the grains are reoriented at 65^0 to the axis X in the shear direction. The ECAP microstructure evolution indicates a close relationship to simple shear deformation in region B and non-uniformity of deformation especially in region D. After extrusion of one ECAP pass samples, the structure presents the fine grain structure with corrugated and spiral shape. Extruded samples after four ECAP deformations have only fiber lines with dense surface aspect.

References

[1]. *** *Nanomaterials.* European Commission. Last updated 18 October (2011).

[2]. H. Gleiter - *Nanostructured Materials: Basicn Concepts, Microstructure and Properties,* Forschungszentrum Karlsruhe, Institut fur Nanotechnologie, Postfach 36 40, D-76021 Karlsruhe.

[3]. Ruslan Z. Valiev, Terence G. Langdon - *Principles of equal-channel angular pressing as a processing tool for grain refinement*, Progress in Materials Science 51 (2006) 881–981.

[4]. A. Azushima, R. Kopp, A. Korhonen, D.Y. Yang - *Severe plastic deformation (SPD) processes for metals*, Manufacturing Techology 37, (2008) 716-735.

[5]. M.A. Meyers et al. - Progress in Materials Science, 51 (2006) 427–556.

[6]. A.R. Eivani, A. Karimi Taheri - *A new method for estimating strain in equal channel angular extrusion*, Journal of Materials Processing Technology 183 (2007) 148-153.

[7]. A. A. Gadzer, F. Dalla Torre, C.F. Gu, C.H.J. Davies, E.V. Pereloma - *Microstructure and texture evolution of bcc metals subjected to equal channel angular extrusion*, Materials Science and Engineering 415 (2006), 126-139.

[8]. A. Gadzer, F. Dalla Torre, C. F. Gu, C. H. J. Davies, E. V. Pereloma - *Progressive structure during equal channel angular extrusion*, Materials Science and Engineering A 437 (2006) 259-267.

[9]. Wei Q, Kecskes L, Jiao T, Hartwig KT, Ramesh KT, Ma E. - Acta Mater (2004); 52:1859–69.

[10]. Jia D., Wang YM, Ramesh KT, Ma E, Zhu YT, Valiev RZ. - Appl Phys Lett (2001); 79:611–3.

[11]. Wang YM, Ma E., Chen M.W. - Appl Phys Lett (2002); 80:2395–7.

[12]. Jia D., Ramesh K.T., Ma E. - Scripta Mater (2000); 42:73.

[13]. Meyers M., Pak H.R. - Acta Mater (1986); 34:2493.

[14]. Meyers M.A., Subhash G., Kad B.K. -Prasad L. Mech Mater (1994); 17:175.

[15]. Andrade U.R., Meyers M.A., Vecchio KS, Chokshi AH. - Acta Metall Mater (1994);42:3183.

[16]. Chen R.W., Vecchio KS. -J Phys IV (1994); 4: C8-4591.

[17]. Murayama M, Howe JM, Hidaka H, Takaki S. - Science (2002); 295: 2433–5.

[18]. Xu Y.B., Zhong W.L., Chen Y.J., Shen L.T., Liu Q., Bai Y.L., et al. - Mater Sci Eng A, (2001); 299: 287.

[19]. Li Q., Xu Y.B., Lai Z.H., Shen L.T., Bai Y.L. - Mater Sci Eng A (2000); 276:127.

THE ANNALS OF "DUNAREA DE JOS" UNIVERSITY OF GALATI.
FASCICLE IX. METALLURGY AND MATERIALS SCIENCE
N^0. 2 – 2012, ISSN 1453 – 083X

NEUTRALIZATION OF HAZARDOUS WASTE IN VITREOUS MASS OF GLASS

Maria VLAD, Gelu MOVILEANU, Iuliana MARCUS, Gheorghe FLOREA, Alina CANTARAGIU

[1]"Dunarea de Jos" University of Galati, Faculty of Metallurgy and Materials Science,
[2]"Valahia" University of Târgoviste, Faculty of Environment Engineering and Biotechnology
email: mvlad@ugal.ro

ABSTRACT

The paper presents studies concerning the neutralization of hazardous waste containing metal ions by embedding them in vitreous matrix which are chemically stable materials. The main analysed factors are: chemical composition of the charge based on packaging glass waste, amount influence of waste added in the charge on the physical-mechanical properties of analysed materials, the structure and the capacity for inclusion of metallic oxides from hazardous waste, the thermal treatment of vitreous or vitreous-ceramic materials.

KEYWORDS: glass, oxides, hazardous waste, structure

1. Introduction

Through the neutralization of dangerous waste in the matrix of oxidic glasses which are stable from the chemical point of view, the polluting potential of the waste decreases substantially [1].

The recovery of glass waste in view of elaborating the vitreous matrix for the inertisation of dangerous waste was studied in the present paper due to the fact that it represents a research field which may reveal very important technical and economic advantages.

Through incorporating various composites (some metal oxides, salts, heavy metal hydroxides) into the vitreous matrix, decorative glasses may be obtained, whose colour varies in keeping with the nature of the metallic ion, the quantity added and the work temperature [2].

Vitroceramic materials may combine specific properties to ceramic and specific properties to glass. To obtain the designed properties, the stabilisation of the appropriate chemical composition and the achievement of an adequate thermal treatment must be taken into account.

The concept of controlled crystallisation involves the separation from the vitreous phase of a crystalline phase under the form of fine crystals, whose number, growth speed and final size are controlled through an appropriate thermal treatment [3]. The inertisation of wastes in the vitreous matrix mainly consists in their incorporation through melting in a glass with a particular composition, which allows the incorporation of certain chemical elements present in the waste [4, 5].

The complexity of the correlation between the chemical composition and the properties of the base glass functioning as a vitreous matrix which incorporates the waste makes the choice of composition be of a a great importance.

The production of vitroceramics with improved properties is highly dependent on the phases of the crystalline microstructure developed during the heat treatments of the base glass.

Some glass compositions have their own crystallisation centres, but others need specific components to be added so as to ensure the internal formation of crystallisation centres. In glass factories, glass chips are used to a high extent (almost up to 100%) in the fabrication process as raw material, also known as adding material.

2. Experimental results

In present are known three broad categories of vitro-ceramic materials used for their special properties. The first is based on a base glass with a composition close to eutectic Al_2O_3-SiO_2-MgO system (MAS), the second system becomes very important is ternary system Li_2O-Al_2O_3-SiO_2 (LAS), the third class of vitro-ceramic materials refers to those which contain the main crystalline phase keatitul (polymorphic form of SiO_2) from the system

Al_2O_3-SiO_2 (AS), with outstanding thermal properties.

Results for stoichiometric compositions 2CaO Na_2O $3SiO_2$ (NC_2S_3) and $2Na_2O$ CaO $3SiO_2$ (N_2CS_3) which are based on the ternary system SiO_2-CaO-Na_2O, Figure 1, were discussed by Gonzales - Olivier and James [4] which studied nucleation speeds, viscosity and thermodynamic data in stationary regime.

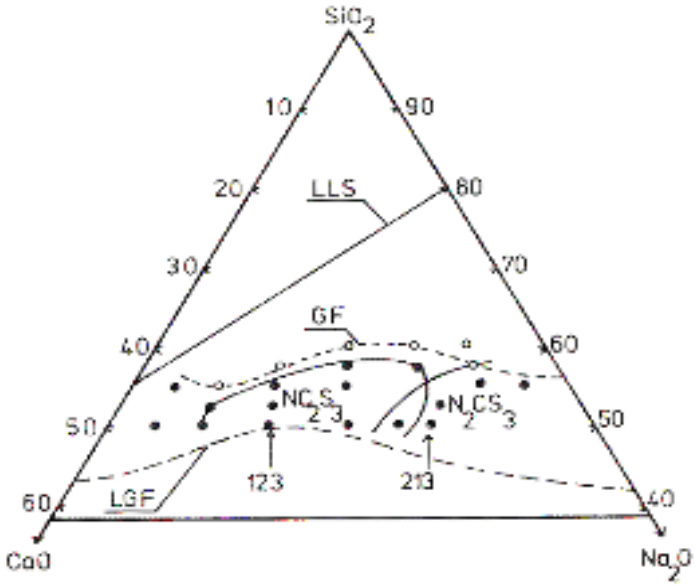

Fig. 1. *Section of Na_2O-CaO-SiO_2 system with compositional fields vitrogene (GF, LGF) with imiscibilitaty (LLS) and crystallization in volume of the N_2CS_3 NC_2S_3 compounds [3]*

Table 1. *The main stages in the elaboration of glass*

No	Name of stage	Temperature range
1	Formation of silicates in the solid phase and of the first melt volumes	It begins at 300 ° C and ends at 800 - 1000^{o}C
2	Glass formation	It begins at 800 – 1000^{o}C and ends at 1300 – 1500^{o}C
3	Refining of the glass melting	1350 – 1550^{o}C
4	Homogenization of the glass mass	It begins at the upper limit of the melting interval and ends at temperatures corresponding to the glass clarification
5	Cooling of the glass mass	At temperatures 200-600^{o}C lower than those of the melting interval

More types of glasses go into the recycling flux, each having different chemical compositions and physical properties. The most frequently used vitreous material is the glass based on silicon dioxide (SiO_2), sodium carbonate (Na_2CO_3), calcium carbonate ($CaCO_3$) or limestone and other minor additives.

Most of the recycled glass is made up of packaging and plane surface glass. The main stages in the treatment and elaboration of glass are shown in table 1.

The samples were made of chipped packaging glass, aluminium oxide, zinc oxide, arsenic trioxide, metal oxide wastes with a granulation of under 300µm. The casting form were filled with these chipped materials which were heated in an oven with silit bars, at a temperature of up to 1450^{o}C.

The quantity and the dimensions of the pieces of glass, as well as the metallic oxide resulting from industrial waste are of a great importance for the melting time, and also for the end product. The granulation of the transparent glass chips which change colour following melting and in the presence of oxides plays an important role in the colour homogeneity and uniformity. The smaller the granule size, the better the colour uniformity. The homogenisation of the glass melt consists in the levelling of the physical and chemical characteristics of the whole mass of glass, a phenomenon which is usually based on reciprocal solubility.

The non-uniformity of colour may appear as a result of an insufficient mixing of the chips with the waste which contains a certain metallic oxide that influences the structure of the glass.

The intensity of the colour and its nuance depend on the concentration of oxide, the valence of the colouring ion, the latter's modification due to the atmosphere of the oven and the chemical composition of the glass. An extremely important role in finalising the homogenisation of the glass is played by high temperature diffusion, at the atom-molecular level. In glass melts, diffusion is the slowest stage and it depends especially on raising the temperature, which also leads to a reduction in viscosity.

Glass without gas bubbles is obtained through refining the glass melt during its elaboration.

Figure 2 presents a sample of dark green glass obtained with the aid of iron oxide resulting from the scale, which is a waste from the metallurgical industry, grinded at sizes of under 200 μm, in a reducing medium.

The used materials for obtaining vitreous materials when added waste with nickel ions are presented in charge, are presented in table 2.

Fig 2. *Green glass obtained by adding in charge of iron oxide*

Table 2. *Raw materials for glasses which neutralisation wastes containing nickel oxide*

Materials charge	wt (%)
Waste glass	63.37
Aluminium oxide	12.25
Zinc oxide	17.42
Arsenic trioxide	0.47
Waste with nickel oxide content	6.48

The melting temperature has increased to over 1450^{o}C through adding the concentration of nickel oxide. After the temperature of 1450^{o}C was reached, it was maintained at this temperature for 150 minutes in view of homogenisation and degasification.

Fig. 3. *Glass with nickel oxide after thermal treatment*

The melt from the refractory crucible was poured into the preheated refractory metal form. The samples obtained through casting were subjected to a thermal treatment of afterglow at a temperature of 600ºC. NiO can be introduced as $Ni(OH)_2$ which decomposes during melting.

Depending on glass composition and melting temperature, glass shades range from yellow to brown, violet or gray. After maintaining the temperature at 600ºC for 2 hours, the oven was stopped and the samples were left inside until completely cooled. Following the afterglow thermal treatment, the sample is gray-green in colour, Figure 3.

The obtained samples were analysed at the SEM in view of emphasising their structure and the inclusions present in their mass. Figure 4 presents the structure of the glass sample, for their obtaining were used green glass waste, other oxide additions and waste containing iron oxide.

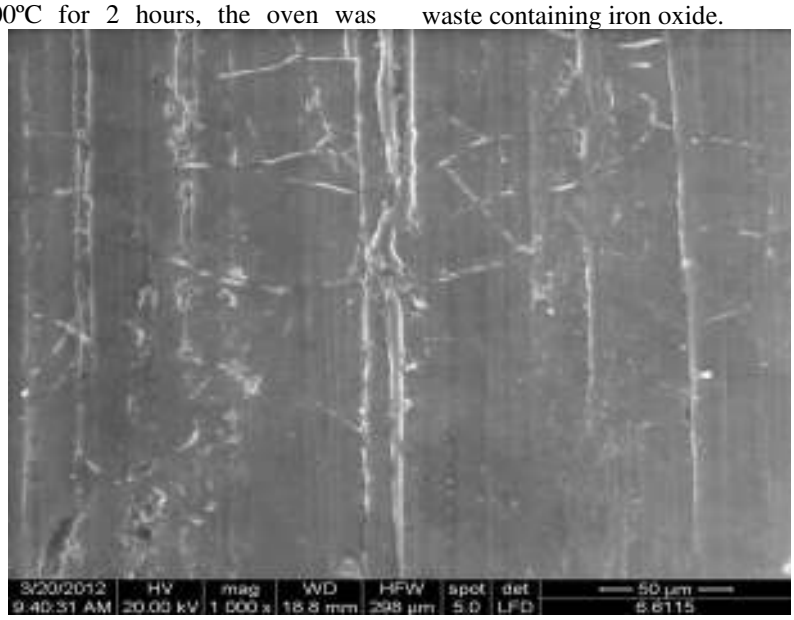

Fig. 4. *Microstructure of a green glass plate with iron oxide*

For casted glass, the base structure is amorphous, which is specific to a vitreous mass. Figures 5 and 6 present the microstructures of the studed glasses which were achieved through the re-melting of glass wastes mixed with othercomponent such us dried mud which contains nickel ions, following then the casting and the afterglow thermal treatment.

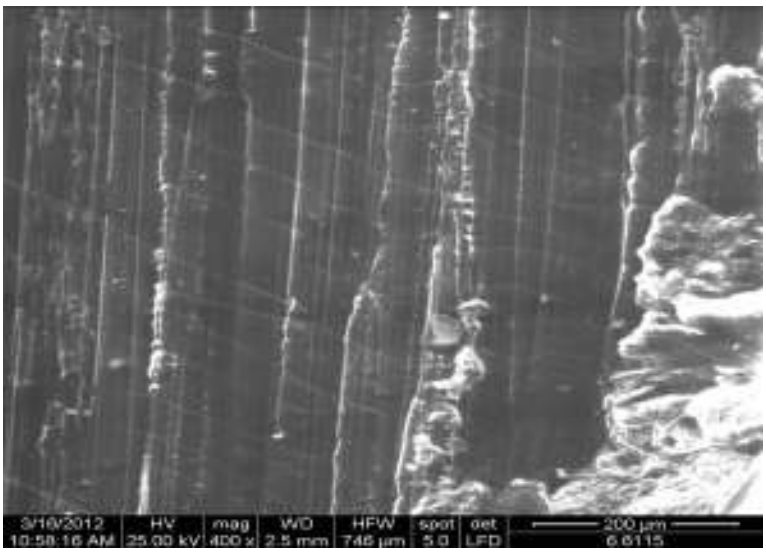

Fig. 5. *Microstructure of glass with nickel oxide, thermally untreated*

In the microstructures of glasses obtained by re-melting of glass waste in the presence of iron oxides or nichel and other components, has revealed the presence of crystals in the vitreous matrix which is specific to oxide glasses.

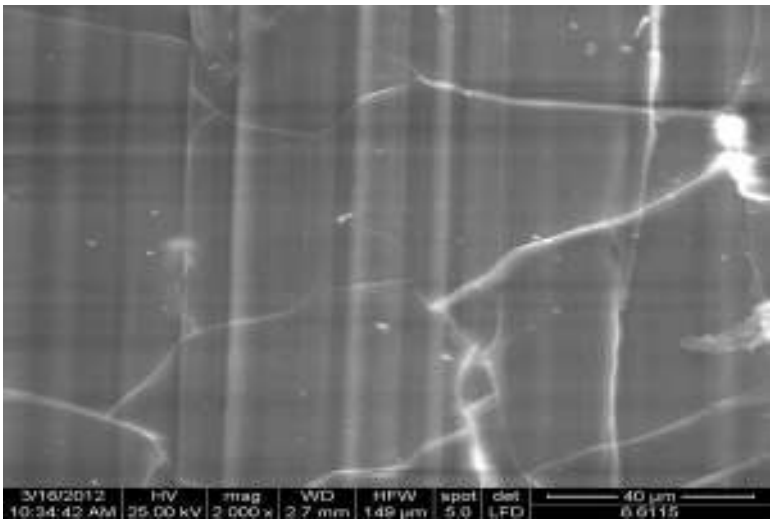

Fig. 6. *Microstructure of glass with nickel oxide, after thermal treatment*

The crystals formed thanks to the thermal of the vitreous phase have determined at the same time a gradual change in the composition and structure of the base glass.

4. Conclusions

The main conclusions of these experimental researches are:

1. Incorporating metallic oxides (contained by industrial waste) into the vitreous matrix determines the decrease of their polluting effect, favourably influences on the temperature of elaborating or thermally treating of the vitreous or vitroceramic materials, and sometimes improves their physico-mechanical properties.

2. Crystals formed as a result of neutralization of waste with metal oxide content in the vitreuos matrix and of the thermal treatment determining at the same time a gradual change in the composition and structure of the base glass.

3. To ensure the designed properties of the glasses, the establishing of the appropriate chemical composition and achieving an adequate thermal treatment are very important.

References

[1]. Luminita-Daniela Ursu, Adriana Diaconu, B.A. Sava, Lucica Boroica, Ileana Mitiu, Elisabeta Rosu, D. Radu, M. Dinulescu, M. Eftimie - *A study of the industrial waste incorporating in glass*, Advanced Materials Research Volumes. 39-40, (2008), pp 675-678.

[2]. Holland W., Beall G., Glass - *Ceramic Technology, by the American Ceramic Society,* Westerville, Ohio, (2002).

[3]. James P.F. - *Nucleation in Glass-Forming Systems a Review, Advances in Ceramics,* Vol. 4, Nucleation and Crystallization in Glasses, 1-48, by the American Ceramic Society, Columbus, Ohio, (1982).

[4]. Gonzales C.J.R., James P.F. - *Crystall Nucleation and Grwoth in an $Na_2O{\cdot}2CaO{\cdot}3\ SiO_2$ Glass, J. Non –Crist. Solids*, 38-39, 699-704, (1980).

[5]. Garcia M.,Valles, G. Avila, S. Martinez, R. Terradas and J.M. Nogués - *Heavy metal rich waste sequester in mineral phases through a glass–ceramic process.* Chemosphere Volume 68, Issue 10, August 2007, pp 1946-1953.

THE ANNALS OF "DUNAREA DE JOS" UNIVERSITY OF GALATI.
FASCICLE IX. METALLURGY AND MATERIALS SCIENCE
N^0. 2 – 2012, ISSN 1453 – 083X

THE INFLUENCE OF STEAM TREATMENT ON MECHANICAL PROPERTIES AND ABRASIVE WEAR BEHAVIOR OF SINTERED P/M STEELS

Mihaela MARIN, Florentina POTECAŞU, Elena DRUGESCU, Octavian POTECAŞU, Petrică ALEXANDRU
"Dunarea de Jos" University of Galati
email: mihaela.marin@ugal.ro

ABSTRACT

In this paper is a study of the influence of steam treatment on sintered P/M steels, for three different types of powder. The abrasive wear of steam-treated sintered iron is analysed by abrasion tests. The specimens were produced from atomised iron powders (Hoeganaes Corporation) with different sizes (<45, 45-63, 63-100, 100-150, >150μm). They were compacted at pressures 600MPa, sintered for 60 minutes at 1150 ºC and then subjected to continuous steam treatments at 550 ºC for 45 minutes. The abrasion tests were conducted under constant load and speed conditions. The wear properties of sintered iron were improved by steam treatment and by the addition of alloying elements. An increase in hardness was associated with an increase in wear resistance. The results reveal that the samples (P_2 and P_3) prealloyed with Cu, Ni and Mo can improve wear resistance of sintered steels.

KEYWORDS: powder metallurgy, sintering, steam treatment, abrasive wear

1. Introduction

The growth of ferrous powder metallurgy (P/M) over the past three decades has been considerable as this technology proves to be an alternate lower cost process if compared with other metal working techniques such as machining, casting, stamping, forging, etc. The parts manufactured by powder metallurgy are broadly used, mostly in the automotive industry. The powder metallurgy parts of complex shapes are obtained and close to final form, with precise surface. Also, specific parts made by powder metallurgy processing help to save time, energy, material, labor and money [1]. Steam treatment is one of the surface treatments applied to sintered components. At first, this treatment was used as an economical way to seal the interconnected pores, sintered iron characteristic, making the component impervious to liquid and gases. This treatment is claimed to improve the superficial properties of sintered materials because the water vapor in the steam will begin to react with the iron in the part to form the oxide iron - magnetite (Fe_3O_4) [2–15].

The oxide layer formed on the sintered iron components is thicker than on the conventional wrought ferrous parts steam treated [13]. In this paper, the mechanical properties and abrasive wear behavior of steam treated sintered iron alloys are studied. The abrasion tests were conducted under constant load and speed conditions.

2. Experimental procedure

2.1. Materials

The specimens prepared from atomized iron powder and from pre-alloyed iron base powders were analyzed in this paper.

***Table 1**. Chemical composition of analyzed powders*

Powder type	Cu	Mo	Ni	C
P_1	0.096	0.008	0.046	<0.01
P_2	1.50	0.50	1.75	<0.01
P_3	1.50	0.50	4.00	<0.01

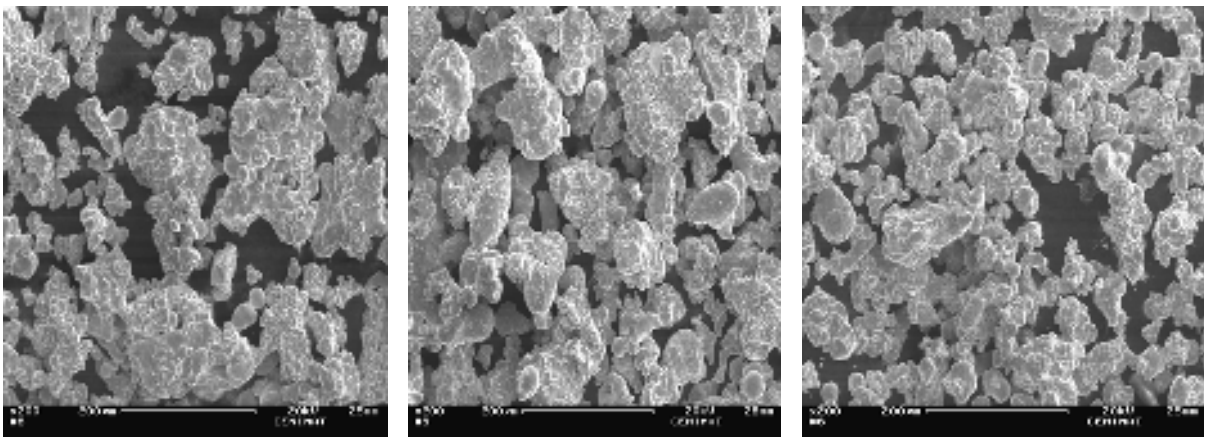

a b c

***Fig. 1**. SEM images of the water- atomized iron powder: a) P_1, b) P_2, c) P_3*

The chemical composition of the powder samples, pure iron and iron-based prealloyed powder with Cu, Ni and Mo is presented in Table 1, whereas Figure 1 shows SEM images of analysed powders.

To evaluate the mechanical properties, such as Vickers microhardness and abrasive wear, a die for making the samples in the form of a cylinder was produced. The powders were mixed with 1% zinc stearate. The samples were compressed in a universal mechanical testing machine to a pressure of 600 MPa, the dimensions of disc specimens are $\phi 8 \times 6$ mm.

The uniaxial pressing in the mold is used effectively for mass production of simple components. In Figure 2 are presented the surface of sintered and stream treated samples.

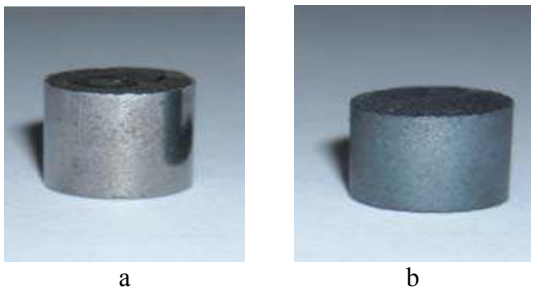

a b

***Fig. 2.** The aspect of sample surface: a- sintered; b- steam treated*

The green samples were sintered in a laboratory furnace, in a controlled atmosphere. The sintering temperature was approximately 1.150°C and the sintering time was 60 minutes with a heating rate of 30-40°C/minutes.

All the samples were kept in the furnace for slow cooling to room temperature. Before the sintering temperature is reached, the parts were maintained during 30 minutes at 500°C to burn lubricant, respectively the zinc stearate. After cooling to room temperature the samples were steam - treated.

The steam treatment was carried out in a furnace with steam atmosphere at 550°C for 45 minutes. The steam-treated specimens were air-cooled to room temperature. It can be seen that on the surface of the samples a blue layer of iron oxide–magnetite (Fe_3O_4), typical for this process, was formed (Fig. 2).

2.2. Mechanical properties

The steam-treated samples were analyzed according to their mechanical properties. The microhardness tests were performed by measuring Vickers microhardness, and the test parameters are: the penetrator is a diamond pyramid diameter and the load of 100 g. The microhardness was the average of three indentations on the top and another on the bottom surfaces of the samples.

2.3. Abrasion wear tests

The abrasive wear is a process of removal and the destruction of the surface tested material. It is affected by many factors such as mechanical properties and abrasive materials, microstructure, loading condition, etc. The steam-treated specimens were tested for abrasion wear test (Fig. 3).

***Fig. 3**. Worn surface after the abrasion test*

The samples were weighed using a precision balance with a sensitivity of 10^{-4} before and after each test, so it was possible to evaluate the wear mechanism undergone by the material. The SiC particles on the abrasive papers were the size of 80µm and the load applied was 855g.

The distance traversed in each case was limited to 150 cycles corresponding to 76.5m. The samples were subjected to circular motion over the wheel on which the abrasive paper was stuck.

The abrasion wear process in which the abrasion test was carried out included the steps: fixing the abrasive paper on the wheel machine; the samples of known weight were loaded on the machine tester and then the load was applied.

The surface of the sample and the abrasive paper were always in strong contact with each other under the predetermined load, and the samples were cleaned and weighed prior to and after each test interval. After tribological tests, the worn surfaces were examined by optical microscope, in order to identify and characterize the dominant wear mechanisms.

3. Results and discussion

3.1. Microstructure

Because the steam treatment is not a treatment that can produce structural changes, all the sample structures consist of ferrite and pores filled with iron oxides and a growth porosity for sample P_1. The optical micrographs are reported in Fig. 4a) – f) and were obtained at a magnification of 400x.

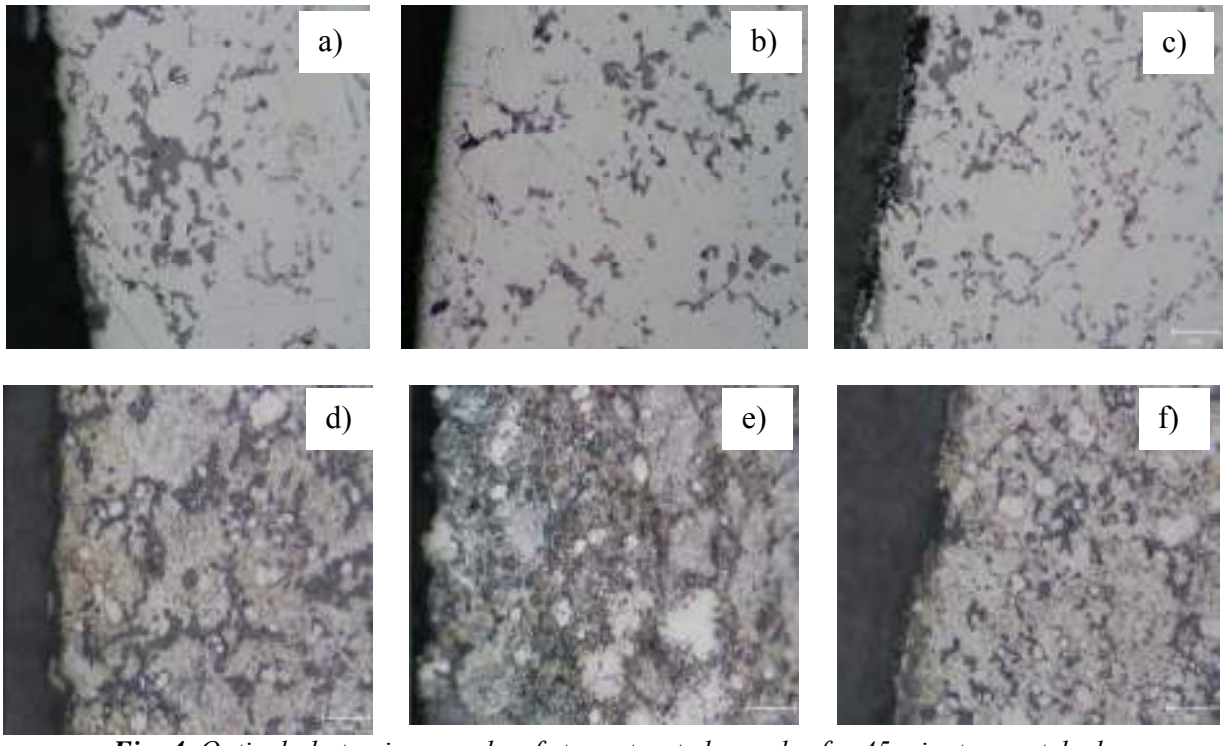

Fig. 4. *Optical photomicrographs of steam-treated samples for 45 minutes unetched: a) P_1, b)P_2, c) P_3 and etched with 2% Nital: d) P_1; e) P_2, f) P_3*

Table 2 shows the values of Vickers microhardness of the studied steam-treated samples, when powder type P_1 (pure iron) was used as a reference.

Table 2. *Vickers microhardness of the steam treated samples*

Powder type	Microhardness [µHV100]	Difference [%]
P_1	221	0.00
P_2	243	9.954
P_3	245	10.859

It is found that all three samples have a difference of approximately 10% in Vickers microhardness values.

3.2. Tribological tests

The worn surfaces of the steam treated samples after abrasion tests were examined with an optical microscope the typical aspects of the abraded surfaces are presented in Fig. 5. The depth and width of wear grooves of steam-treated samples P_1 are greater compared to steam-treated samples with higher microhardness values P_2 and P_3. The wear tracks are in the same direction and the pores are areas that have propagated the wear grooves.

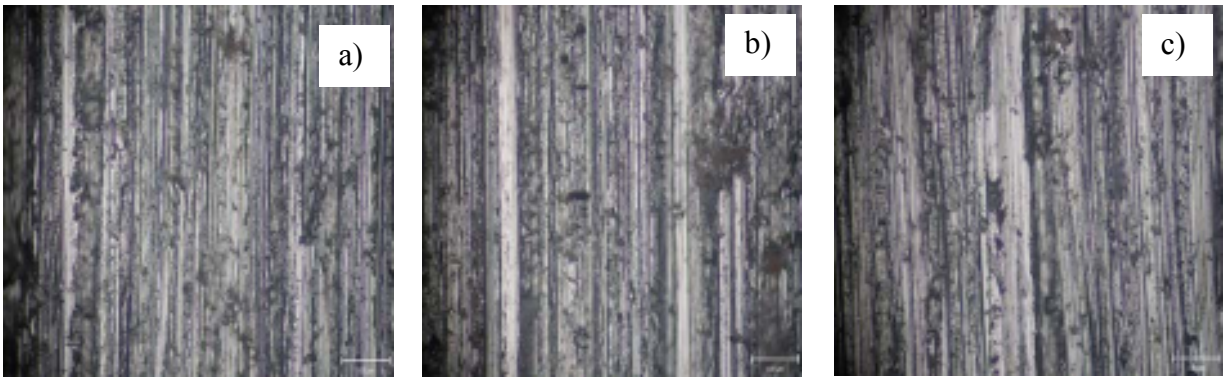

Fig. 5. *Optical photomicrographs of worn surfaces for steam treated samples (x200): a) P_1, b) P_2, c) P_3*

The wear rate was measured as the weight loss and is expressed in Table 3; the sample P_3 provided the greatest weight loss.

Table 3. *Mass loss of steam-treated samples tested to abrasion test*

Powder type	Initial mass	Final mass	Mass loss
	[g]		
P_1	2.271	1.882	0.389
P_2	2.285	1.922	0.363
P_3	2.286	1.935	0.351

4. Conclusions

According to the experimental results in this study, the following conclusions may be discussed:

- As generally observed, composition plays a significant role in the resistance to abrasive wear of PM steels. In this regard, the best behavior was observed for the more hardenable steam-treated samples with higher Ni and Mo content, respectively P_3.
- Based on microhardness measurements, the samples P_2 and P_3 show higher values compared to P_1 (the reference) because of the formation of homogeneous phase according to the largest diffusion in solid solution by the elements used in the preparation of samples, respectively Cu, Ni and Mo.
- The steam-treated sample P_1 presents a greater depth and width of wear grooves; consequently, there is a possibility that it offers less resistance.
- The steam-treated samples P_2 and P_3 present a much smaller wear groove width that can ensure good resistance.
- The weight loss is smaller for the steam-treated samples P_2 and P_3.

References

[1]. V. B. Akimenko, I. A. Gulyaev, O. Y. Kalashnikova, M. A. Sekachev - *The Prospects for Russian Iron Powder*, Central Scientific-Research Institute of Ferrous Metallurgy, Vol. 37, No. 5, p. 472–476.

[2]. P. Franklin, B.L. Davies - *The effects of steam oxidation on porosity in sintered iron*, Powder Metallurgy, Volume 20, pages 11–16, (2001).

[3]. K. Razavizadeh, B. L. Davies - *The effects of steam treatment on the wear resistance of sintered iron and Fe-Cu alloys*, Wear, Volume 69, Issue 3, pages 355-367, (1981).

[4]. J.D.B. De Mello, I. M. Hutchings, *Effect of processing parameters on the surface durability of steam-oxidized sintered iron,* Wear, Volume 250, Issues 1-12, pages 435-448, (2001).

[5]. J.D.B. de Mello, R. Binder, A.N. Klein, I.M. Hutchings - *Effect of compaction pressure and powder grade on microstructure and hardness of steam oxidized sintered iron*, Powder Metallurgy, Volume 44, Number , pages 53–61, (2001).

[6]. G. Straffelini, D. Trabucco, A. Molinari -*Oxidative wear of heat-treated steels*, Wear, Volume 250, Issues 1-12, p. 485-491, 2001.

[7]. K. Razavizadeh, B.L. Davies - *Combined Effects of Steam Treatment and Age Hardening on Mechanical Properties of Sintered Fe-Cu Alloys*, Powder Metallurgy, Volume 25, p. 11–16, (1982).

[8]. A. Molinari, G. Straffelini - *Surface Durability of Steam Treated Sintered Iron Alloys*, Wear, Volume 181-183, p 334–338, 1995.

[9]. A. Molinari, G. Straffelini - *Surface durability of steam treated sintered iron alloys*, Wear, Volumes 181-183, p. 334-341, (1995).

[10]. S.L. Feldbauer, *Steam Treating; Enhancing the Surface Properties of Metal Components*; Aabbott Furnace Company; 2003.

[11]. A. Molinari, G. Straffelini - *Tribological Steam Treated Ferrous Parts*, Int. J. Powder Metallurgy, Volume 33, p. 55–62, (1997).

[12]. G. Strafelini, A. Molinari, *Dry sliding behaviour of steam treated sintered iron alloys*, Wear, Volume 159 , Issue 1, p. 127-134, (1992).

[13]. W.M. da Silva, R. Binder, J.D.B. de Mello -*Abrasive wear of steam-treated sintered iron*, Wear, Volume 258, Issues 1-4, p. 166-177, (2005).

[14]. C. Petot, F. Armaneta, H. Klimczyk, G. Petot-Ervas - *Influence of the demixing of impurities on oxidation kinetics*, Solid State, Volume 50, Issues 1-2, p. 87-97, (1992).

[15]. P. Beiss - *Steam treatment of sintered iron and steel parts*, Powder Metallurgy, Vol 34, No3, p. 173–177; (1991).

THE ANNALS OF "DUNAREA DE JOS" UNIVERSITY OF GALATI.
FASCICLE IX. METALLURGY AND MATERIALS SCIENCE
N^0. 2 – 2012, ISSN 1453 – 083X

PERFORMANCE MANAGEMENT SYSTEM FOR PURIFYING POLLUTED INDUSTRIAL WATER

Stefan DRAGOMIR, Georgeta DRAGOMIR
Marian BORDEI
"Dunarea de Jos" University of Galati
email: ddragomir@ugal.ro

ABSTRACT

In this paper we show an integrate system of water management and an efficient solution that is a floating dock, placed in the harbour area. Water quality is one of the most important elements for life support and contributes to the sustainable development of human society. Following the technical and economic transformations taking place in industry, the waste water remediation system required new approaches to management in this area. It recorded an increase in the variety and complexity of the types and quantities of waste generated in the last years and for administration of this situation are necessary new methods and equipments of waste neutralisation or its transformation in raw materials for industries of profile.

KEYWORDS: management system, cleaning water, polluted water, shipyard

1. Introduction

Water management, in accordance with the European request, has the duty to improve the ways to eliminate all substances which pollute the water sources in a considered location (plant, enterprise, in urban or rural area).

Water management is the activity of planning, developing, distributing and optimum use of water resources under defined water polices and regulations. It may mean:

-management of water treatment of drinking water, industrial water, sewage or wastewater;

-management of flood protection;

-management of the water table. Water supply and the cleaning system are the most critical part for good water management and high yields. Often the water supply is experienced as the most critical part of the water management system. As a cure for the insufficient water supply the control structures are closed. However this will work counter-productive, because it will decrease percolation and consequently increases the toxicity levels in the field. The system should aim at increasing both water supply and improving drainage.

The Water Management system consists of three important components:

-a proper operation of the drainage system should benefit the yield levels and the potentials for crop diversification. The water management should aim to promote the ripening of the soft soils by permitting the drying of the surface layers during the dry season. Deep plowing followed by intensive pudding for land preparation will benefit the yields.

-traditional developed areas usually have a well organized institutional infrastructure. It are usually the more difficult to operate areas where there are problems. Lack of understanding to apply the proper Soil and Water Management system and the lack of Operation & Maintenance budget and facilities are the key limitations for improvement [1].

The flows should be able to flow for drainage as well as for supply, depending on the needs of human communities. That could include leaching of toxic elements. Also the type of crops and the rainfalls and land elevations against flood levels determine if drainage or supply is required. Double connection always means need for water system control including control of hazard of "over-drainage".

The South East Region for Waste Management Plan (SERWMP) is composed of several sections showing the current situation in the region, objectives, alternatives for treatment and final methods of determining the minimum cost. In short, it includes the current situation that presents information on the current situation on waste management in the South Region:

-objectives and targets relating to regional waste management: sets targets to be consistent with national and EU objectives;

-forecast on the generation, collection, treatment, disposal, recycling and minimize quantity of waste: provides generation, collection, treatment, recycling and waste disposal, taking and investment and implementing actions to be undertaken;

-assessment of possible technical alternatives: study various technical alternatives that may be considered for the collection, recycling, treatment and disposal of waste;

-benchmarking: contributes to the choice of the lowest cost scenario for waste water management;

Assess the degree of supportability by people: take into account operating costs, financing and investment, including costs necessary to support implementation of grant schemes - implementation of measures SERWMP.

Implementation measures include a list of actions planned to allow the regional Plan, relating to a reduction in the amount of biodegradable waste and packaging of municipal solid waste, an investment (equipment, utilities) a measure of training and preparation for an awareness and public participation continue a financial measures, incentives and tools, legal measures.

2. Theoretical elements about mechanical cleaning

Mechanical cleaning methods ensure that the sewage of large bodies circulating in the impurities which are deposited and those floating or can be brought into an area and then processed. The method is generally used as pre-filtering or purifying single (final), depending on the degree of cleaning required, as should be followed or not by other purification steps. The mechanical cleaning step is to retain matter occur and fine. For their detention are used grills, slipped for fat materials, equipment for separating the sand from water and installations for decanting substances with a high density of water.

According to interstitial size, grills can be classified as follows:

-*rare grills bars* (used to capture paper, cardboard, plastics bodies, diverse fiber of materials etc.), have the gap of 40 - 50mm (and sometimes 100mm) between their bars. Bars are inclined at 1/3, and the speed of water flowing that through the grill bars is maintained at 60 - 100cm/s, in order to avoid the deposition of waste on the bottom of the deck. The materials retained on the grill drop on the bottom of the deck and can be manually cleaned although it is preferable to to this operation mechanically. These materials are discharged as such to be deposited into landfill or incinerated. In some cases the recovery materials can be shredded by cutting in 0.5 to 0.1mm pieces. The shredding machines are installed directly into the floating dock close to the land, so that the disintegrated matter can pass through the grill and can be discharged at the same time by using a mobile carrier on the land. So, in general, the cleaning of the grill bars can be done manually or mechanically. Manual cleaning is used for smaller plants, with small quantities of materials accepted. Raking is made by hand on a platform situated above the maximum level of the water. Mechanical cleaning is used when the quantities of materials that are retained are so great that frequent cleaning or continues racking are required.

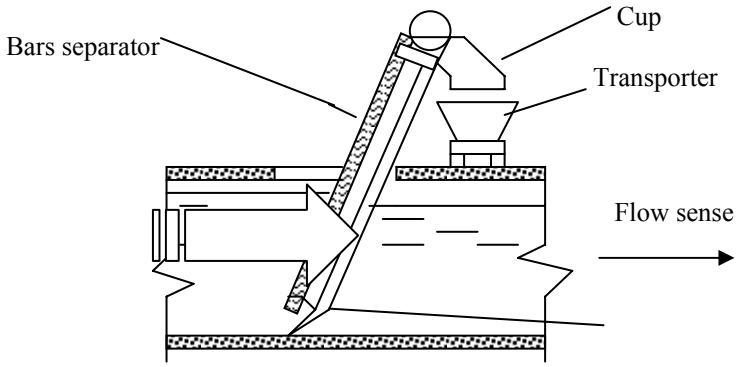

Fig. 1. *Automatic cleaning system with motion rack*

There are a lot of grill types with different mechanical cleaning systems of the water in the floating dock. For example, in a 4m depth floating dock cleaning rotary racks can be used. At greater water depths, straight grills are used, and racks with translation motion (Fig. 1) are used for cleaning. After grill size and degree of mechanization adopted for the cleaning station, deductions from barbecues can be moved mechanically, hydraulically or manually sorted to recover ferrous materials. The nonferrous materials and organics and composted or incinerated. Granulation and cutting material retained on grills can be made with plants placed in water or power outside it. Facilities installed in the water current advantages of a hygienic - sanitary. The material grinding in the water current is done with

shredder equipment. At low and medium flows, they are mounted so that the whole current of water passing through the chip, and thereby to be large bodies crumble. For small quantities of waste, shredder is mounted near the grill that has horizontal bars and mechanical cleaning with rotary rake [2]. In this case, the deductions from grill are collected by a rake with rotating vertical shaft rotation and transported laterally to the machine for waste grinding material positioned below the water.

3. Original solution for fats separation performing equipment

The fat separator may use to remove natural impurities or flotation or flotation with air. Flotation is carried out in natural ponds routine in which, because of the small gears that move water, light particles rise to the surface.

Air flotation may be low pressure or under pressure: in the latter case of air bubbles entering the water adheres to the material in suspension and help reach the surface of the liquid or solid colloidal particles in the mass.

Flotation is used as additional purification step before biological purification of water.

For cleaning industrial wastewater, flotation is used in many cases, for example, water from the oil industry, mining, food, especially when sewage must be treated biologically, either separately or together with other sewage.

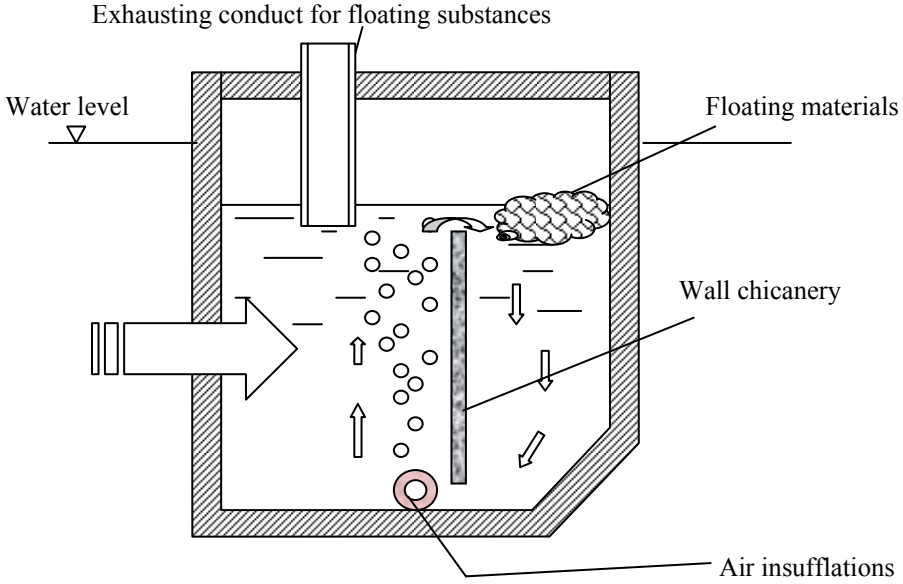

Fig. 2. *Section throws floating dock and schedule of waste separation*

The use of flotation and removal of heavier particles from water is too very important.

The restraint is the nature of fats and namely:

-fat free, that tend to raise the water surface;

-fat soaps, in the colloidal dispersion or in the form of emulsions, which do not naturally tend to rise to the surface;

-tars, which tend to lodge.

To the fat in the first group, the method based on decreasing the rate of flow of water, fat distinguishing the surface in an area arranged for this purpose. Greases from the second group, pools are formed in three sections. In the central basin is insufflations of air and separation of fats, which are directed to collecting trough water and then is discharge in the lateral compartment (Fig.2).

The main parameters for fat separator are:

-time parking: 5 - 10minutes;

-the quantity of air: 0.2 - 0.8m^3 air/m^3 water;

-water depth, 1.20 – 2.75m.

An interesting device for the separation of fat that is combined with air injection vacuum maintained afloat by a vacuum pump. For this purpose it uses a pool covered airtight. For an efficiently purify of water should be introduce an air flow at half from floating dock.

Air bubbles that formed rise to the surface and take after them floating materials and decanted easily. Layer of foam is formed which is collected by a blade that leads to the mouth of the exhaust.

4. Measurements and results

Decanted material is deposited on the bottom of the basin, where they scrape by and discharged. Before and after the cleaning operation we take samples of water and in our laboratory we analyzed these samples. We can see the result of this measurement in the Table 1.

Table 1

No.	Quality indicators		Maximum acceptable level		
		NTPA 001-National and European standardized	**Recorded before water cleaning**	**Recorded after water cleaning**	**u. m.**
1	Temperature	25	25.5	25	^{o}C
2	pH	6.5 – 8.5	8.8	7.9	unities pH
3	Suspension in water	35	300	57	mg/L
4	CBO_5	20	300	18	
5	CCO - Cr	125	500	117	
6	ammonia nitrogen NH_4^+	2	30	4.2	
7	nitrogen total N	10	14	11.5	
8	Sulphides and H_2S	0,5	1,2	0.7	
9	Phosphorus	1,0	5	1.8	
10	Synthetic detergents	0,5	26	8.2	
12	Substances extractable	20	30	19	
13	Total iron ion Fe^{2+}, Fe^{3+}	5.0	-	3.7	
14	Total Cyanide	0,1	1,6	0.16	
15	Nickel, Ni^{2+}	0,1	1,2	0.14	
16	Chromes trivalent Cr^{3+}	1,0	1,8	0.9	
17	Chromes hexavalent Cr^{6+}	1,0	1,1	0.8	
18	Copper Cu^{2+}	0,1	1,5	0.19	
19	Chlorides Cl	500	584	483	
20	Phosphates PO_3^-	1	3,2	1.4	

To investigate potential issues in improving the quality of life for residents of Galaţi city and surrounding region and reducing pollution levels in the Danube River and its downstream locations it is necessary to implementing an automated monitoring system of water parameters, which integrates satellite images using GPS technology.

The main indicators of quality of water, the limits of detection, and the most used methods of analysis is shown in table no.1. In this table are given standardized methods nationally and European (third column) and in the next columns the results recorded before and after using the floating dock for cleaning operation. For determined the parameters of water quality we used own laboratories equipped with these techniques of analysis, such as:

-ionic chromatography (IC);
-atomic plasma spectrometry (APS);
-atomic absorption spectrometry (AAS);
-gas chromatography (CG);
-chromatography liquid high-pressure (HPLC).

Statistical Processing permits a better interpretation of the parameters evolution according to specialists will is performing. Data acquisition for water parameters developing, permit to compare the pollution waters water parameters at precisely time periods.

A specialized computer controls the system that have instruments and devices for coupling at measuring interface, based on real information about quantity of diverse substance dissolved in water samples.

This automated monitoring integrated system must to give information for decisional support and for the measurement that can be taking.

This equipment can decanted the most of the substances in suspension in sewage. After the direction of flow of water decanted equipment are divided into: horizontal and vertical. After the section the decanted equipment may be rectangular (rarely square) and circular.

In terms of processing noted in mud decanted, they can share the space without decanter fermentation (fermentation is done in separate building), or with floor decanter (Imhoff or Emscher), including spaces and fermentation [3]. After place it occupies in the scheme of purification, they are divided into: primary decanter (placed before biological cleaning step) and secondary decanted (after biological cleaning step).

Channel to collect deposits from the upstream head is several times daily to prevent fermentation of using the hydraulic or mechanical means.

Vertical decanted equipment have circular cross section, less square, in which water circulates from the bottom up with a speed Ascension of about 0.7mm/s. The water enters the decanter through a central tube provided at the bottom with a deflection for a more uniform distribution and exits at the upper side over a circular overflow. During normal station

is 1.5 h. Removal of deposits is done by a hydraulic tube vertically on differential pressure [4].

Chemical cleaning is more known as chemical-mechanical cleaning, since it is preceded, in most cases, mechanical cleaning facilities presented above.

Chemical-mechanical cleaning is done in a whole building that includes:

-the construction preparation, determination and introduction of coagulation reagents in treated water;

-decanted.

For mechanical and chemical reagents are used for removal by coagulation and flocculated dispersed fine material and the colloidal.

A colloidal suspension consists of extremely small particles, which possess certain surface with electrical charged. The electrical load induces rejection force. This is of a force between neighbouring particles, which explains the great stability of these suspensions. If, by any means whatsoever, for example, changing the pH or the introduction of a colloid electrical load, it fails to cancel or reduce partially the tasks of electrical particles in water filter, these particles are formed and crowded precipitated relatively bulky (flocculate) capable of rapidly decanted.

5. Conclusions

Precipitation agents most widely used for urban effluent is ferrous sulphate and ferric chloride. Usual doses coagulants used are about 35g/m^3 of water for ferric chloride, and about 55g/m^3 water for ferrous sulphate, which may vary from case to case.

The action of ferrous sulphate at a pH between 6 and 7 (sometimes 5), ferric chloride on the contrary, at alkaline pH is very important. In some cases, precipitation (flocculate) and are hampered by variations in pH, temperature or low level of water do that the floccus results that are very light and make hard. In such cases, a good factor that activate the flocculated process is silica, an element that helps prevent electrical tasks and to obtain a compact precipitate.

Separators pools of flotation aimed at removal of waste water to oils, fats and, in general, all substances lighter than water, which rises to the surface, in quiet areas and low horizontal velocity water. Fat separators mounted, after equipment for separate the sand from water are located where the drainage network has been built into the system unit and after bars grill, when the network has been built into a complex system.

Other substances that can activate the flocculated process are tannin, some clays etc... The coagulants involves in water treatment with a good mastery and knowledge of flow treated. Also, depending on the coagulant, it is necessary a pH of the water that is cleaning.

The time required for reaction with coagulants sewage is 10-20min., a process that occurs in specific basins, to cavil, which provides a mixture intimae. Sometime these pools are replaced with the reaction chamber, where mixing is provided by agitators with large water based and where 15-30min.

Using coagulants is producing a volume of decanted sludge 2-3times higher, than the result from decanted process without coagulant.

The process of chemical treatment of water is falls between simple decantation and biological cleaning. By adding disinfection can sometimes achieve by this method, the efficiency of the biological step. The flocculated process can be doing in separately floating dock or in commune tank with decanted equipment. This equipment is part from new strategy of water management that shipyard administration must do in practice. Sing of floating dock like separated and cleaning system, have the advantage that he avoids the cracked of floccules and their dispersion and too all dangerous substances from waste water are eliminate.

References

[1]. Tchobanoglous, G., Burton, F.L., and Stensel, H.D. - *Wastewater Engineering (Treatment Disposal Reuse) / Metcalf & Eddy, Inc.* (4th ed.). McGraw-Hill Book Company. ISBN 0-07-041878-0, (2003).

[2]. Beychok, Milton R. - *Aqueous Wastes from Petroleum and Petrochemical Plants* (1st Ed.). John Wiley & Sons. LCCN 67019834, (1967).

[3]. *** - International Journal of Water Resources Development, ISSN: 1360-0648 (electronic) 0790-0627 (paper).

[4]. *** - Journal of Water and Health, ISSN: 1477-8920, IWA Publishing.

THE ANNALS OF "DUNAREA DE JOS" UNIVERSITY OF GALATI.
FASCICLE IX. METALLURGY AND MATERIALS SCIENCE
N^0. 2 – 2012, ISSN 1453 – 083X

THE DENTAL TECHNOLOGY IN ART FOUNDRY

Gheorghe FLOREA[1], Ana DONIGA[1], Bogdan FLOREA[2]
[1]"Dunarea de Jos" University of Galati
[2]Politehnica University of Bucuresti
email: gflorea@ugal.ro

ABSTRACT

The paper presents results of a study undertaken to implement the dental casting technique of small parts characterized by extremely complex drawings of surfaces and thicknesses reduced specific objects. During the study there was a similarity between this technique and casting forms obtained with models used to obtain spare fuses in the car industry. They could highlight differences between the materials and the equipment used in dental technology and art foundries.

KEYWORDS: dental, foundry, design, casting technique

1. Introduction

Achieving a work of art or decorative, or cultural, is a challenge to any existing foundry and, especially, informer. For the production of small objects, whether jewelery or religious objects or souvenirs or ornaments, with accessibile, economical technology, can be a profitable productive activity. The dental technique, with specific castings and tools developed to produce them, is an alternative to large, massive machines that require large space for installation and operation, and high consumption of materials and energy.

In addition, this technique provides the possibility to obtain thin-walled parts without surface defects, which usually requires no further machining. The possibility to obtain complex parts attracts the attention of artists and art foundry, giving at the same time, ideas to dental technicians.

Time has moved from manually operated centrifugal cast machine or vacuum has changed the construction of the fuse model, forms and methods of implementing the execution model etc.

In general the phases of dental technology are the same as those encountered in the casting of precision engineering industry, with differences in the chemical composition consisting of alloys and training materials, equipment size, etc.

2. Making mold and fuse model. Owner results

Making a model casting part that the subject of this study, taking into account the complexity and difficulty of its exectuției was not possible for this purpose using a brass icon whose design had a very complex: design complex and reduced height and thickness of the reduced model details as seen in Figure 1.

Fig. 1. *Metal model used in the study*

Unlike dental technique which fuses are easily realizable models for each paper in the study to obtain models chosen for making a mold capable of providing a large number of children in terms of reproduction and fine detail, the suitable material for obtaining them are caucicul silicone. By this method we adopted is different and quite common procedures foundries to manufacture precision molds which are currently used metallic materials, easily fusible metals, plastics etc.

Again, the main conditions imposed molds are perfect:

-play configuration model as the original metallic, precision piece depends, largely, the

dimensional accuracy of the model, a goal achievable through more precise machining and finishing mold advanced as the active surface or, if metal molds, chrome plating work surfaces thereof;

-keeping the size as well during the manufacturing technology fuses models, not to produce the dimensional deviations between tracks;

-making it at least cost to the number of parts is poured.

Taking shape piece (making mold - Fig. 2) was quite easy by pouring silicone rubber, in turn, form the two cavities separated by surfaces and contraformele piece of plaster made previously, the separation plan, configuration, model, representing it its flat surface.

Fig. 2. *Matrix used to obtain models fuses*

Fuses to obtain models (Fig. 3) was used dental wax, which melted, was injected into the mold. Injecting wax into the mold, the mold melt extraction model and its finish, before being put on stream operations is seen with conventional precision casting.

Fig. 3. *Model easily fusible*

"Frame" used to achieve form a metallic cylinder with a diameter of 100 mm, closed at one end with a cover that is integral with the casting funnel model, centrally located. The icon, different in shape and dimensions of castings usually in dental technology workshops, also meant a disposition otherwise shaped patterns (Fig. 4): back to back, evenly spaced about the stem of the funnel and the rods of wax it, and ventilation channels, all the wax, fixed to the back of each.

Network hardware is made based on the same criteria as for casting accuracy, making sure that it has little weight as possible to achieve a minimal casting alloy, condition very important, especially for alloys high cost.

Fig. 4. *Layout models as a whole form-fitted models on the table vibrating, ready pentru turnarea mass packaging*

Generally, the material used in dental technology training is a mixture of refractory material (usually silicon dioxide), binder (calcium sulfate, phosphate, ethyl silicate etc..).

And other chemicals, used to ensure certain properties physical. This material, marketed as "packing table" not specified composition representing Supplier's secret.

To obtain the mixture of training, all materials used in dental technique, using a container (bowl) and a clean spatula, scrap material enhanced hardness can reduce interference, change and modify the setting time dilation. Have the manufacturer's requirements fully, being about a particular product.

Mixture was mixed in vacuum forming, thus ensuring uniform mixing of air and remove it, then

was cast in the form carefully placed on a vibrating table. Forms manually tamping method is inadequate, because on the one hand wax models can be damaged and the other does not get a uniform compaction of the mixture and the complete elimination of air bubbles which form to fill box saturated mixture. After hardening and cooling shape at 35-40^{o}C (the process of strengthening the reaction mixture creates heat), it is placed in an oven pre-heating (Fig. 5), cone down on such support that they can escape wax, which will be heated to remove the wax and bring it to the casting temperature.

***Fig. 5**. The oven used to dry forms.*

Casting alloy to form precision models in forms fuses is warm, with temperatures above 800^{o}C, to ensure their proper filling. The temperature inside the oven to start the heating process of the form is the environment.

Turning water into steam in form, with increased intensity, starting at a temperature of 110^{o}C. During evaporation, the temperature remains at 110-120^{o}C shape, and when it reached the center temperature of 120^{o}C, the evaporation is finished and the temperature rises again.

Cristobalitului transformation starts at a temperature of 220^{o}C form increased in intensity up to 255^{o}C, where transformation reached its climax, and ends at a temperature of 270^{o}C. In the phase where cristobalitul turns itself form temperature should be between 255^{o}C and 270^{o}C. In the packed mass heating, quartz transformation does not begin until the temperature reach 570^{o}C, and between 570 to 580^{o}C in a period of 30 minutes, to create optimal conditions for transformation of quartz. It is important that this temperature is reached inside the shape.

Quartz sintering occurs between 820-860^{o}C and is not subject to time. This process takes place without causing movement of expansion or contraction. This phase is particularly important for precision work. Working temperature of the packed mass must always reach 900^{o}C to ensure smooth and accurate surface detail molded cast part.

Casting icon was made of two alloys used throughout the dental technique, respectively gaudent (9.65% Al, 4.25% Ni, 2.07% Fe, 1.18% Mn, remainder Cu) and niadur (62% Ni, 24.5% Cr, 10.3% Mo, 1.7% Si, 1.5% Fe) and electric resistance was melting. (Fig. 6)

***Fig. 6.** Electric molding furnace*

***Fig. 7.** Centrifugal casting in plant field*

a b

Fig. 8. *Finished piece: a - from gaudent; b - from niadu*

To achieve piece molding technique was used centrifuge machine used for this purpose is shown in Figure 7.

After cooling the alloy, form was destroyed in order to extract part of it, they are subject to further removal process known network hardware and finishing, obtaining finally finished icons (Fig. 8).

3. Conclusions

Forms of plaster, usually are part of permanent forms, while they are forms of temporary dental service, the packaging of this model requiring fuses.

Forms obtained with fusible models allow casting a special dimensional accuracy even in art, where models are highly complex and can not be "copied". In modeling does not take too much account of contraction.

Forms of plaster used in the study will produce parts with very smooth surfaces, what if parts of the category of art is a basic ceriţă. The high percentage of water in mixtures used to obtain forms, requires the use of their hardware only after their complete drying, the difference, the net favorable dental technique, consisting in reducing the period of 10 to 12 times.

By casting models forms easily fusible, the technique adopted, it can get pretty thin walled parts, and can thus significantly reduce the weight of the object.

Casting method in accordance with fusible models in precision casting, allows recovery of burnt material, while in dental technology that burns thus lost.

Materials used to obtain the forms in the studies normally use dental technique, are trade secrets of companies supplying and using them is by their recommendations. Plaster forms, even when used for packaging weight, are relatively inexpensive compared to other precision casting processes.

References

[1]. Florea, Gh., Chiriac, Al., Mărginean, I. - *Procedee performante de punere în formă*, Editura Europlus, (2008).
[2]. Buzilă, S. - *Tehnologia formării*, Editura Didactică şi Pedagogică, Bucureşti, (1981).
[3]. Chira, I., ş.a. - *Procedee speciale de turnare*, Editura Didactică şi Pedagogică, Bucureşti, (1980).
[4]. Fedelman, S. S. - *Turnarea de precizie*, Editura Tehnică, Bucureşti, 1953
[5]. Buzilă, S. - *Procedee speciale de formare,* Editura Didactică şi Pedagogică, Bucureşti, (1978).

THE ANNALS OF "DUNAREA DE JOS" UNIVERSITY OF GALATI.
FASCICLE IX. METALLURGY AND MATERIALS SCIENCE
N^0. 2 – 2012, ISSN 1453 – 083X

AN OVERVIEW OF ASSESSMENT OF THE BLAST FURNACE SLAG TRANSFORMATION INTO VALUE ADDED BY-PRODUCTS ON BASIS OF ITS CHARACTERISTICS KNOWLEDGE

Anișoara CIOCAN
Faculty of Metallurgy, Materials Science and Environment
"Dunarea de Jos" University of Galati
email: aciocan@ugal.ro

ABSTRACT

The slags are the main by-products generated during iron and crude steel production and the steel industry is committed to increasing and improving their recycling. Today the quantity of slag produced and its utilization are one of the important indicators of sustainable steel industry. There are different forms of BF slag by-products depending on the method used to cool the molten slag. The by-products can be an excellent source of constructional materials, finding applications in road building, concrete aggregate, as thermal insulation (mineral wool), and as a clinker substitute in cement production, biological filter media, glass making etc. In addition to products obtained from fresh slag, was studied the possibility to utilize the old and the stockpiled blast furnace slags. The knowledge of the chemical, mineralogical, and morphological properties plays an essential key role in the utilisation of old and stockpiled blast furnace slags. This paper summarizes the characteristics of BF slag and its possible application.

KEYWORDS: blast furnace slag, by-products, morphology, mineralogy, chemical and physical properties

1. Introduction

The target of the current metallurgical industry is to recycle and utilize all their by-products, so as to close the sustainable production loop. Wastes, particularly solid wastes generated unavoidably, should be converted into useful, value added by-products. Slags are the main waste generated during iron and crude steel production and the steel industry is committed to increasing and improving their recycling. These are generated in a parallel route of the main processes of hot metal production in ironmaking and steelmaking and therefore the slag generation process is considered as a part of the whole steel production process [1].

Today the quantity of slag produced and its utilization are one of the important indicators of sustainable steel industry. An average of about 400 kg of solid by-products is generated in the steel industry per tone of crude steel.

Major share of this (70-80%) consists of blast furnace slag and basic oxygen furnace slag. Due to the large slag quantities and the stricter environmental regulations, recycling and utilization of slag are an attractive alternative in order to reduce and eventually to eliminate the disposal cost, to minimize the related environmental pollution, and to save the resource conservation.

The sustainable use of slag contributes to natural resources saving, to CO_2 emissions reduction, to energy consumption reduction, to the formation of a society founded on the recycling practice (as landfilling is avoided) and to the promotion of the iron and steel industry sustainability. Therefore potential economic and environmental benefits make slag by-products that can be further recovered and used. For all these reasons, the effective utilisation of slag turns it into high value added product and allows to improve competitiveness of the iron and steel industry [2].

Based on the information in literature, this paper summarizes the characteristics of BF slag and its possible application.

Its generation process is correlated with the environmental impact. In respect to slag characteristics is evaluated the possibility to transform blast furnace slag into value added by-products for various domains.

2. Blast furnace slag, environmental and economical considerations

A blast furnace is a closed system into which iron-bearing materials (iron ore lump, sinter and/or pellets), additives (slag formers such as limestone) and reducing agents (i.e. coke) are continuously fed from the top of the furnace shaft through a charging system that prevents escape of blast furnace gas (BF gas). Iron ore processed nowadays contains a large content of hematite (Fe_2O_3) and sometimes small amounts of magnetite (Fe_3O_4). In the blast furnace, these components become increasingly reduced, producing iron oxide (FeO) then a partially reduced and carburised form of solid iron. Finally, the iron charge melts, the reactions are completed and liquid hot metal and slag are collected in the bottom. The reducing carbons react to form CO and CO_2. Fluxes and additives are added to lower the melting point of the gangue, improve sulphur uptake by slag, provide the required liquid hot metal quality and allow for further processing of the slag.

The slag floats on the surface of the molten iron and is subsequently drawn off and allowed to cool to produce a semi-dense porous crystalline material (light weight aggregate) known as air cooled blast furnace slag.

From the environmental point of view, the blast furnace has a significant role in the ore based steel production. The manufacture of iron by chemical reduction of iron ores by coke (carbon) in a blast furnace is accompanied by the production of large wastes quantity. The most important is the slag. About 70 years ago, slag generation in blast furnace was 980 kg/t. Recently, due to a better understanding of the slag formation mechanisms and of the overall BF process, it is also currently possible to control, optimize and minimize slag production. The specific quantity of slag generally lies in the range of 175 – 350 kg/t hot metal produced [3, 4].

The slag amount depends very much on the charging material, for example, the grade of iron ore, its sources are the gangue content of iron ore and lime content added to adjust the chemical composition of molten slag. The slag quantity has decreased today by using enriched iron ore and coke with low ash content. From the viewpoint of preservation and protection of the global environment, the main issue concerning the use of ferrous slag is the question whether it is a waste or a by-product. In order to market them, the better way is to consider them by-products because the term "waste" indicates a material to be deposited instead of being used [2, 5].

The driving force for the valorization of the slag is the stringent legislation for environmental protection concerning the use of slag that includes other laws, as follows: the Kyoto protocol, the Reference Document of Best Available Techniques, Harmonization Committees TC 351 Dangerous Substances and TC 154 Aggregates, the REACH directive. The Waste Framework Directive (WFD) (2006/12/EC) is the most important document governing the use of slag. [2].

By other hand, recycling and utilization of the slag is an attractive alternative in order to reduce and eventually to eliminate the disposal cost, to minimize the related environmental pollution, and to save the materials resource and energy. Slag recycling has been successful in different fields of application, in a variety of industries, starting with ironmaking and steelmaking. Ironmaking slag is used in different ways with high added value.

2.1. Utilization of BF slag

Different forms of slag product are produced depending on the method used to cool the molten slag. These products include air-cooled blast furnace slag (ACBFS), expanded or foamed slag, pelletized slag, and granulated blast furnace slag (GBFS), Figure 1.

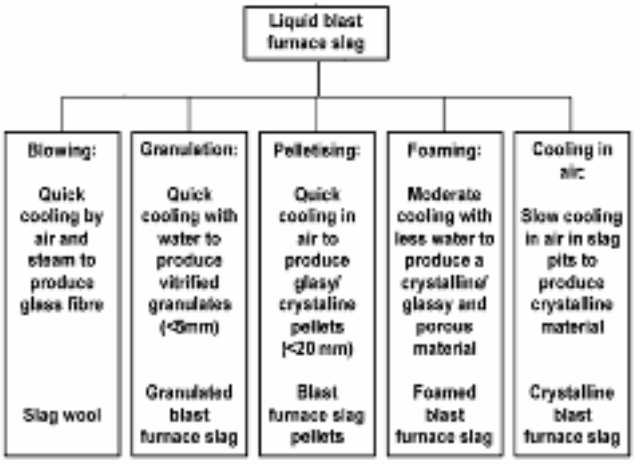

Fig. 1. *Methods of processing the liquid BF slag*

If the liquid slag is poured into beds and slowly cooled under ambient conditions, a crystalline structure is formed, and a hard, lump slag is produced, which can subsequently be crushed and screened. This is the air-cooled BF slag.

If the molten slag is cooled and solidified by adding controlled quantities of water, air, or steam, the process of cooling and solidification can be accelerated, increasing the cellular nature of the slag and producing a lightweight expanded or foamed product.

Foamed slag is distinguishable from air-cooled blast furnace slag by its relatively high porosity and low bulk density. If the molten slag is cooled and solidified with water and air quenched in a spinning drum, pellets can be produced.

By controlling the process, the pellets can be made more crystalline, which is beneficial for aggregate use, or more vitrified (glassy), which is more desirable in cementitious applications.

At more rapid quenching results a greater vitrification and less crystallization. If the molten slag is cooled and solidified by rapid water quenching to a glassy state, little or no crystallization occurs.

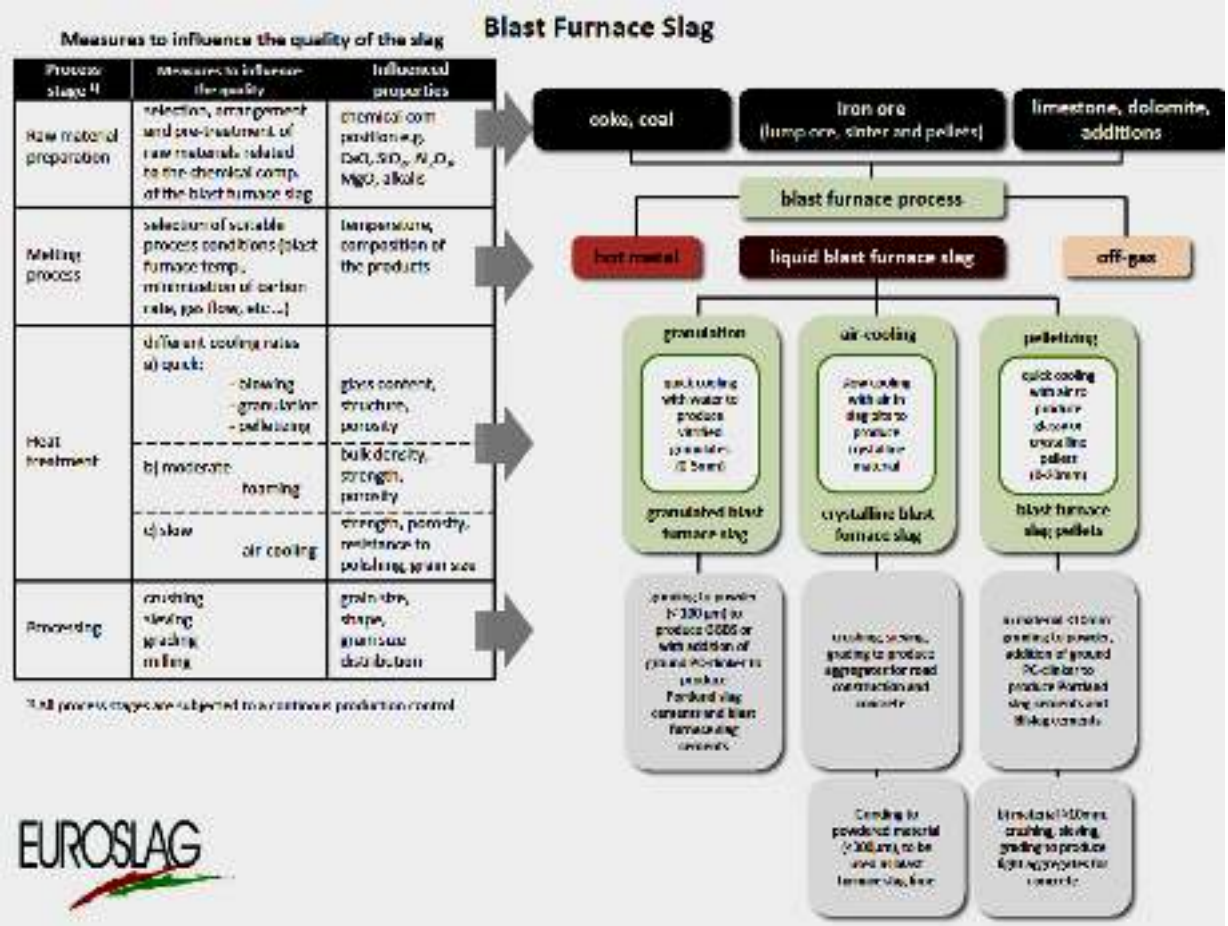

Fig. 2. *Measures to influence the quality of the slag*

Thus is obtained the granulated BF slag. This process results in the formation of sand size (or frit-like) fragments, usually with some friable clinker like material.

The physical structure and gradation of granulated slag depend on the chemical composition of the slag, its temperature at the time of water quenching, and the method of production.

When crushed or milled to very fine cement-sized particles, ground granulated blast furnace slag (GGBFS) has cementitious properties, which make a suitable partial replacement for or additive to Portland cement [6].

The utilization of ironmaking slag has a long history. The use of by-products from steel industry goes back to many centuries ago. The first appearance of slag was recorded as early as the year 700 B.C. In 350 BC Aristotle already stated "When iron is purified by fire, there forms a stone known as iron slag. It is wonderfully effective in drying out wounds and results in other benefits". The history of slag use in road building dates back to the time of Roman

empire, some 2000 years ago, when broken slag from the crude iron-making forges of that area were used in base construction. The cast iron slag stones were used for masonry work in Europe of the 18th century. As early as 1589, Germans were making cannon balls cast from iron slag [4]. In later centuries slag has been used as construction material. The discovery of the hydraulic properties of granulated BF slag gave birth to a new era in slag exploitation: slag has been used as binding agent and/or addition for concrete. The first modern roads in the building of which slag was utilized were built in England, in 1813 [8], and after that the use of slag spread fast to the American continent as well. The use of slag in road building was recorded there for the first time in 1830. Granulated blast furnace slag was first developed in Germany in 1853. Ground slag has been used as a cementitious material in concrete since the beginning of the 1900s.

The traditional use of slag as landfill material, after the increase of steel production since the mid-1970's, has reached its limit and the pressure for natural resources and energy saving have driven steel industry to increase the recycling of this material, by facing other important challenges (such as technologies development, production facilities maintenance and ferrous slag products certification) in order to improve their application in different sectors [2, 7]. To transform blast furnace slag into value added by-products some measures must be applied in accordance with its chemical characteristics, Figure 2.

2.2. Characteristics of the BF slag in accordance with its utilization domains

Blast furnace slag can be an excellent source of constructional materials, finding applications in road building, concrete aggregate, as thermal insulation (mineral wool), and as a clinker substitute in cement production, biological filter media, glass making etc. In addition to fresh slag based products, has been developed the possibility to utilise old, stockpiled blast furnace slags. Such can be re-utilised the several million tones of old slags, previously considered unusable. Availability and areas of applications of BF slag are:

- *Environmental products*: production of Portland slag cement using BF slag; production of roadmaking aggregate and soil conditioner using BF slag and BOF slag

Use of BOF slag as rail ballast; use of fly ash as partial replacement of cement, in manufacture of cellular concrete, bricks and sintered light-weight aggregate, and in road construction.

- *Altogether new products*: glass-forming material; prime western grade zinc; high-purity zinc oxide crystal; glass-ceramic family of materials; Portland cement; iron oxide powder for use in manufacture of ferrites, pigments, etc.; ceramic floor and wall tiles; synthetic granite tiles; wear-resistant ceramic products; heat and sound insulation sandwich panels; natural organic fiber reinforced door panel; sisal fiber cement corrugated roofing sheet.

Knowledge of the chemical, mineralogical, and morphological properties of BF slag is essential because these play a key role in their utilization. The chemical, mineralogical, and morphological characteristics of BF slag are determined by the processes that generate this material. The slag formation is the result of a complex series of physical and chemical reactions between iron bearing raw materials (iron ores, concentrates, sinter, and pellets), the non-metallic charge (limestone), the energy sources (coke, injected coal, etc.), refractory lining etc. at temperature range from 1450 to 1550°C. Also the chemical compositions of the slag depend on the feeding raw materials, and cooling rate. The amount of slag produced depends upon the gangue content of the blast furnace, the ferrous burden, the coke ash and ash from the injection material, e.g. coal, and the amount of flux required to achieve the necessary hot metal quality. In order for blast furnace slag to be acceptable for use outside the iron and steel works, it is necessary to take additional measures to ensure that the slag chemistry and/or physical properties are requisite.

BF slag is made of silicates and alumino-silicates of calcium and magnesium together with other compounds of sulphur, iron, manganese and other trace elements. Their iron content is usually below 0.5% since they result from a reduction process [8-10]. The four major constituents of blast-furnace slag - silica, alumina, lime and magnesia - constitute about 95% of the total composition. In the operation of a blast-furnace the composition of the slag must be closely controlled so that the amount of silica plus alumina balances (wise quantity) with the total of lime and magnesia to produce a composition of slag which will readily melt and flow from the furnace at the temperature of molten iron.

These limitations on the chemistry of blast-furnace slag to permit efficient furnace operation provide quite a narrow band in the chemical composition of all blast furnace slag, Table 1. There may be a limited variation between the silica plus alumina and lime plus magnesia constituents, however, the ratio of the composition fluctuates only to a small amount. The chemistry usually has a narrow ratio of basic to acid components. The most BF slags are characterized by $CaO:SiO_2$ ratio of 1.0-1.3.

Calcium and magnesium oxides content, reported as silica and alumina, normally results in a 0.85 to 1.20 basicity ratio.

The pig iron for the steelmaking purposes has 1.1-1.3 $CaO:SiO_2$ ratio and $(CaO+MgO):(SiO_2+Al_2O_3)$ = 1-1.2. For the high Al_2O_3 content ($SiO_2:Al_2O_3<2.5$) the $(CaO+MgO):(SiO_2+Al_2O_3)$ ratio decreases to 0.9. The presented data suggest that these have remained relatively consistent for all blast furnaces and over the years [6].

Table 1. *Typical composition of blast furnace slag*

Constituent	Percent, %							
	1949[a]		1957[a.]		1968[a.]		1985[a.]	
	Mean	Range	Mean	Range	Mean	Range	Mean	Range
Calcium Oxide (CaO)	41	34-48	41	31-47	39	32-44	39	34-43
Silicon Dioxide (SiO_2)	36	31-45	36	31-44	36	32-40	36	27-38
Aluminum Oxide (Al_2O_3)	13	10-17	13	8-18	12	8-20	10	7-12
Magnesium Oxide (MgO)	7	1-15	7	2-16	11	2-19	12	7-15
Iron (FeO or Fe_2O_3)	0.5	0.1-1.0	0.5	0.2-0.9	0.4	0.2-0.9	0.5	0.2-1.6
Manganese Oxide (MnO)	0.8	0.1-1.4	0.8	0.2-2.3	0.5	0.2-2.0	0.44	0.15-0.76
Sulfur (S)	1.5	0.9-2.3	1.6	0.7-2.3	1.4	0.6-2.3	1.4	1.0-1.9
a. Data source is the National Slag Association data: 1949 (22 sources); 1957 (29 sources); 1968 (30 sources) and 1985 (18 sources).								

The potential mineralogical composition of the BF slag is established from the chemical composition based on the phase diagram of the $CaO-SiO_2-Al_2O_3-MgO$ quaternary system. The place of these usual metallurgical slags on $SiO_2-Al_2O_3-MgO-CaO$ quaternary system is delimited by the Al_2O_3 content that is lower than 20 %. Also the MgO content not higher than 20 % is used to established this location. Thus established, the domain of BF slag is given in Figure 3 (it is presented the compositional zone for the main products in which it is used). The quaternary system of SiO_2, Al_2O_3, MgO, CaO oxides for the 10 % MgO plane is given in Figure 4 and for the 10% and 15% $A1_20_3$ planes in Figure 5 [12, 13].

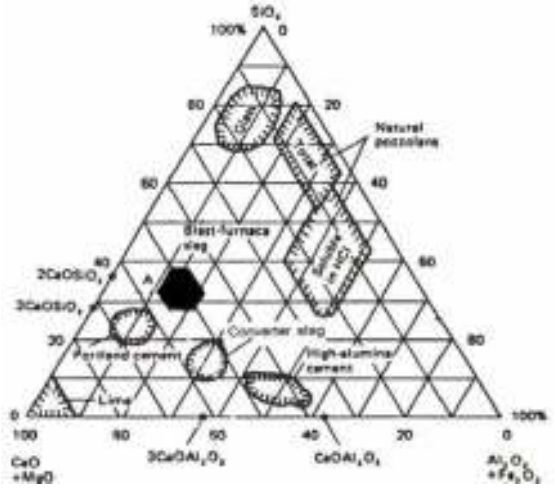

Fig. 3. *Position of the BF slag on thernal diagram with respect to its chemical composition and its utilization possibility [11]*

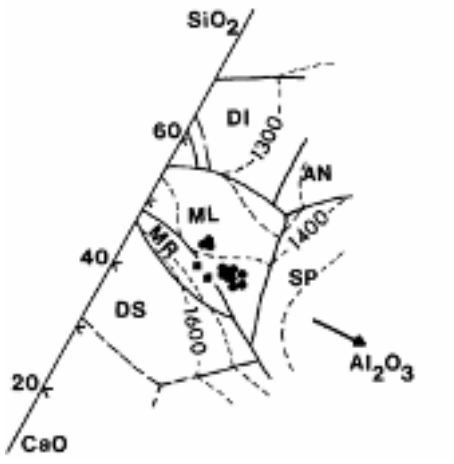

Fig. 4. *Section through the $CaO-SiO_2-A1_20_3-MgO$ system at 10 % MgO with chemical data of slags plotted for some French slags (squares) and Scunthorpe and Redcar slags (circles): DI: diopside. AN: anorthite. ML: melilite. MR: merwinite. SP: spinel. DS: dicalcium silicate. Dashed lines are isotherms in ^0C [13]*

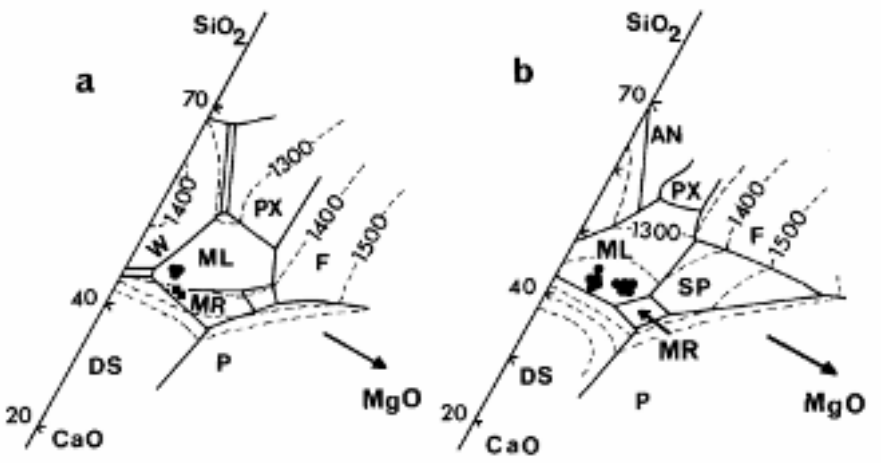

Fig. 5. *Sections through the CaO-SiO_2-Al_2O_3-MgO system at 10 % Al_2O_3 (a) and 15 % Al_2O_3 (b):PX: pyroxene. F: forsterite. W: wollastonite. ML: melilite. MR: merwinite. DS: dicalcium silicate. P: periclase. AN: anorthite. SP: spinel. Chemical data for low Al (<11 % Al_2O_3) Scunthorpe (circles) and French slags (squares) plotted on a. Scunthorpe and Redcar slags with >11 % Al_2O_3 a plotted on b. [13]*

The absence of any quaternary compound is certainly in this quaternary system. The oxides, binary and ternary compounds, binary, ternary and quaternary solutions were identified. The mineralogical compounds from quaternary system CaO-SiO2-Al203-MgO that can be found after crystallization from acid and basic blast-furnace slag are: pseudo-wollastonite (CS), rankinite (C_3S_2), dicalcium silicate (C_2S), melilite, merwinite (C_3MS_2), monticellite (CMS), diopside (CMS_2), anorthite (CAS_2), Figure 6.

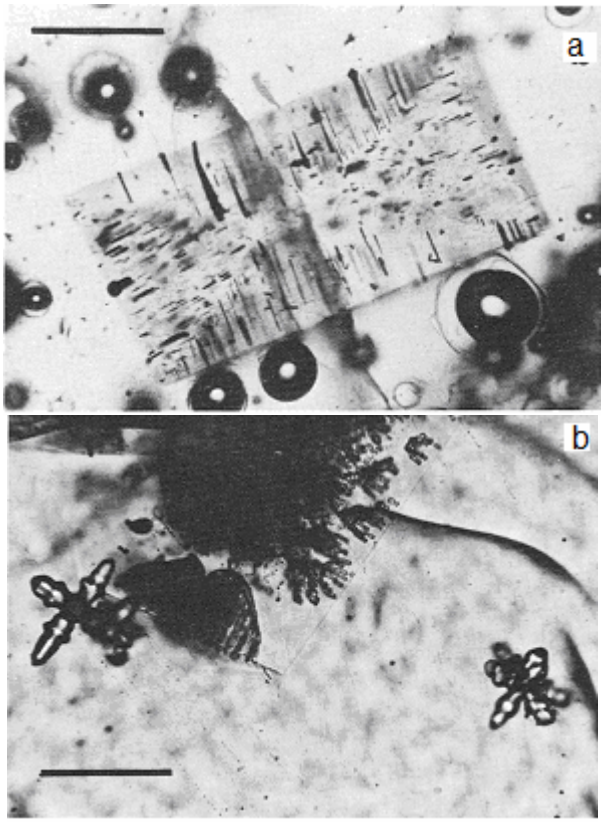

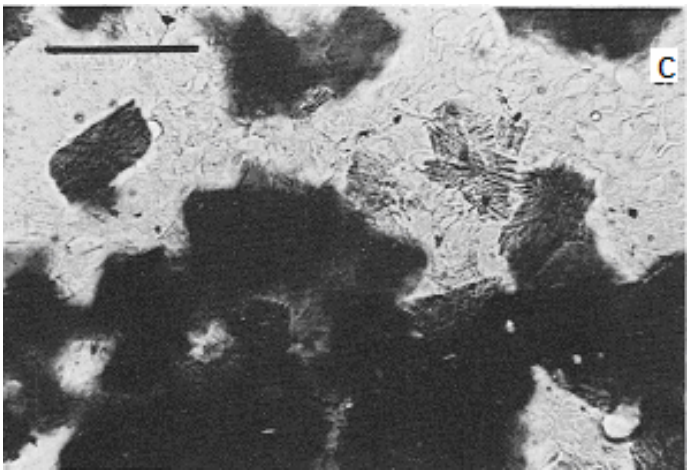

Fig. 6. *Micrographs of granulated slag: (a) Sector-zoned euhedral melilite with orientated inclusions of iron. Some of the iron extends beyond the crystal forming a spherical globule attached to the surface. Sample 3. Plane polarized light. Scale bar 0.10 mm. (b) Stellate oldhamite crystals and dendritic growth of oldhamite. (c) Cluster of merwinites within glass [13]*

When molten blast-furnace slag is rapidly chilled and is being quenched in water as granulated slag, the solid phase is amorphous, predominantly a granular and cellular glass. When such molten slag is more slowly cooled, crystallization takes place while the slag is cooling. The air-cooled BF slag is a mixture (crystalline and amorphous). The crystal phase predominant in air-cooled blast furnace slag is melilite, a name applied to any series of solid solutions extending from akermanite ($2CaO{\cdot}MgO{\cdot}2SiO_2$) to gehlenite ($2CaO{\cdot}Al_2O_3{\cdot}SiO_2$). Spinel is also present. The compositions of spinel ($MgO{\cdot}Al_2O_3$), merwinite ($3CaO{\cdot}MgO{\cdot}2SiO_2$) and periclase are close to their stoichiometry. In addition, in certain conditions other minerals found to be present in blast furnace are pseudowollastonite, monocalciumsilicate, olivine, pyroxene, merwinite, calcium sulfide, ferrous sulfide and manganous sulfide [13, 15].

Figure 7 shows well the quenched liquid slag in equilibrium with melilite (Figure 7a) and spinel (Figure 7b) respectively.

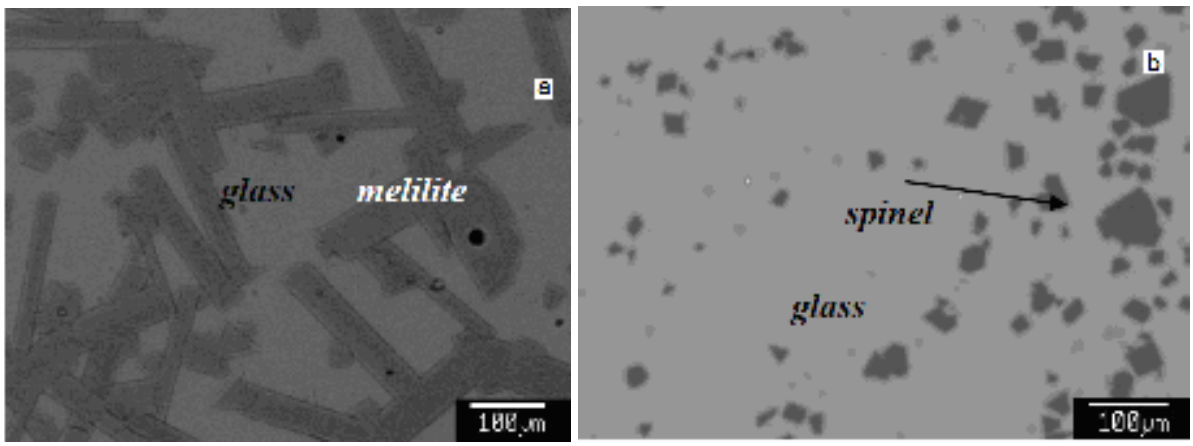

Fig. 7. *Typical microstructures of quenched slags from a) melilite and b) spinel primary phase fields in air [15]*

a. b.

Fig. 8. *Ground granulated blast-furnace slag (a) and its SEM micrograph (b) [16]*

The physical appearance shows that the blast furnace slag is a dull white color, and it has rough and angular-shaped particles, Figure 8.

When BF slag is crushed and screened it produces an aggregate with a rough surface texture and relatively high porosity. Crushed air-cooled BF Slag (ACBFS) is angular, roughly cubical, and has textures ranging from rough, vesicular (porous) surfaces to glassy (smooth) surfaces with conchoidal fractures. The 1-5 mm granulate particles are very angular with a vitreous appearance. Their colour varies from pale honeybrown to grey-brown and rarely almost black. This reflects the chemical variability, the darker slags being richer in Mn (0.98-1.65 %). Small vesicles (<1 mm) are common in the larger pieces. Occasional vitreous fibers occur. The internal structure of the granulate particles has many cracks visible in thin section, some of which are perlitic. There are abundant vesicles varying considerably in size and quantity within a single grain. These often aggregate to form linear, curved or irregular clusters of single sized vesicles. Overall, glass dominates. In every sample it is >80% by volume, but usually >95% and often >99% of the granulate. Individual granules, however, sometimes contain up to 30% crystals [13].

The mineralogy of the solid state determines the material properties such as the durability, the solubility and the reactivity. Generally, an amorphous material is less soluble than a crystallized phase with a similar chemical composition, due to the very slow kinetics for a re-crystallization and reactions with the surrounding liquid media [17]. However, rapid cooling (quenching) and enhancing the amount of amorphous material is also a process that increases the reactivity of a material with puzzolanic properties, such as ironmaking slag [18-20]. Rapid cooling is also a means of reducing the content of unstable silicates, as well as free CaO and periclase, MgO that expand at phase transformation [21].

From the point of view of the hydraulic power of the blast-furnace slag, this depends for one part on their chemical composition and for another on their microstructure. Most of the authors estimate that the vitreous structure is the controlling condition because the vitreous state makes possible and explains the reactions which would not be possible from the crystallized material. Blast-furnace slags entirely crystallized of normal composition do not have hydraulic property or only a very limited one. Other estimate that "vitreous-crystalline" slag has higher potential hydraulic properties than slag vitrified up to 100%. Also the size and the distribution of crystals in the vitrified blast furnace slag have an effect upon hydraulic power. In conclusion, for an identical chemical composition a perfect vitrification is not the criterion of a highest reactivity. The increase of Al_20_3 rate in a quaternary slag glass gives an improvement of hydraulic properties. Particularly the increase of Al_20_3 rate in a quaternary slag glass gives an improvement of hydraulic properties [22-25].

Blast furnace slag is mildly alkaline and exhibits a pH in solution in the range of 8 to 10. Although blast furnace slag contains a small component of elemental sulfur (1 to 2 percent), the leachate tends to be slightly alkaline and does not present a corrosion risk to steel in pilings or to steel embedded in concrete made with blast furnace slag cement or aggregates. Also as a matter of fact, slag is frequently used to eliminate acid conditions in industrial operations as well as to neutralize acid soil conditions in agriculture [14].

Relatively low bulk density of BF slag is typically 1300 kg/m^3 for air-cooled and stable with no expansion tendencies. Instability problems with blast furnace slag are relatively rare. Fresh-made (i.e. new) blast furnace slag should in fact have no instability problems. However, some older sources of blast furnace slag, after a period of weathering, may contain pockets of unstable material.

The most likely form of instability in this type of slag is when, as a result of weathering, a significant proportion of the sulphur oxidises to sulphate, often present as gypsum. This, under given conditions, may take part in chemical reactions resulting in the formation of a sulphoaluminate hydrate phase, apparently similar to that taking place in sulphate attack on concrete. The result is volumetric expansion and disruption of the mass [14].

In certain situations, the leachate from blast furnace slag may be discolored (characteristic yellow/green color) and have a sulfurous odor. These properties appear to be associated with the presence of stagnant or slow moving water that has come in contact with the slag. The stagnant water generally exhibits high concentrations of calcium and sulfide, with a pH as high as 12.5 [26]. When this yellow leachate is exposed to oxygen, the sulfides present react with oxygen to precipitate white/yellow elemental sulfur and produce calcium thiosulfate, which is a clear solution. Aging of blast furnace slag can delay the formation of yellow leachate in poor drainage conditions but does not appear to be a preventative measure, since the discolored leachate can still form if stagnant water is left in contact with the slag for an extended period [27-30].

The physical properties of blast furnace slag have a considerable variability depending on the iron production process. Table 2 compares the key physical properties of air-cooled blast furnace slag and a common natural aggregate [8]. Of all the slag types generated, air-cooled blast furnace slag (ACBFS) is the type that is most commonly used as an aggregate material.

Processed ACBFS exhibits favorable mechanical properties for aggregate use including good abrasion resistance, good soundness characteristics, and high bearing strength. Table 3 lists some typical physical properties of air-cooled, expanded, and pelletized blast furnace slags [33].

Table 2. *Typical properties of BF slag compared to a natural aggregate*

Property	BF slag	Carboniferous limestone
Apparent density	2.55	2.72
Water absorbtion (%)	4	0.7
Impact dry value (%)	34	19
Crushing value (%)	34	21
10% fines soaked -kN	85	160
Polished stone value	53-57	38-48
Abrasion value (%)	5-7	8

Table 3. *Typical physical properties of blast furnace slag*

Property	Slag Type and Value		
	Air-Cooled	Expanded	Pelletized
Specific Gravity	2.0 - 2.5	—	—
Compacted Unit Weight, kg/m^3	1120 – 1360	(800 - 1040)	840
Absorption (%)	1 - 6	—	—

Granulated blast furnace slag is a glassy granular material that varies, depending on the chemical composition and method of production. Grinding reduces the particle size to cement fineness (Figure 8a), allowing its use as a supplementary cementitious material in Portland cement concrete. The GGBF slag has the lowest percentage of large particles. The fines specification requires that < 20 wt % of the material be retained by the 45 micron sieve during wet sieving.

The particle size distributions (PSDs) of the slag powder (with the chemical composition given in Table 4) in deionized water and obtained by laser light scattering indicate that many fine particles (<1μm) are present, Figure 9 [34].

Also were determined other physical properties of this slag: the mean diameter volume for two samples is 8.80, respectively 9.10; the medium diameter volume is 6.74 and 7.83; the a mean diameter number is 0.63 and 0.73 as a mean value, respectively 0.52 and 0.58 as a medium value; the particles density is 2.70 and the aerated and tapped densities measured for slag are around of 0.80 and respectively 1.26 (tapping deaerates the powder, allowing the particles to compact within the graduated cylinder to produce a greater density than the one measured for the aerated materials); the value of ratio of the two densities (tapped/aerated) that is the Hausner Ratio is about 1.56…1.59 and provides an indication of the degree of compaction that a dry powder can undergo in handling and storage.

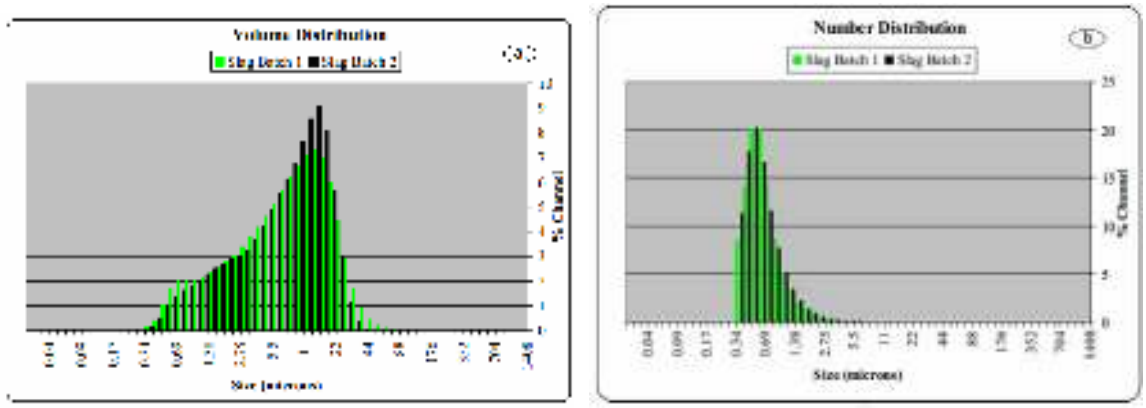

Fig. 9. *PSD (volume based) (a) and PSD (number based) (b) for GGBF slag [34]*

Table 4. *Chemical compositions of two samples of BF slag [34]*

Sample	Al_2O_3	CaO	Fe_2O_3	K_2O	MgO	Na_2O	SO_4	SiO_2	TiO_2
1	8.4	38.5	0.4	0.3	12.9	0.3	1.0	37.9	0.4
2	6.6	35.0	0.3	0.5	13.1	0.3	2.5	40.4	0.3

The porosity of expanded blast furnace slag aggregates is higher than ACBFS aggregates. The bulk relative density of expanded slag is difficult to determine accurately, but it is approximately 70 percent of that of air-cooled slag. Typical compacted unit weights for expanded blast furnace slag aggregates range from 800 kg/m^3 to 1040 kg/m^3. Unlike air-cooled and expanded blast furnace slag, pelletized blast furnace slag has a smooth texture and a rounded shape. Consequently, the porosity and water absorption are much lower than those of ACBFS or expanded blast furnace slag. Pellet sizes range from 13 mm to 0.1 mm, with the bulk of the product in the minus 9.5 mm to plus 1.0 mm range. Pelletized blast furnace slag has a unit weight of about 840 kg/m^3.

Because of their more porous structure, blast furnace slag aggregates have lower thermal conductivities than conventional aggregates.

Their insulating value is of particular advantage in applications such as frost tapers (transition treatments in pavement subgrades between frost susceptible and nonfrost susceptible soils) or pavement base courses over frost-susceptible soils [35].

3. Conclusions

The global emphasis on stringent legislation for environmental protection has changed the scenario of slags dumping into slags management.

Because of the natural drive to be cost-effective, there is a growing trend of adopting such slags management measures that would convert slags into wealth, thereby treating these wastes as by-products.

This has led to aiming at the development of zero-waste technologies.

In addition to the environmental achievements, the recycling practices produced economic benefits, by providing sustainable solutions that can allow the steel industry to achieve its ambitious target of "zero-waste".

To satisfy environmental and technical requirements of international and national standards, it is necessary to know the chemical, mineralogical, and morphological properties of BF slag.

The chemical composition and the cooling rate determine the phases and the particle shape of slag. These are in correlation with its physical and mechanical properties.

All of these Bf slag characteristics are essential because these play a key role in their utilization.

References

[1]. **** - Integrated Pollution Prevention and Control* (IPPC) – Best Available Techniques Reference Document on the Production of Iron and Steel – December, (2001), European Commission, Brussels.
[2]. Branca, T.A., Colla, V. - *Possible Uses of Steelmaking Slag in Agriculture: An Overview, Material Recycling – Trends and Perspectives*, 335-356, Available on http://cdn.intechopen.com/pdfs/32571/InTech-Possible_uses_of_steelmak-ing_slag_in_agriculture_an_overview.pdf.
[3]. **** Eurofer,* Review blast furnace slag processing, (2007), p. 5
[4]. Joulazadeh, M.H. Joulazadeh, F. - *Slag; Value Added Steel Industry Byproducts, Archives of Metallurgy and Materials*, Volume 55, Issue 4, (2010), 1137-1145.
[5]. Kobesen, H. – *Legal Status of Slag Valorisation, Proceeding of the First International Slag Valorisation* Symposium, Leuven, Belgium, April 6-7, (2009).
[6]. **** User Guidelines for Waste and Byproduct Materials in Pavement Construction,* Available on http://www.fhwa.dot.gov.

[7]. *** *The Japan Iron and Steel Federation* – Nippon Slag Association (July 2006). The Slag Sector in the Steel Industry, Available on http://www.slg.jp/e/index.htm.

[8]. Dunster, A.M. – *The Use of Blast furnace Slag and Steel Slag as Aggregates*, Proceedings of the Fourth European Symposium on Performance of Bituminous and Hydraulic Materials in Pavements, 257-260, (2001), Nottingham.

[9]. Geiseler J. – *Use of slags from iron and steelmaking.* Proc. Gorham/Intertech's 13th International Iron & Steel Development Forum – Managing Steel Mill Wastes & By-Products: Crisis and Opportunity. 11.-14.5.1998, Antwerp, Belgium, 8p. Geiseler, (1998).

[10]. Mäkikyrö M. – *Converting Raw Materials into the Products – Road Base Material Stabilized with Slag-Based Binders*, Academic Dissertation Faculty of Technology, University of Oulu, (2004).

[11]. Monsi, A., Asgarani, M.K. – *Producing Portland cement from iron and steel slag and limestone,* Cement and Concrete Research **29**, 1373-1377 (1999).

[12]. Levin, E. M., Robbins, C. R., and McMurdie, H. F. – *Phase diagrams for ceramists. American Ceramic Society*, Columbus, Ohio, (1964), pp. 601.

[13]. Scott, P.W., Critchley, S.R., Wilkinson, F.C.F. – *The chemistry and mineralogy of some granulated and pelletized blast furnace slags*, Mineralogical Magazine, March 1986, Vol. 50, pp. 141–147

[14]. *** *Slag and Its Relation to the Corrosion Characteristics of Ferrous Metals*, National Slag Association, NSA 172-13 Available on www.nationalslagassoc.org.

[15]. Dianwei Zhang, Evgueni Jak, Peter Hayes, Baojun Zhao – *Investigation and Application of Phase Equilibria in the System Al2O3-CaO-MgO-SiO2 Relevant to BF Slag, High Temperature* Processing Symposium 2012, Swinburne University of Technology

[16]. Harbour, J.R., Hansen, E.K., Edwards, Williams, V.J., Eibling, R.E., Best D.R., and Missimer, D.M. – *Characterization of Slag, Fly Ash and Portland Cement for Saltstone*, Process Science and EngineeringSavannah River National Laboratory Aiken, SC 29808.

[17]. White, W.B. – *Dissolution mechanism of nuclear waste glasses: A critical review. Advances in Ceramics, 20 Nuclear Waste Management II,* Editor: Clark DE, White WB, Machiels AJ. the American ceramic Society, (1986), p. 431-442.

[18]. Daugherty KE, Saad B, Weirich C. Eberendu A. – *The Glass Content of Slag and Hydraulic Activity,* Silicates Industriels, (1983). 4-5, p 107-110.

[19]. Murphy JN, Meadowcroft TR, Barr PV. – *Enhancement of the cementitious properties of steel-making slag,* Canadian Metallurgical Quarterly, Vol 36, No 5, (1997), p 315-331.

[20]. Shij C. – *Steel slag – its Production, Processing, Characteristics, and Cementitious Properties*, Journal of Materials in Civil Engineering. ASCE, (2004), p 230-236.

[21]. Tossavainen, M., Lind, L. – *Leaching Results of Reactive Materials,* Building Materials, September (2005).

[22]. Bunikov, P.O. - *Znacko Javorskij, Laitiers de Haut Fourneau Granules et Cimente au Laitier* Gosstrojizdat Moscow, 1953

[23]. Smolczyk, H.G. – *Structure et Caracterisation des Laitiers,* 7th International Congress on the Chemistry of Cement - Paris, 1980, Volume I – Rapports principaux - pages III 1/3 to 1/16.

[24]. Demoulian, E. - *Gourdin P. et Autres, Influence de la Composition Chimique et de la Texture des Laitiers sur leur Hydraulicite*, 7th International Congress on the Chemistry of Cement - Paris, 1980, Volwne II - Communications pages III 89 to III 94.

[25]. Galibert, R. – *Glass Content Influence upon Hydraulic Potential of Blast - Furnace Slag*, National Slag Association, NSA 184-2, Available on www.nationalslagassoc.org.

[26]. *** *National Slag Limited. Letter*, April 4, 1995, D. Horvat, National Slag Limited to P. Verok, MTO Construction Office, with Attachment, Overview Report, Leachate Mechanism, Blast Furnace Slag Technical Committee, Hamilton, Ontario, March 17, (1995).

[27]. *** *I*ron and Steel Slag for Road Construction*,* JIS A 5015, Japanese Industrial Standards, (1992).

[28]. * Guide to the Use of Slag in Roads***,* Australian Slag Association, (1994).

[29]. *** *Interim Policy: Use of Blast Furnace and Steel Slag,* State of Ohio Environmental Protection Agency, June 6, (1994).

[30]. *** *National Slag Limited. Letter*, April 4, 1995, D. Horvat, National Slag Limited to P. Verok, MTO Construction Office, with Attachment, Overview Report, Leachate Mechanism, Blast Furnace Slag Technical Committee, Hamilton, Ontario, March 17, (1995).

[31]. *** *Fax memorandum, S. Szoke, Ontario Ministry of Transportation to D. Horvat, National Slag Limited,* April 7, (1995).

[32]. Noureldin, A.S., McDaniel R.S. – *Evaluation of Steel Slag Asphalt Surface Mixtures,* Presented at the 69th Annual Meeting, Transportation Research Board, Washington, January, (1990).

[33]. *** American Association of State Highway and Transportation Officials. Standard Specification for Materials, "*Blended Hydraulic Cements,"* AASHTO Designation: M240-85, Part I Specifications, 14th Edition, (1986).

[34]. Harbour, J.R., Hansen, E.K., Edwards, T.B., Williams, V.J., Eibling, R.E., Best D.R., and Missimer, D.M. – *Characterization of Slag, Fly Ash and Portland Cement for Salts*tone, February (2006), Available on http://sti.srs.gov/fulltext/2006/TR200667resub.pdf.

[35]. Emery, J.J. – *Pelletized Lightweight Slag Aggregate,* Proceedings of Concrete International 1980*,* Concrete Society, April, (1980).

THE ANNALS OF "DUNAREA DE JOS" UNIVERSITY OF GALATI.
FASCICLE IX. METALLURGY AND MATERIALS SCIENCE
N^0. 2 – 2012, ISSN 1453 – 083X

INCREASE THE STEELS PURITY CAST IN VACUUM

Valentin MINCU, Nicolae CONSTANTIN
Politehnica University of Bucharest
emails: valentin.mincu1@yahoo.com, nctin2010@yahoo.com

ABSTRACT

The need to develop products with special characteristics and high mechanical properties led to the introduction of plastic deformation of semi-finished materials. Special purpose products are produced from slabs, blooms, billets or from different size ingots. One of the critical conditions to meet quality expectations after plastic deformation is that the material must be as high quality as possible. For refining steels, a range of methods have been developed that can remove harmful elements from the physical and mechanical product properties. For these products, the chosen casting method is one of the most important factors that can ensure product quality because casting can easily remove the beneficial effects of the refining process conducted during the development of the steel melt by contamination with refractory material from the casting assembly, re-oxidation of the metal bath and others. Depending on the complexity of the casting product and to obtain a superior quality product, several methods of casting have been developed.

The usual method of casting high quality large ingots is in vacuum, the advantage is that the steel stream is protected from the surrounding atmosphere, this paper aims to highlight the benefits of vacuum casting with wide stream on the improvement of ingot quality by increasing purity and decreasing gas content.

KEYWORDS: vacuum casting, big ingots, increase the purity, decreasing gas content

1. Introduction

The wide range of applications for steel products made it necessary to develop certain methods and equipments for developing and refining steels leading to increased productivity and improved quality. Product quality is given by the chemical composition and physico-mechanical properties, therefore, to be able to obtain them, steel undergoes a series of processes to increase its purity. Imposing special treatment installations is due to the negative influence of endogenous and exogenous inclusions on steel quality.

Appearance of nonmetallic inclusions (exogenous) in cast steels is a common problem because it involves additional costs for repairs or can lead to the rejection of the product. The results of mechanical properties are closely related to the degree of the steel purity, as the size, composition, morphology and distribution of inclusions have a huge impact on product quality. For example, ductility and tensile strength decreases significantly with increasing oxides or sulfides content in the material. It is important that the number and size of inclusions be controlled.

2. Necessity of refining steels

Refining on secondary treatment installations is successful in removing these inclusions through chemical reactions and slag making but great attention must be paid to the chosen method of casting and molding equipment used because steel can absorb gases from the atmosphere forming defects on the surface of the casted steel part. The exposure of the steel melt to the uncontrolled atmosphere during casting is very harmful because liquid steel absorbs atmospheric gases (N, O and H) to form compounds that prevent solidification in optimal conditions (appearance of gas pockets, internal and external shrinkage hole, fissures and cracks).

Nitrogen influence

Nitrogen is generally unwanted in steel because of its influence on steel properties: it lowers cold deformability (deep drawing) and resilience,

resistance to corrosion and shock. In combination with hydrogen, it causes the formation of small pockets of gas and steel aging in castings because of nitrides forming on the structural grain boundaries [3]. Nitrogen is absorbed in the liquid steel from the metal scrap charge, de-oxidation and alloying elements and from the furnace atmosphere as a result of dissociation taking place in the electric arcs of the electric arc furnace.

Hydrogen influence

Hydrogen is always present in the metal bath, but completely unwanted because it produces flakes and porosities during the solidification process. Hydrogen is one of the main causes of porosities in steel ingots and castings it also reduces the plasticity and toughness and affects electrical and magnetic properties [3].

Oxygen influence

Oxygen is a main element in the development of steel, the energy released from burning gas or solid fuel is used to melt the scrap metal, gaseous compounds resulting from combustion help removing non-metallic inclusions from the liquid metal.

Oxide inclusions resulted from reactions between oxygen and metals or non-metals cause an increase in susceptibility to brittle fracture, they reduce fatigue (especially in bearings, springs, and machine parts) and affect the surface quality of parts [3].

Depending on the steel destination, it can be molded into various shapes that can ensure good conditions in the next stages of processing, depending on the shape and size of the products, costs and quality.

To maintain the purity and quality of cast steel ingots, it is necessary to take into account the advantages and disadvantages of the main methods of casting (castings, vacuum castings, bottom pouring).

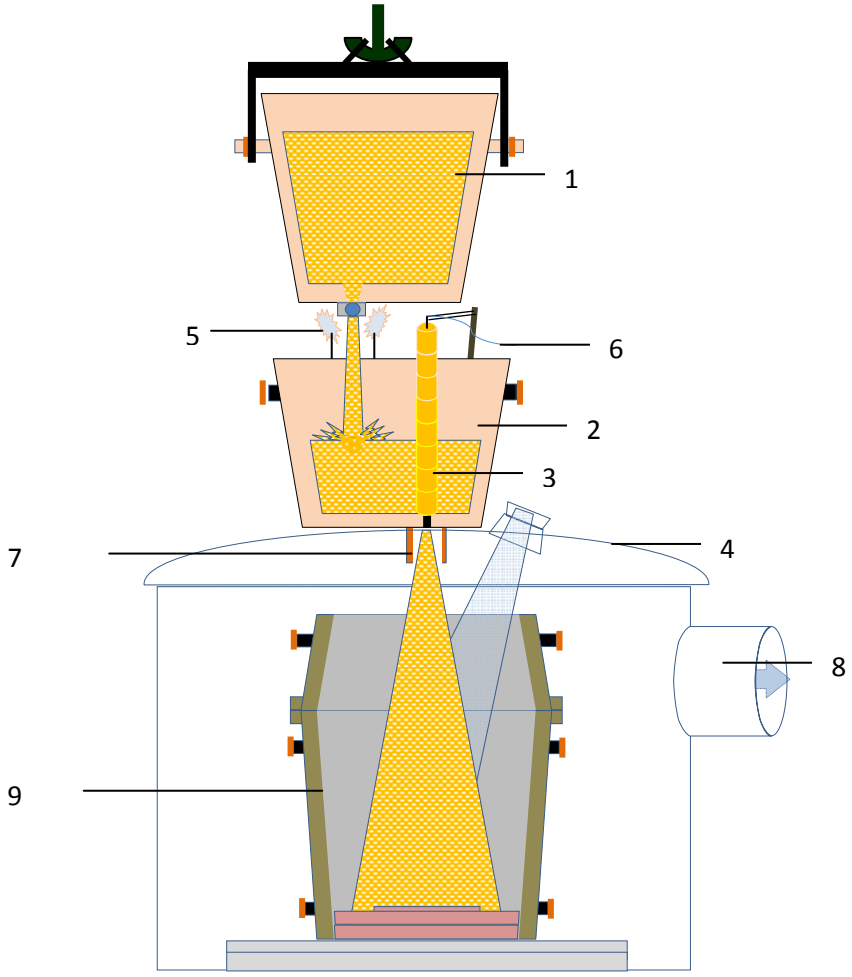

Fig. 1. *Pouring assembly:*
1 – refining ladle; 2 – pony ladle; 3 – stopper rod; 4 – vacuum tank; 5 – argon protection; 6 – argon to the stopper rod; 7 – stream jet; 8 – steam ejector; 9 – mold.

3. The methods casting and refining

This paper presents the benefits obtained from vacuum casting with wide stream.

Using this method (Fig. 1), an advanced degassing of the liquid steel is achieved due to the vacuum created in the casting tank (4), obtaining a high quality ingot. To obtain the necessary vacuum, a pony ladle is required (2) with a stopper rod (3). Argon is injected inside lance (6) to ensure the formation of wide stream (7) in order to obtain a bigger contact surface between the steel droplets and the vacuum inside the tank.

The analyzed heats were melted and refined on an electric arc furnace (Fig. 2) with the following features:

Construction type → Water cooled roof and side panels;
Capacity → 55-73 T;
Lining → Magnesia-carbon;
Hearth interior diameter → 5500 mm;
Transformer power →30 MVA;
Electrode diameter → Ø500mm (UHP);
Electrode placing diameter → 1350 mm;

This also helps avoiding the appearance of strong convection currents that could transport inclusions to the ingots center, letting them float to the surface metal bath. To emphasize the degassing efficiency of steels during casting, nine heats of carbon steel were analyzed, material S34MnV and weighing 71Tons, each used in the manufacture of crankshafts for the marine industry.

To achieve the required mechanical properties imposed by the operating conditions, the cleanliness of the material must be increased by removing trace elements and gas from the metal bath during secondary treatment.

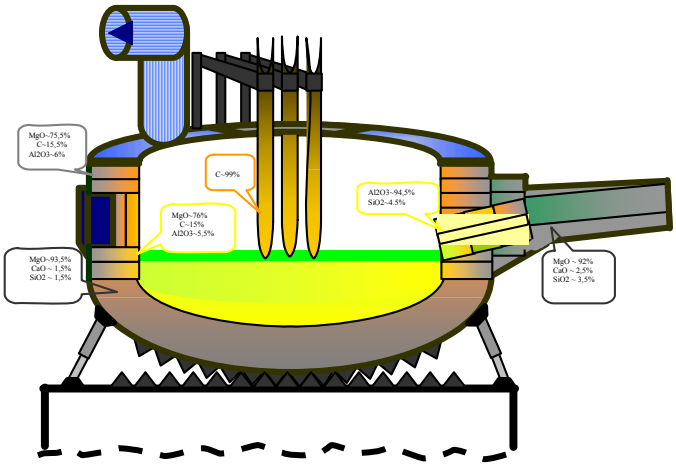

Fig. 2. *Electric Arc Furnace*

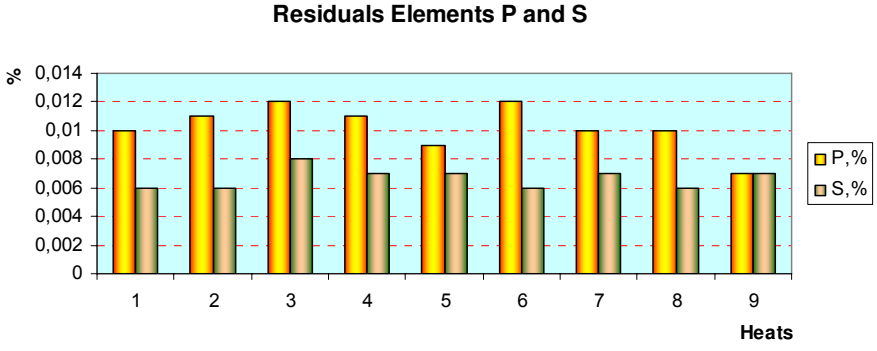

Fig. 3*. Residual elements P and S at the end of the EAF refining*

The reduction of residual elements P and S was made by classical methods: phosphorus removal - intense oxidation of metal bath, slag removal and sulfur removal - high temperature and the use of synthetic slag. The oxidation of the metal bath is made to reduce the residual elements by oxidation and by transferring them in the slag.

The order of oxidation reactions is:

$$[Si] + 2[FeO] = (SiO_2) + 2[Fe]; \quad (1)$$
$$[Mn] + [FeO] = (MnO) + [Fe]; \quad (2)$$
$$2[Fe_2P] + 5[FeO] = (P_2O_5) + 9[Fe]; \quad (3)$$
$$[C] + [FeO] = \{CO\} + [Fe]; \quad (4)$$

The oxidation of carbon and release of CO causes a stirring effect on the liquid metal bath ("boiling effect") increasing the contact area between slag and metal bath, ensuring homogeneous temperature and chemical composition of the metal bath also eliminating much of the gases (hydrogen and nitrogen) and nonmetallic inclusions contained in the liquid steel [1]. For the reduction of oxygen contained in the metal bath, such powerful de-oxidation materials were used as, Al, SiCa, FeSiMn. By injecting an inert gas (argon) during the de-oxidation period, some of the gasses contained in the liquid metal are removed.

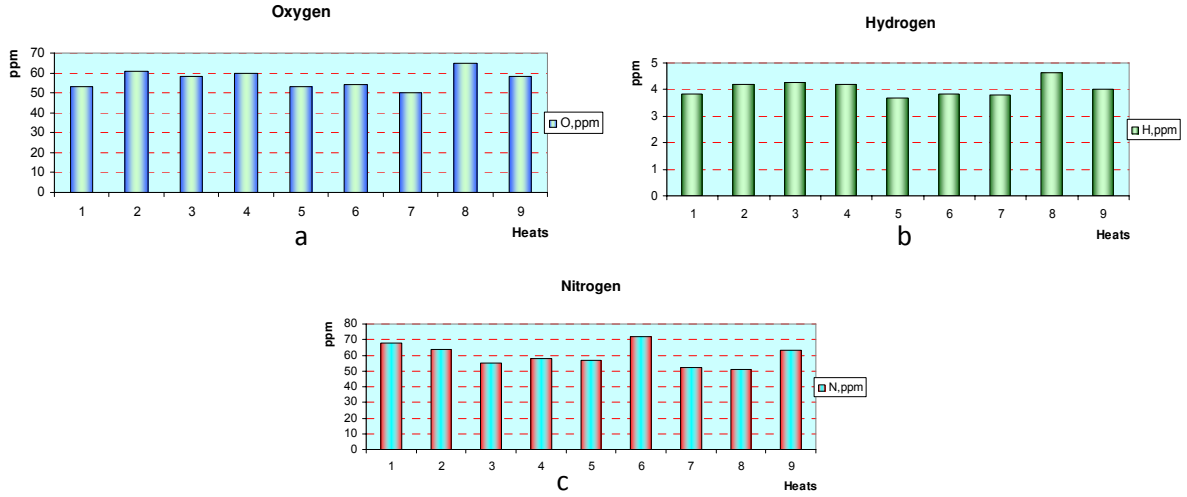

Fig. 4. *Gases present in the metal bath at the end of the EAF refining period: a - Oxygen, b - Hydrogen, c-Nitrogen*

4. Gas absorption in metal bath

To tap the steel from the EAF a ladle must be preheated to a temperature of 1150°C in order to reduce temperature loss and thermal shock. To ensure optimal pouring temperature (1580+/-5ºC) the liquid metal will be tapped from the EAF at 1700°C. The big temperature difference between tapping and pouring is due to time losses (Fig. 5), transport and re-ladling the liquid steel into the pony ladle (Fig. 6).

Fig. 5. *EAF tapping in ladle*

Fig. 6. *Steel re-ladling*

Pouring speed, spout length and the distance between the ladle and spout are critical factors in the absorption of gases from the atmosphere into the liquid metal. When re-ladling, to reduce the harmful effects of exposing the steel stream to the surrounding atmosphere an intermediate device between the ladle and pony ladle is used that protects the steel stream by injecting argon gas.

The transfer between the ladles takes about 4 minutes, at the end the temperature is close to the steel pouring temperature. Gas analysis from the molten steel bath after tapping from the EAF indicates a slight increase, especially hydrogen and oxygen (Fig. 7.)

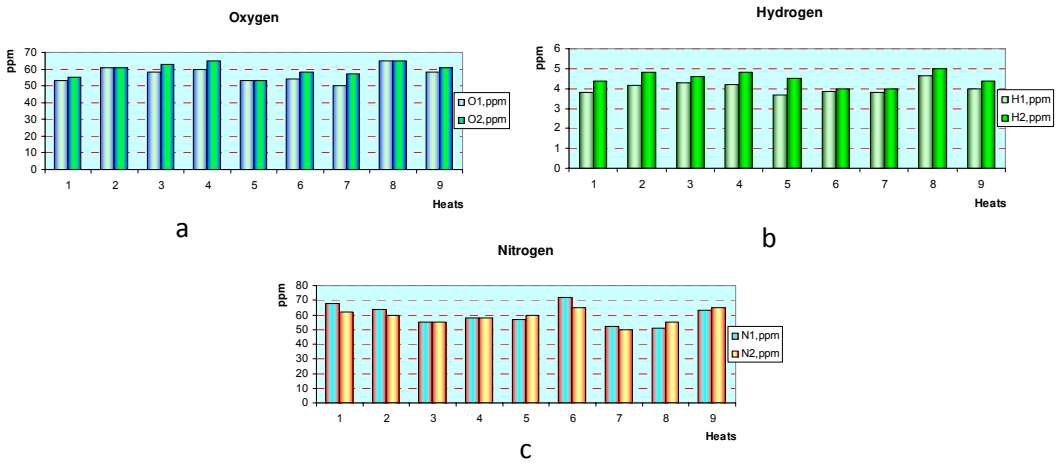

Fig. 7. *Gases present in the metal bath after tapping from EAF: a - Oxygen; b – Hydrogen; c-Nitrogen.*

The pouring assembly has an important role in ensuring product quality because it can contaminate the liquid metal with oxides and refractory materials, so it is very important to properly clean and preheat (to lower the humidity). Low vacuum is an important factor to achieve because the degassing efficiency is even higher when the pressure is at its lowest point [2].

The vacuum pump type used is ULVAC, the vacuum is made by steam ejectors. The steam must have a minimum temperature of 200° C and a pressure of 20 (see Table 1).

Table 1. *The vacuum pump features*

Capacity	Ejectors	Condensers	Steam pressure	Min. Steam temperature	Lowest vacuum
[kg/h]			[Bar]	[ºC]	[Torr]
650	7	3	20	200	0,250

5. Stream Degassing

The injected argon flow in the stopper rod during pouring directly influences the steel stream. It is established according to the following: temperature steel (fluidity), the amount of steel that is present in pony ladle, distance between stopper head and pony ladle nozzle (pouring speed) and the inside diameter of the pony ladle nozzle used.

Excessive flow of argon leads to a large stream of steel that can adhere to the cold pouring equipment thus contaminating the steel (future mass ingot crystallization centers) but a low flow decreases the metal degassing efficiency [2].

For the analyzed heats, the wide stream was done differently by increasing or decreasing the speed of ingot pouring, keeping a constant argon flow and pressure (5 bar) in the stopper rod, the casting speed was modified by decreasing or increasing distance between the stopper rod and the pony ladle nozzle obtaining different types of wide stream: large, medium and strong.

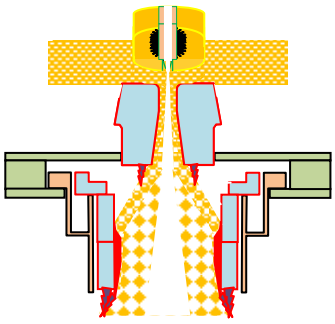

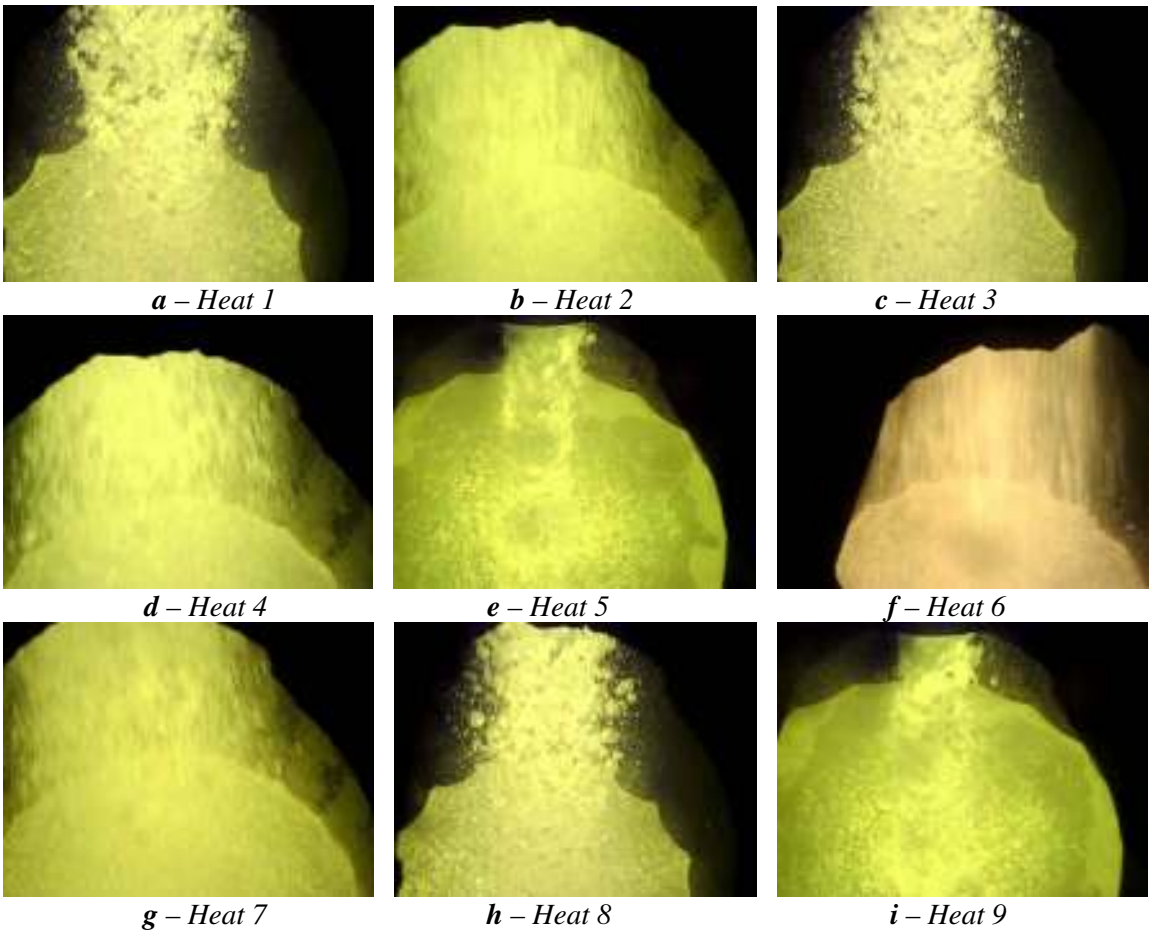

***a** – Heat 1* ***b** – Heat 2* ***c** – Heat 3*

***d** – Heat 4* ***e** – Heat 5* ***f** – Heat 6*

***g** – Heat 7* ***h** – Heat 8* ***i** – Heat 9*

***Fig. 8.** Stream Jet in pouring time:*
b, d, f, g – wide stream; a, c, h – medium stream; e, i – narrow stream.

***Table 2.** Degassing efficiency*

Stream		**WIDE**				**MEDIUM**			**NARROW**	
Heats		Heat 2	Heat 4	Heat 6	Heat 7	Heat 1	Heat 3	Heat 8	Heat 5	Heat 9
Casting rate [t/min]		6.0	6.1	6.3	6.2	6.8	7.0	6.7	7.5	8.2
Vacuum degree [Torr]		**0.360**	**0.314**	**0.337**	**0.333**	**0.388**	**0.330**	**0.303**	**0.325**	**0.363**
Hydrogen	Before Tapping [ppm]	4.18	4.2	3.85	3.8	3.83	4.28	4.65	3.7	4
	After Tapping [ppm]	4.8	4.8	4	4	4.4	4.6	5	4.5	4.4
	After Pouring [ppm]	1	1.1	1.25	1.2	1.3	1.3	1.3	1.6	1.8
	η degassing. [%]	**79.2**	**77.1**	**68.8**	**70.0**	**70.5**	**71.7**	**74.0**	**64.4**	**59.1**
Oxygen	Before Tapping [ppm]	61	60	54	50	53	58	65	53	58
	After Tapping [ppm]	61	65	58	57	55	63	65	53	61
	After Pouring [ppm]	27	24	25	24	25	27	25	25	25
	η degassing. [%]	**55.7**	**63.1**	**56.9**	**57.9**	**54.5**	**57.1**	**61.5**	**52.8**	**59.0**
Nitrogen	Before Tapping [ppm]	64	58	72	52	68	55	51	57	63
	After Tapping [ppm]	60	58	65	50	62	55	55	60	65
	After Pouring [ppm]	35	40	36	35	40	37	45	32	40
	η degassing. [%]	**41.7**	**31.0**	**44.6**	**30.0**	**35.5**	**32.7**	**18.2**	**46.7**	**38.5**

A wide stream is supposed to cover around 80% of the ingot bottom surface while medium stream covers about 50% (below this value it is considered to be narrow stream. resulting low degassing efficiency).

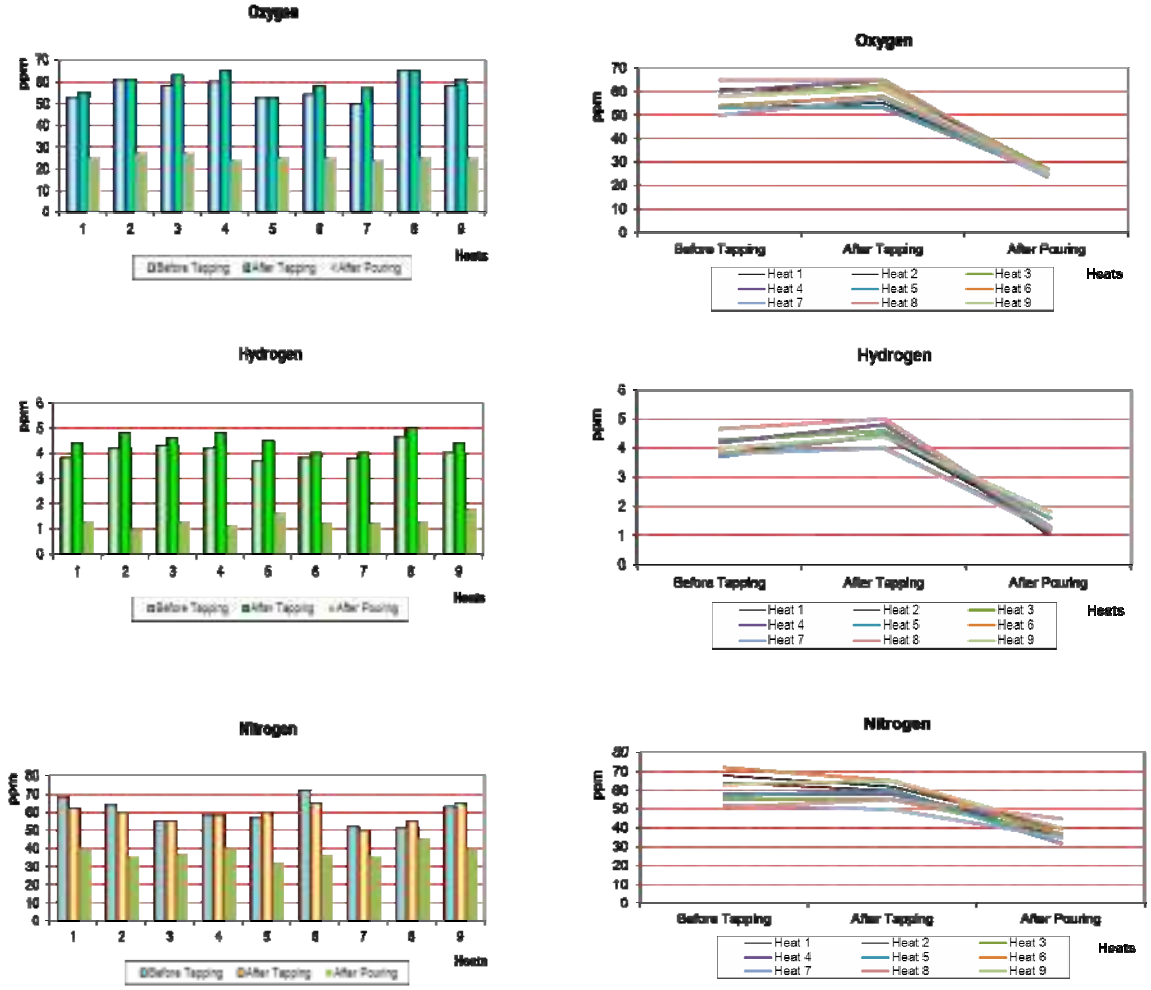

Fig. 8. *Graphical representation of the gas evolution on heats*

The importance of obtaining wide stream when pouring can be easily observed. The steel stream is divided into small drops after argon gas injection in the stopper rod. the pouring stream looking like a summer rain. Increasing the contact surface between the droplets of steel and the vacuum is the main factor that can boost the degassing process.

Fig. 9.

The metal bath is not agitated by the strong convection currents like we would have seen if we had had narrow stream and the risk of inclusions in the body of the ingot is small. Non-metallic inclusions with lower density always remain on top of the ingot, remaining in the hot top.

6. Conclusions

Vacuum pouring with wide stream helps increase purity by decreasing gas content and keeping the inclusions to the surface. You can see a very good degassing yield from the analyzed heats as follows: for [H] - η = 79% for [A] - η = 63% for [N] - η = 46%;

The condition of the stream during the pouring process directly affects the degassing and purity of the cast ingot because a narrow jet has a smaller contact surface with the vacuum atmosphere (low efficiency degassing) and it creates a high convection

current which causes inclusions to appear in the ingots body.

After the assessment of the wide stream it has been shown that the stream created by argon injection through the stopper rod creates optimal conditions for advanced degassing. obtaining increased purity and uniform distribution of spherical particles that stimulates floating inclusions and prevent creating convection currents.

Acknowledgment

The work has been funded by the Sectoral Operational Programme Human Resources Development 2007-2013 of the Romanian Ministry of Labour, Family and Social Protection through the Financial Agreement POSDRU/88/1.5/S/60203.

References

[1]. Takashi Ubukata, Tadashi Suzuki, Sou Ueda, Takashi Shibata, (Japan Steel Works. Ltd.. Muroran Plant. Muroran. Hokkaido (Japan)) – *Dehydrogenation in large ingot casting process.* Nippon Seikosho Giho, (no.60), Oct. (2009), Volume 41, Issue 21, p. 8-14.

[2]. Mincu Valentin, Negru Malin and Constantin Nicolae – *Increase the ingots quality cast in vacuum,* Solid State Phenomena, Volume 188 (2012), p. 339-345.

[3]. Mincu Valentin and Constantin Nicolae – *Influence of Vacuum on the Quality Steels,* Conference Proceedings of the Academy of Romanian Scientists, 5-7th May, (2011), Volume 3, p. 211-220.

THE ANNALS OF "DUNAREA DE JOS" UNIVERSITY OF GALATI.
FASCICLE IX. METALLURGY AND MATERIALS SCIENCE
N^0. 2 – 2012, ISSN 1453 – 083X

PHYSICO-CHEMICAL WATER TREATED WITH SONIC GENERATOR AND $Al_2(SO_4)_3$ COAGULANT

Anca ȘERBAN, Marian BORDEI, Aurel CIUREA, Mariana Carmen BURTEA
Dunarea de Jos University of Galati
email: mbordei@ugal.ro

ABSTRACT

This paper is a study on the problem of using ultrasound in the treatment of raw water. It highlights the effect of ultrasounds produced by the experimental sonic ultrasound generator through the physico-chemical analysis of raw water, as well as of the treated water, namely turbidity, pH and dissolved oxygen. Also, to reduce the dose of coagulant used in water treatment plants, we studied the influence of ultrasound on water treated with coagulant based on the physico-chemical parameters analysis.

The aim of this paper was to determine the effects of ultrasound and of the coagulant on the physico-chemical parameters of water by treating raw water with ultrasonic gas-dynamic generators, or by adding coagulant, with reference to water quality before treatment. We followed the environmental impact by allowing the use of the sonic generator technology treatment leading to significant reduction in the amount of chemicals commonly used in water treatment stations in view of clotting suspension.

KEYWORDS: water treatment, physico-chemical, sonic generator

1. Introduction

This paper treats the problem of developing new methods of water treatment using ultrasound gas-dynamic generators. Ultrasound production facilities [1] can be used in processes taking into account construction, media used, working frequency, acoustic intensity, irradiation time. In analyzing any process related to the application of ultrasound technology, the first problem that arises is to produce ultrasonic vibrations of a determined frequency and intensity [2]. Generators produce ultrasounds in certain areas of propagation for certain frequency ranges [3] and therefore for each technological process a type of ultrasonic generator is used. Based on the analysis of the types of generators, the best gas-dynamic generator type was Hartmannrod with rod [4], which is stable in operation and can ensure high enough work gas flow, as required in water treatment.

2. Experimental stand and working methodology

The gas-dynamic axial sonic generator used (Fig. 1) was chosen because of its construction characteristics that determine operating parameters corresponding to laboratory conditions [5].

Thus, to study water treatment using a sonic generator (ultrasonic and concomitant bubbling) a hydro-pneumatic scheme [5] of the experimental facility it was achieved (Fig. 2).

The plant can use compressed air or oxygen as working agent to generate ultrasounds depending on technological needs.

In our case, the system uses air as working medium for sonic generator power, which leads simultaneously to producing ultrasonic waves and to aeration-bubbling phenomenon, thus ensuring the sonic treatment of the technologic liquid.

Air, as working medium for generating ultrasound, was taken from an air compressor with a capacity up to 6 bars.

They collected water samples from the Danube according to the appropriate standard and samples of 1 liter of fresh water were used as samples and treated with a sonic generator under certain conditions.

The experimental stand operated at a supply pressure of 0.4MPa generator, or frequency ν=27.4kHz and acoustic intensity level L = 131.0dB.

Also, during water treatment with sonic generator varied in the range of 5-40 seconds.

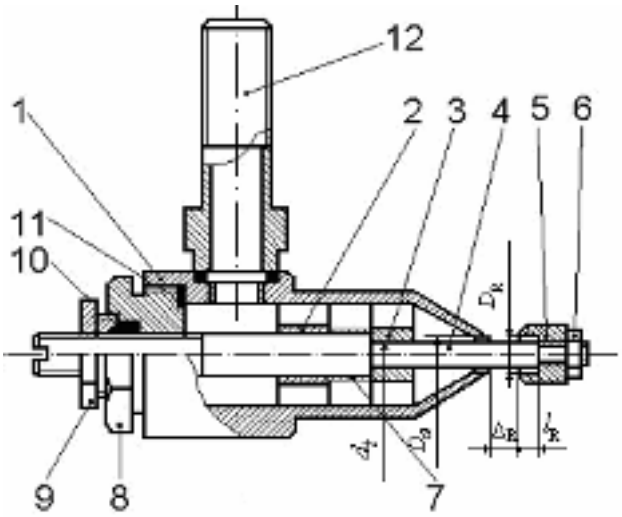

Fig. 1. *Axial gas-dynamic sonic generator: 1 - nozzle, 2, 3 - cross support; 4 - rod, 5 - resonator, 6 - nut, 7 - bush, 8 – cover, 9 - nut, 10 - gasket, 11, 13 - ring; 12 - socket; D_a- nozzle diameter, d_t - rod diameter, D_R, L_R - diameter and depth resonator, D_r - distance granting resonator*

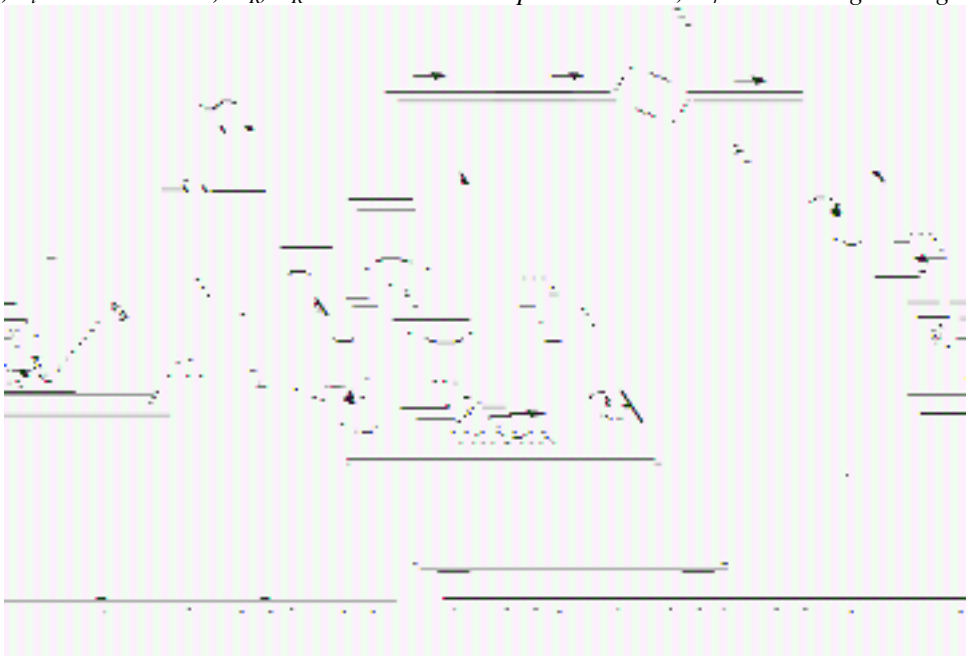

Fig. 2. *Experimental stand for water treatment technology: 1-compressor, 2-tank battery, 3-pneumatic reducer, 4-electric motor, 5-air filter, 6-gauge, 7-gas-dynamic ultrasonic generator, 8-gauge with electro-contact, 9 -cylindrical vessel, 10 - desk, V_1-drain valve, V_2 -valve, V_3-regulating valve*

For comparison and to highlight the effect obtained by using an experimental sonic generator, an aluminum sulfate $Al_2(SO_4)_3$ coagulant was introduced in the raw water sample, before treating the samples with ultrasound.

Water quality has been shown in both studied cases by analyzing some physical and chemical parameters namely: turbidity, pH, dissolved oxygen (DO), according to current standards.

3. Results and discussion

3.1. Dynamics of the water treated with experimental sonic generator

Five one liter of raw water samples were considered each, treated at different periods of time, namely 5, 10, 20, 30, 40 seconds under optimum working regime.

A one-liter water sample was also considered to determine the raw water characteristics and to compare them with the test data submitted to the sonic treatment. The generator operating mode was determined according to the best results obtained from the physico-chemical indicators of the sonic raw water treated at the working pressure of 0.4MPa, to which following acoustic parameters correspond: acoustic intensity L = 131.0dB and frequency ν=27.2kHz [6].

The sonic treatment of raw water leads to a sharp decrease of turbidity (Fig. 3).

The sonic treatment effect occurs from time t=5s treatment [7].

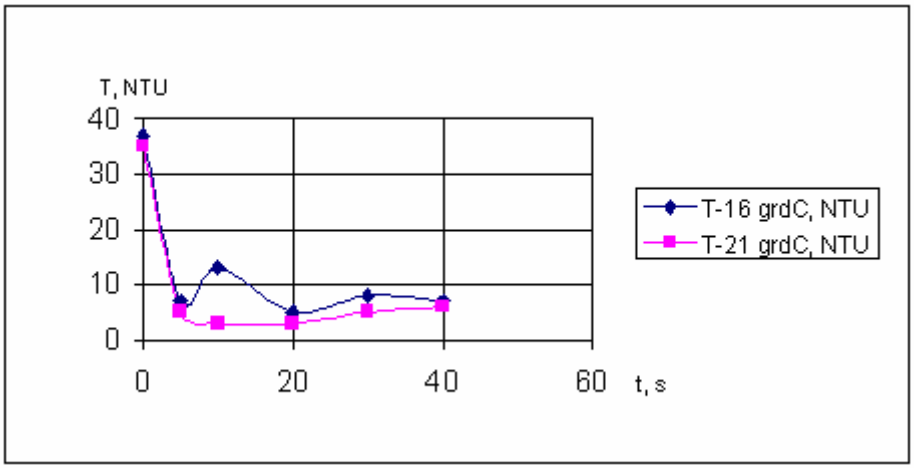

Fig. 3. *Turbidity variation depending on the time of sonic treatment of water*

After an initial turbidity of 35NTU (nephelometric turbidity units) at a temperature of 21^{0}C to 16^{0}C and 37NTU, the same time, with increasing sonic treatment turbidity varies quasi-periodically around an average of T=5NTU (nephelometric turbidity units) respectively T=7NTU. The analysis of the results shows that after 10 seconds of sonic treatment of raw water turbidity reduction occurs on an average of 5-7 times compared with the value determined in untreated raw water.

In the case of pH (Fig. 4), the influence of ultrasonic waves is negligible at both considered temperatures [7] and its evolution is relatively constant.

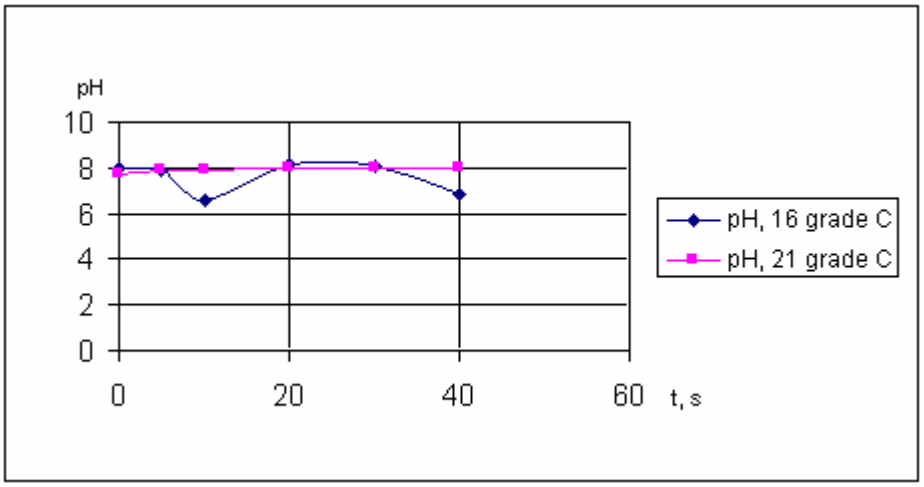

Fig. 4. *pH variation depending on the time of sonic treatment of water*

The initial base value of the control sample was 8.02 and it is within quality limits. From Figure 5 it is noticed that at a temperature of 21^{0}C, the quantity of dissolved oxygen in untreated raw water is 5.8mgO_2/L, so under the limit prescribed by law (7mgO_2/L). However, after the first 5 seconds of ultrasonic treatment, the oxygen level increases to a normal value for a given temperature and the recorded values with increasing treatment time vary between 8 and 9 mg O_2/L.

The necessary level of dissolved oxygen content in water occurs at a less time treatment that does not exceed 10 seconds. The sonic treatment time influence on the content of dissolved oxygen [7] indicates that during the sonic treatment two different processes occur simultaneously: the aeration and the degassing of water. Degassing occurs due to ultrasonic cavitation, and aeration occurs after the penetration of the working air resulting from the functioning of the gas-dynamic generator.

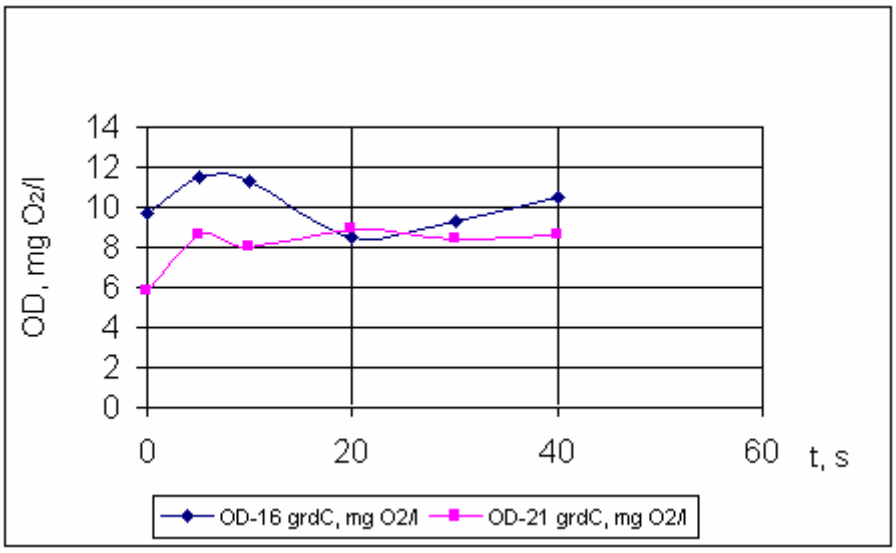

Fig. 5. *Variation of dissolved oxygen with the time of sonic treatment*

In this case, the two processes - degassing and aeration net each other and optimal results are obtained for the required oxygen content necessary in water at certain temperatures.

The results presented above allow us to choose the minimum length of sonic treatment time to which water can get optimal parameters, namely 5-10 seconds for a liter of water sample.

3.2. Dynamics of the water treated with coagulant and experimental sonic generator

The main purpose of using coagulants in water treatment technology [5] is increasing the sedimentation process from decanters. From economic and environmental points of view, solutions to reduce the dosage of coagulants or the use of environmentally friendly technologies are demanded.

We studied the possibility of reducing the dosage of coagulants to protect the environment and public health using an ultrasonic generator, and a coagulant commonly present in sewage systems, aluminum sulphate $Al_2(SO_4)_3$. In the study, it was considered the maximum dose of coagulant of 40 mg/L $Al_2(SO_4)_3$, while the dose of coagulant used at present in the water treatment plants is 40-60 mg/L $Al_2(SO_4)_3$.

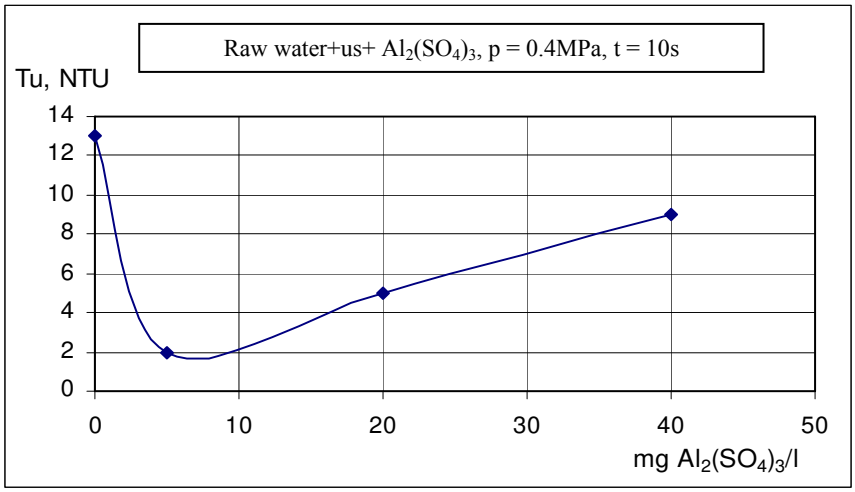

Fig. 6. *Water turbidity variation depending on the dose of coagulant $Al_2(SO_4)_3$*

To determine the minimum dose of coagulant, to which the effect is observed, the influence of coagulant concentration was studied and the ultrasonic produced by the ultrasonic generator on turbidity, at the working pressure of 0.4MPa and treatment duration of 10 seconds (Fig. 6). It is observed from sonic generator water treatment, the reduction water turbidity of 7.5 times the initial value of raw water.

Also, by getting the lowest turbidity value at the lowest dose used, we conclude that the coagulant dose decreased by 8 times, respectively, from 40mg/L to 5 mg/L $Al_2(SO_4)_3$.

Given this result, we studied the influence of the treatment time (Fig. 7) on turbidity at a dose of 5mg/L $Al_2(SO_4)_3$, the same supply pressure of 0.4MPa generator.

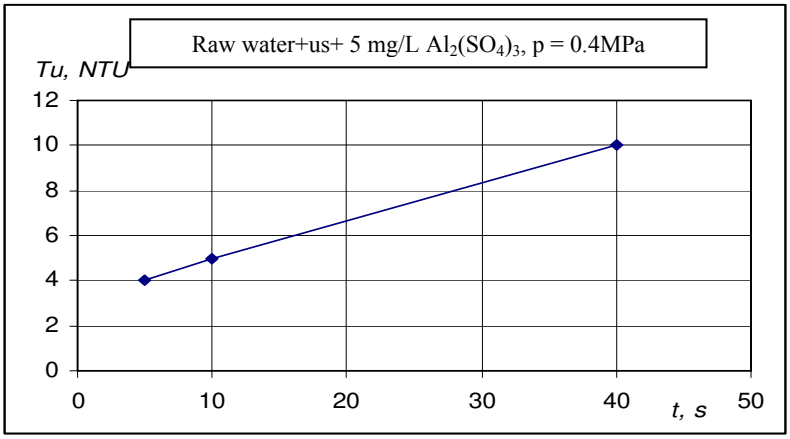

Fig. 7. *Water turbidity variation depending on the time of treatment at a dose of 5 mg/L $Al_2(SO_4)_3$*

The graphic from Figure 7 shows that turbidity increases with increasing treatment time, the treatment time required to achieve minimum turbidity being 5 seconds.

Given the amount of raw water turbidity (Fig. 6), adding minimal coagulant dosage with ultrasounds produces a significant reduction in turbidity. It is noted that at a treatment duration of 5 seconds and 10 seconds, respectively, to register turbidity values as indicated in the standards are recorders (Tu≤5NTU).

Next, we studied the influence of the coagulant dose and the ultrasound on the pH, at the same parameters as for turbidity (Fig. 6).

The dose of coagulant $Al_2(SO_4)_3$ in water does not affect the pH values, as shown in Figure 8.

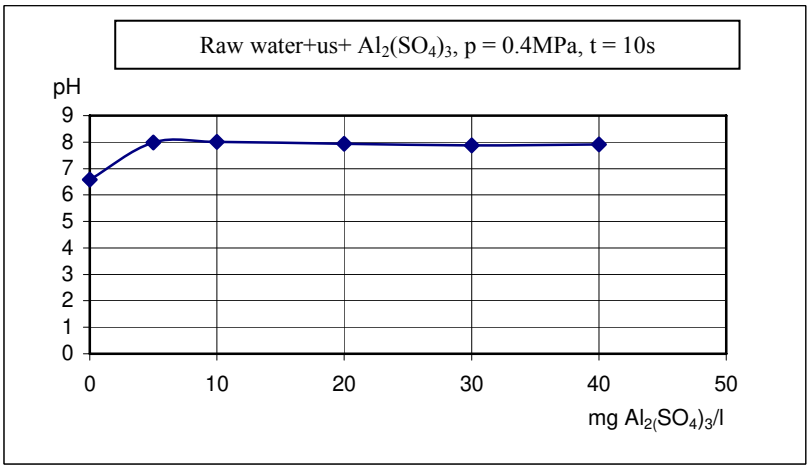

Fig. 8. *pH variation depending on the dose of $Al_2(SO_4)_3$ coagulant*

If in both cases, the pH is not influenced by ultrasound, or by the presence of coagulant and ultrasound, for pH variation depending on the duration of water treatment with 5 mg/L $Al_2(SO_4)_3$, at the working pressure p = 0.4MPa, an increase with 2 units of pH occurs (Fig. 9). It can be concluded that to obtain a neutral pH, under the conditions considered above, a duration of treatment of 20-40seconds it is required.

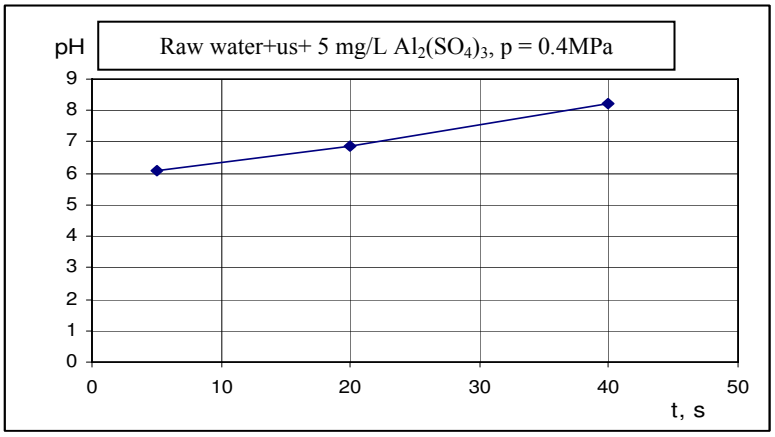

Fig. 9. *pH variation depending on the water during treatment with 5 mg/L $Al_2(SO_4)_3$*

Regarding the evolution of dissolved oxygen content in water in the presence of coagulant and ultrasound, at the same operating parameters previously established for other indicators, a clear change could noticed.

Thus, by increasing the dose of coagulant, the oxygen content (Fig. 10) decreases from 11.2mgO_2/L to 10.5mgO_2/L, so the coagulant dosage with ultrasounds affect the content of dissolved oxygen, in water but to a lesser extent.

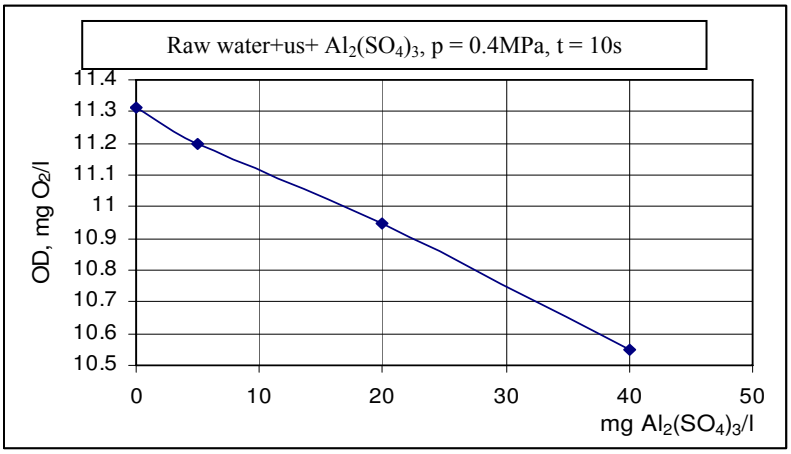

Fig. 10. *Dissolved oxygen variation depending on the dose of $Al_2(SO_4)_3$coagulant*

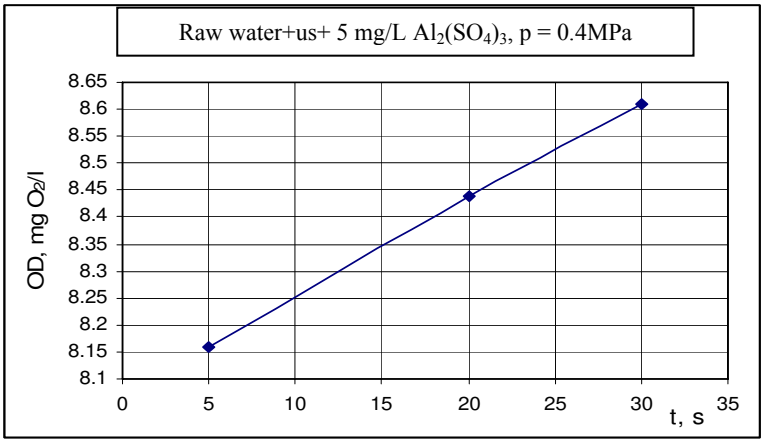

Fig. 11. *Variation of dissolved oxygen according to the time of water treatment with the dose of 5mg/L $Al_2(SO_4)_3$*

The same thing happens in the case of dissolved oxygen variation (Fig.11) according to the time of sonic treatment of water at the dose of 5mg/L $Al_2(SO_4)_3$, the dissolved oxygen concentration increasing from 8.16mg O_2/L to 8.61mg O_2/L.

The parameter variation study highlights the synergistic influence of ultrasound and coagulant, and thus, the possibility of using an ultrasonic generator for reducing chemicals in water treatment plants.

4. Conclusions

By increasing the dose (5-40mg/L) of aluminum sulphate ($Al_2(SO_4)_3$ to sonic treatment (generator working pressure 0.4 MPa, the acoustic intensity L = 131.0dB, frequency ν = 27.2 kHz) with treatment time t = 10s it showed that:

- turbidity increases, so, to obtain minimum turbidity (Tu = 2 NTU), a minimum dose of 5mg/L of $Al_2(SO_4)_3$ is recommended;
- the pH of the water does not change, so it is not influenced by the $Al_2(SO_4)_3$ dose level;
- the content of oxygen in the water decreases from 11.2 to 10.5mg O_2/L.

The influence of the duration (5-40 seconds) of the ultrasound treatment on the physico-chemical parameters of the water, with a coagulant dose of 5mg/L at working pressure of 0.4MPa generator (sound intensity level L = 131,0dB, frequency ν=27.2kHz), was studied and have revealed the following:

- the turbidity increases, which shows that to achieve the best results the treatment time should be considered during treatment to which it is minimal (t = 5 and u = 4 NTU);
- the pH increases by 2 units compared to that determined for untreated raw water (Fig. 8);
- the oxygen content in the water increases from 8.16mg O_2/L to 8.61mg O_2/L with increasing duration of water treatment.

According to limit set of standards (Tu≤5NTU), turbidity reached these values in both cases studied to a minimum coagulant dose of 5mg/L $Al_2(SO_4)_3$ and a treatment duration of 5 to 10 seconds.

The values obtained for water pH in this study are within the limits set by the standards (6.5 ÷ 9.5). In the case of dissolved oxygen, both for its evolution depending on the dose of coagulant and for coagulant according to the duration of treatment and ultrasonic, a decrease is observed in comparison with the value of untreated raw water. This is not desirable because the dissolved oxygen content in the water depends on water temperature and its decrease leads to the loss of water freshness. By contrast, a single action of ultrasound on water increases the dissolved oxygen content, regardless of the temperature of the water sample.

It should be noted that the dose of $Al_2(SO_4)_3$ coagulant recommended in the paper (5mg/L) is 8 times lower than the lowest dose of 40 mg/L $Al_2(SO_4)_3$ used in water treatment plants, which demonstrates the applicability of treatment technology with ultrasonic generator.

References

[1]. Balan G., Ciurea A., Balan V., Bordei M. - *The sonic technologies*, Quatrième Edition Du Colloque Francophone en Energie, Environnement, Economie et Thermodynamique COFRET'08, Nantes, France, pg. 20-29, (2008).

[2]. Bălan, G. - *The sonic technologies and its perspectives*, Proceedings of the Annual Symposium of the Institute Of Solid Mechanics and Session of the Commission of Acoustics of Romanian Academy SISOM - 2009, Bucharest, p.65-76, (2009).

[3]. Amza, Gh. - *Ultrasunetele. Aplicatii active,* Ed. AGIR, Bucuresti, (2006).

[4]. Balan, G. - *Aerogazodinamica,* Ed. Tehnica-INFO, Chişinău, (2003).

[5]. Stefan A., Balan G. - *Efectul tratarii sonice asupra parametrilor fizico-chimici ai apei de Dunare*, Revista Meridian Ingineresc, nr. 3/2009, pag. 11-18, Editura UTM, Chisinau, Republica Moldova, ISSN 1683-853X.

[6]. Stefan A. - *The research of the physico-chemical parameters of water treated with sonic technology*, Journal of Science and Arts, Universitatea Valahia din Targoviste, nr.1(12), pag. 79-82, (2010), eISSN 2068-3049.

[7]. Stefan A., Balan G. - *The Chemistry Of The Raw Water Treated By Air-Jet Ultrasound Generator*, Revue Roumaine des Sciences Techniques - Série de Mécanique Appliquée, Published/Hosted by Romanian Academy, Tome 56, N°1, Bucharest, ISSN: 0035-4074, (2011), p. 85-92.

[8]. Iordache I, Iordache M. - *Sonochimia in epurarea energo-intensiva a apelor*, Editura Casa cartii de stiinta, Cluj, (2009).

THE ANNALS OF "DUNAREA DE JOS" UNIVERSITY OF GALATI.
FASCICLE IX. METALLURGY AND MATERIALS SCIENCE
N^0. 2 – 2012, ISSN 1453 – 083X

INFLUENCE OF MICRO GLASS BEADS ADDED IN A PBT MATRIX ON THE MECHANICAL PROPERTIES OF COMPOSITES

Mihail BOTAN, Constantin GEORGESCU, Lorena DELEANU
"Dunarea de Jos" University of Galati
emails: mihai.botan@ugal.ro, constantin.georgescu@ugal.ro

ABSTRACT

This paper presents the influence of adding materials (micros glass spheres) in a matrix of PBT on several mechanical properties: elasticity modulus, stress at break , elongation at break, energy at break.

The mechanical properties of these composites depend on the glass beads concentration. The additivation of polybuthylen therephtalate with glass beads increases the values of the elasticity modulus, but reduces quite drastically the elongation at break. Using the SEM investigation, the authors pointed out the particular aspects of fracture surfaces: a ductile process at sample margins and a brittle one in the middle of the composite.

KEYWORDS: PBT, glass beads, composite, elasticity modulus, stress at break, elongation at break, energy at break

1. Introduction

It is a basic problem with the tests that the result will vary with the test piece geometry and the test conditions and it may not be easy to extrapolate to different conditions [7-9].

Even if there are many standards related to short-term tensile testing, they endeavor to quantify a number of specific characteristics which relate to the strength and deformation of a material. Knowledge of these characteristics can supply the designers with the potential performances of a material and a reliable basis of comparing materials [8, 19].

The term 'short term mechanical tests' is used as a convenience to describe mechanical properties where the effects of long times and cycling are ignored. This group of tests includes hardness, tensile, compression, shear, flexing, impact and tear. The material properties require to be rated for generating design data, for quality controlling, for predicting their durability and, unfortunately but necessarily for investigating failures. The polymers have a complex behavior thus, more than any material, they have to be evaluated in a useful way by particular or adequately adapted methods [8].

Polymeric materials are non-linear and their stress-strain characteristic is not linear and hence their modulus is not a constant [1, 2, 8, 9].

The use of PBT as an engineering material is a consequence of a balance of good properties rather than of a few outstanding ones. It does not possess the toughness of polycarbonate (PC), the abrasion resistance of an aliphatic polyamide, the heat resistance of a polysulphone, polypheny1ene sulphide (PPS) or polyketone, the low water absorption of a modified poly(p-phenylene oxide) (PPO).

However, PBT, when it is suitably modified by, for example, glass fiber or fire retardants, can contribute to produce very useful compounds.

The particular characteristics of PBT, as pointed out by the suppliers [9, 26, 27], include:

- high softening temperatures (especially for composites with glass or carbon fibers, challenging the use of PC and modified PPOs);
- high rigidity, exceeded only by PPS among the engineering thermoplastics;
- good electrical insulation properties for an engineering thermoplastic as compared to PC, modified PPOs, PPS and the polyether imides;
- low friction and good abrasion resistance;
- good impact strength at low temperatures and excellent creep rupture strength;
- low water absorption and good chemical resistance, including resistance to stress cracking;

- good dimensional stability, a consequence of the low water absorption but also because of a low coefficient of thermal expansion;
- good moldability (easy flow and rapid setting).

A large number of PBT grades is available, including unreinforced, glass- and carbon-fiber reinforced, mineral filler reinforced, impact modified, elastomer modified, flame retardant and various combinations of the foregoing [9, 15, 16, 24, 27, 28].

2. Glass beads as adding material in a polymeric matrix

C type glass is adequate for using in chemically aggressive environments, especially acids. This outstanding chemical resistance is a consequence of its composition, typically as following: at least 60% SiO_2, Li and Na oxides, Yn and Ca oxides and also rare earth oxides with small amounts of Al_2O_3, B_2O_3, Fe_2O_3, TiO_2, MnO and SnO_2 [17, 18].

Adding this type of reinforcing material influences the technological properties [5, 6, 10, 25] the mechanical ones [3, 4, 11-13, 22] and the tribological ones [14, 20]. In 2010, Akiyama et al. [2] reported a modifying tendency of the mechanical properties of the composites with ceramic particles (average diameter of 150 μm) a little greater than the glass beads introduced in PBT for this study and more ragged as compared to almost spherical shape of the glass beads (Fig. 5). Adding 60% of ceramic particles in PBT makes the elastic modulus to increase to 7500 MPa, 2.5 times greater than pure PBT, but the tensile at break decreases with 10...12% and Vickers hardness has a double value.

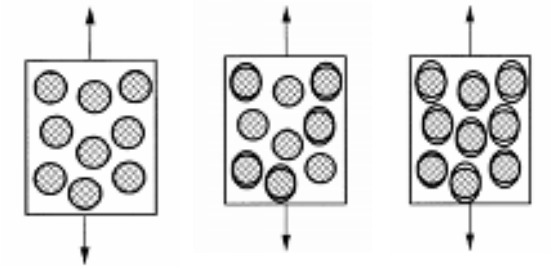

Fig. 1. *Damaging models of the interface in composites with spherical particles [21]*

Medadd and Fisa [21] have proposed a damaging model of the interface when samples were loaded with tensile forces (Fig. 1) that proved to be suitable to explain the PBT + glass beads composite behavior in a qualitative way. Break at traction of a composite with spherical particles depends very much on the chemical and mechanical nature of the interfaces between the polymer and the hard particles:

a) the resistance interface is not damaged under loading and the break is initially developed in the composite matrix;

b) an interface partially damaged, usually dependent on the elasticity modulus, the volume fraction of the adding material without damaged interfaces and the complementary volume fraction of the adding material that is characterized by a damaged interface (the ratio between these two interface categories being very hard to be estimated);

c) a wick defective interface that is easy to be destroyed when applying the load.

The difficulty is that the sample made of such a composite is loaded, all the above-described processes could occur, with different contribution to the final fracture.

Several research works reported that even if the glass beads bearing different treatment, the mechanical properties do not have significant modifications (Fig. 1.7) [21].

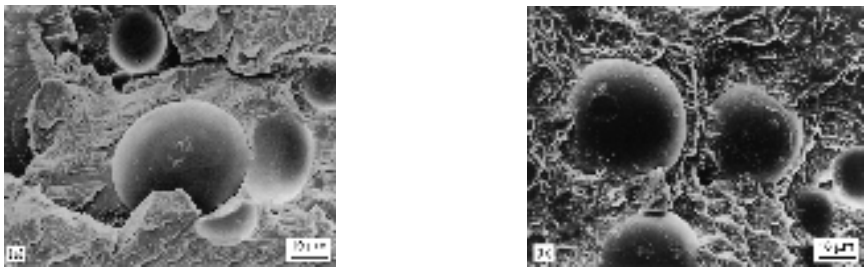

a) untreated *b) treated by silan (SiH_4)*

Fig. 2. *Aspects of tensile fracture surface for a PS+10% GB composite [M12]*

Dekkers and Heikens [12, 13] noticed that, for polymeric composites, the band forming mechanism at traction is fundamentally different, depending on the treatment applied to glass beads. After analyzing the stresses, they concluded that the generation of the bands had occurred in the zones characterized by maximum values for the main shear stress and by maximum values of the strain energy (Fig. 3).

a). a good adherence between matrix and glass beads, using γ-aminopropil silan

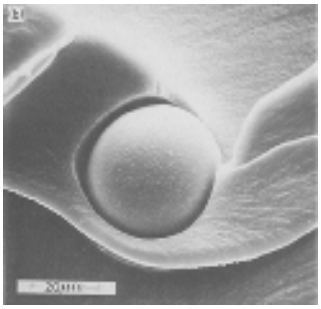

b). without adherence between glass bead and the polymer matrix, as obtained with silicon oil

Fig. 3. *Tensile fracture zones of the PC + GB composite [13]*

3. Testing methodology materials

The samples were obtained by extruding the mixtures of granulated PBT and glass beads (Fig. 5), in three mass concentrations (Table 1), at ICEFS Savinesti, Romania. The polymer had been dried up at a temperature of 100ºC within two hours. There were obtained bone samples with the geometry and dimensions given in Figure 4 and a thermal treatment was applied to the bone samples, as recommended by the producer [27].

The initial distance between the gauge marks on the central part of the test specimen was of 115 mm, the rate of separation of the grips of the testing machine during test 5 mm/min (the speed of testing) and the it was calculated the tensile Stress (engineering), that is the tensile force per unit area of the original cross section within the gauge length, carried by the specimen at any given moment.

The here-presented results include data for at least 5 tensile tests and the average value for each mechanical characteristic was calculated and there also were presented the scattering intervals for each one. Stress was calculated with reference to the initial values of the cross section thus, there are given the engineering stress-strain curves for each material.

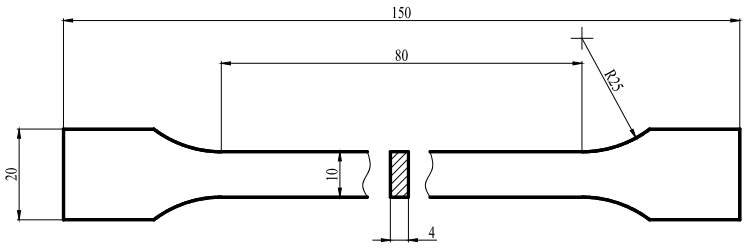

Fig. 4. *Bone sample Type 1A ISO 527-2*

Table 1. *Materials tested*

Material symbol	**Composition** (%wt)	
PBT	neat polymer, grade Crastin 6130 NC010 [10]	
GB10	10% GB	glass bead + 1.5...2% PA + 1% black carbon, for technological reason
GB20	20% GB	
GB30	30% GB	

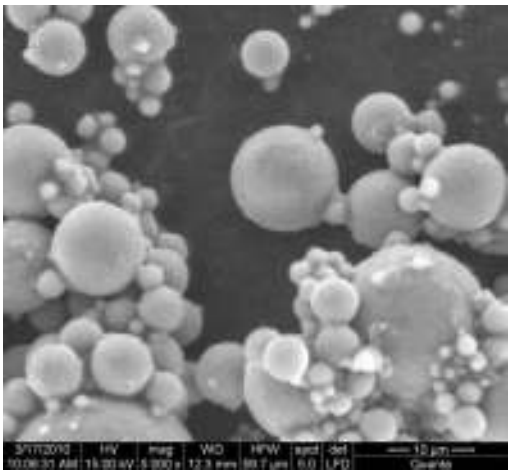

Fig. 5. *Glass beads before being mixed with PBT*

The traction tests were done with the help of the universal testing machine TESTOMETRIC M350-5AT, having a force cell of 5kN, as recommended by EN ISO 527-2 [25], in the Laboratory of Polymeric Materials Research (Faculty of Mechanical Engineering, "Dunarea de Jos" University of Galati).

The values for the mechanical properties were calculated as the average of five tests that the authors consider to have no anomalous features and in accordance with the literature [9, 24, 27, 28].

4. Experimental results

For PBT, the stress-strain curves (Fig. 7a) have the same aspect as presented in [4, 5, 16, 24]; it was noticed a typical creep zone for the thermoplastic polymers, as this polymer could be included in the class of tough materials with a yield stress lower than the failure stress [8]. The composites have the shape of the stress-strain curves typical for brittle materials (Fig. 7b, c and d).

The authors applied Einsteins's model for having a dependency of the mechanical properties on the mass concentration of glass beads,

$$E_c = E_m\,(1 + V_f), \tag{1}$$

where E_m is the elasticity modulus of the matrix and V_f is the volumic fraction of the adding material. For the composite with 10% GB, the value of the elasticity modulus as experimentally determined is greater with 10.8% as compared to the value given by Eq. (1) and for the composite with 20% GB, the experimentally obtained value is greater with 21.3% as compared to the theoretical value given by the same model of mixture. The elasticity modulus and the density for glass beads were taken from literature [13, 21]: E_f=*70000* MPa, ρ_f = 1.6g/cm^3.

Analyzing Fig. 3.4, the following remarks may be made:

- the elasticity modulus of these composites with PBT matrix increases almost linearly with the massic concentration of GB;
- stress at break for the composite with 10% GB is just 10% higher than the polymer but the composites with 10% GB and 20% GB have lower values, 85% and 63%, respectively from the values exhibits by the polymer (Fig. 6b);
- elongation at break decreases with ~72% for PBT + 10% GB and with ~92% for the composite PBT + 20% GB, as compared to the value obtained for PBT.

The composites have reduced elongation at break (Table 2 and Fig. 6c) and none of the samples not presented the typical bottle neck shape characterizing the polymer.

There is a clear tendency of decreasing the value for the strength limit only for the composite with 20% and 30% GB, respectively.

Table 2. *Average values of several mechanical properties for the tested materials*

Characteristic	**Material**			
	PBT	**GB10**	**GB20**	**GB30**
Elasticity modulus, E [N/mm^2]	1923.458	2358.356	2848.581	4087.458
Stress at break, σ_r [N/mm^2]	41.571	40.265	36.543	25.795
Elongation at break, ε_r [mm]	9.404	2.609	0.763	0.411
Energy at break, [N·m]	17.665	2.207	0.701	0.294

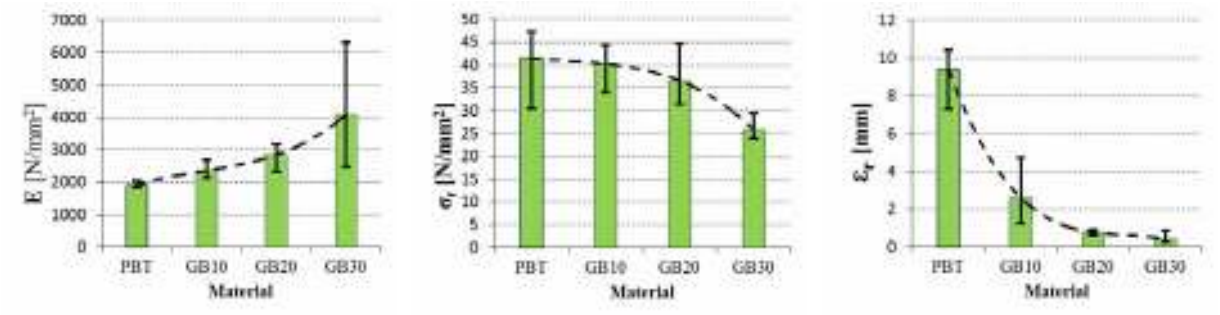

a) Elasticity modulus *b) stress at break* *c) elongation at break*

Fig. 6. *Average values and scattering ranges for the discussed mechanical characteristics of the tested materials*

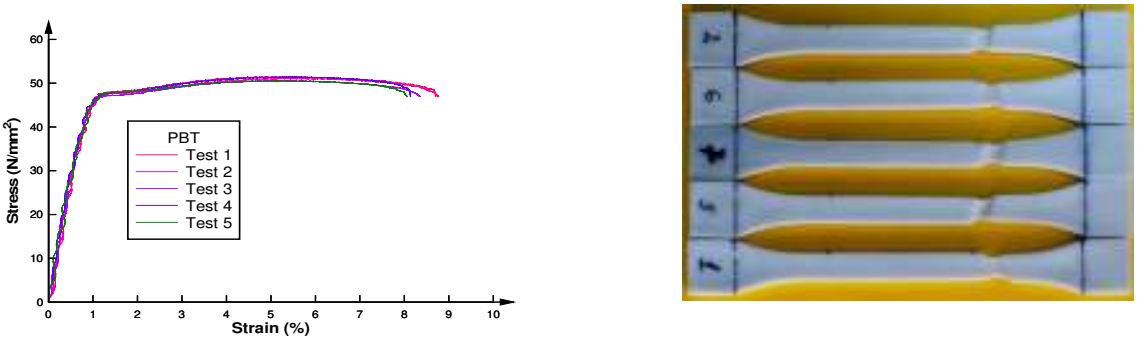

a) curves stress-strain *a) set of five samples, after being tested*

Fig. 7. *Stress-strain curve (left) for PBT and tested samples (right)*

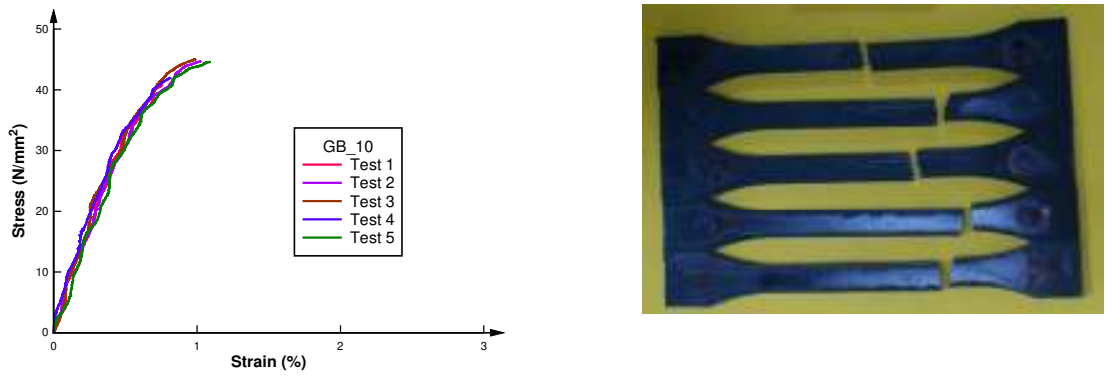

a) *PBT + 10% GB*

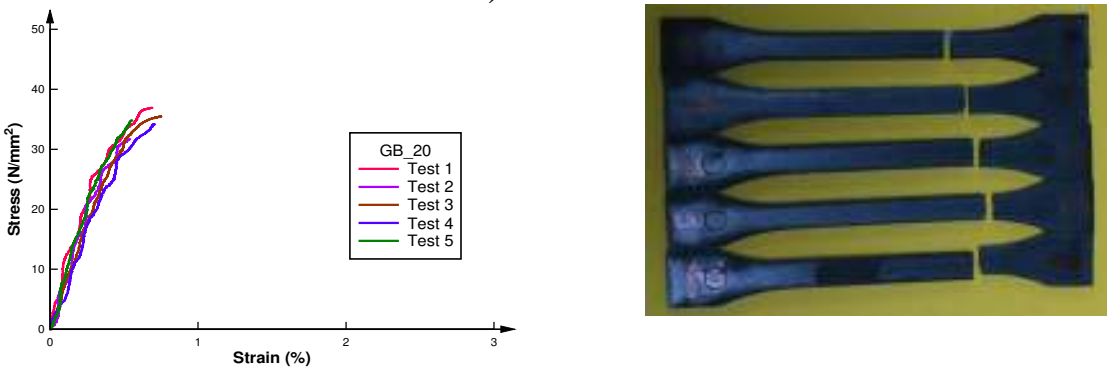

b) *PBT + 20% GB*

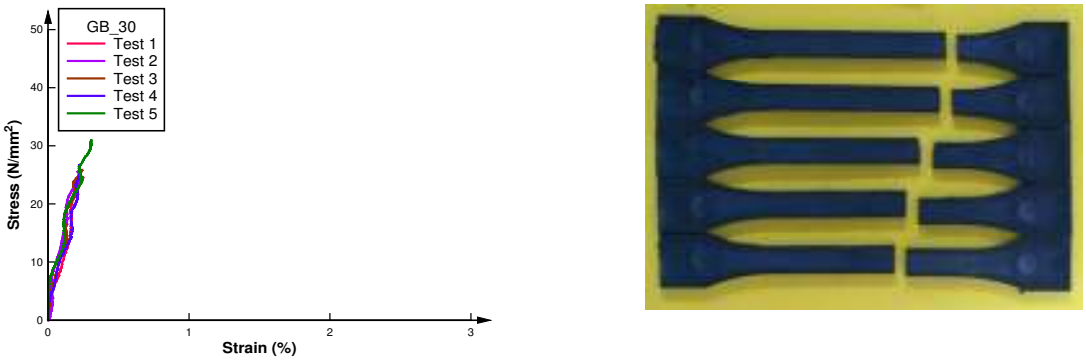

c) PBT + 30% GB

Fig. 8. *The stress-strain curves for the PBT+GB composite (left) and the sets of samples after break (right)*

Table 2. *Data upon the mathematical models attached to the experimental data*

Material symbol	Relation	Correlation coefficient	Standard error about the line
PBT	$y = -0.741 + 50.492\,x + 57.331\,x^2 - 124.096\,x^3 + 89.270\,x^4 - 34.749\,x^5 + 8.185\,x^6 - 1.201\,x^7 + 0.107\,x^8 - 0.005\,x^9 + 0.0001\,x^{10}$	0.999	0.376
	$y = \frac{a \cdot b + c \cdot x^d}{b + x^d}$ (Fig. 4) a =2.886, b =0.1674, c =50.597, d =2.255	0.996	0.667
GB10	$y=-0.356+82.171x - 36.466x^2$	0.999	0.304
GB20	$y=-0.871+ 93.729x - 57.723x^2$	0.999	0.396
GB30	$y = 1.513x+ 119.147 - 88.929x^2$	0.993	0.701

SEM images show that the damaging process of the interface has an intermittent nature (Fig. 8b reveals a bigger glass bead that was discontinuously detached from the matrix). For the tested composites, the 1% PA, even small, could influence the interface resistance, having a greater ductility and adherence to the glass beads as compared to PBT. Analyzing the SEM images from a small scale to larger ones, one may notice the existence of two types of surface aspect. At the sample margins the fracture surface has a ductile nature but towards the center of the sample the aspect becomes brittle (Figs. 7 and 8).

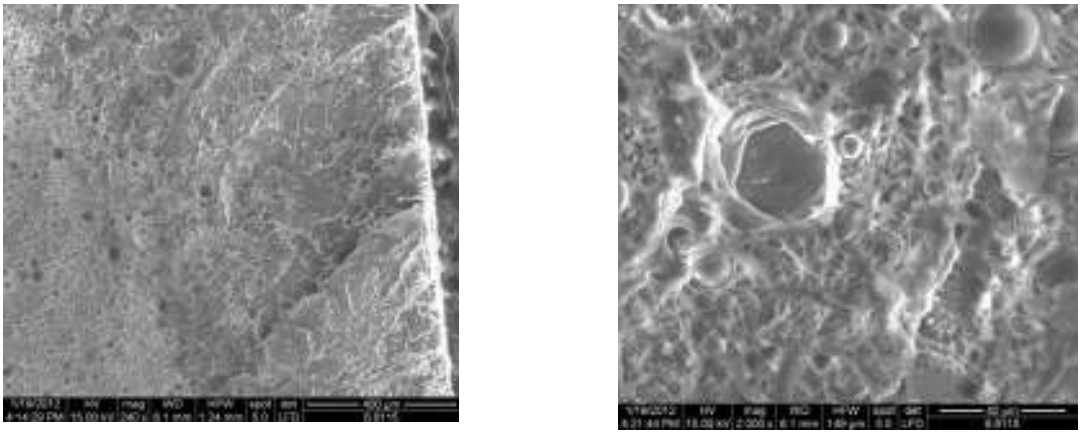

a). Ductile (at the sample margin - right) and brittle (left) aspects of the fracture section

b). Intermittent detaching of glass beads in the middle of the fracture section

Fig. 9. *Typical aspects of the fracture section for samples made of the PBT + 10% GB composite*

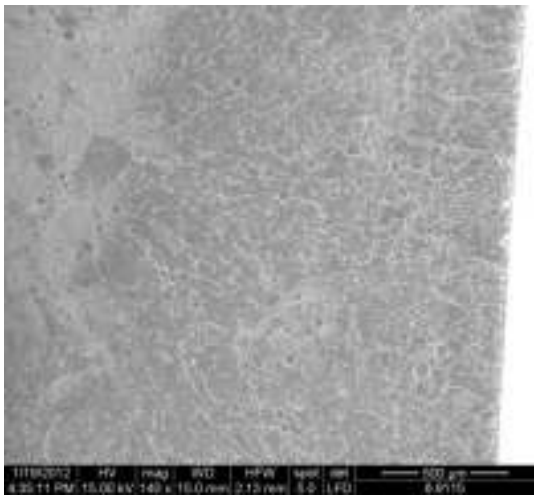

a). Zone of ductile fracture

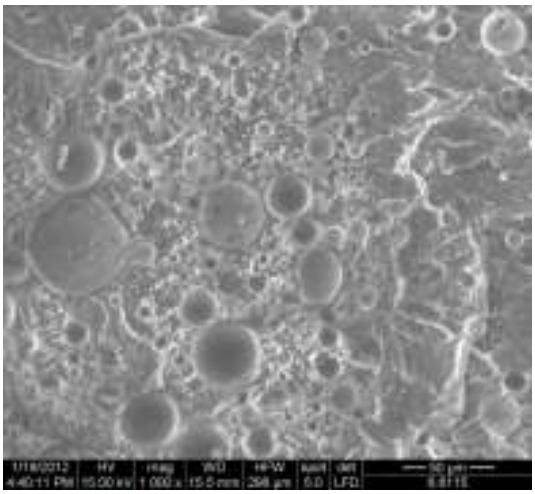

b). Middle zone of the fracture, with brittle aspect

Fig. 10. *Typical aspects for tensile break surface of the PBT + 20% GB composite*

4. Conclusions

The additiveation of polybuthylen therephtalate with glass beads increases the values of the elasticity modulus but reduces quite drastically the elongation at break. The results obtained point out the importance of testing polymers and their composites.

The authors elaborated mathematical models for each tested material. The mathematical models could be useful in analyses with finite elements in the first step evaluation of a design.

References

[1]. Agbossou A., Bergeret A., Benzarti K., Alberola N. - *Modelling of the viscoelastic behaviour of amorphous thermoplastic/glass beads composites based on the evaluation of the complex Poisson's ratio of the polymer matrix*, Journal of Materials Science, pp. 1963-1972, (1993).

[2]. Akiyama, M., Yamaguchi, T., Matsumoto, K., Hokkirigawa, K. - *Polymer Composites Filled with RB Ceramics Particles as Low Friction and High Wear Resistant Filler*, Tribology online, Vol. 5, No. 1, January, pp. 19-25, (2010).

[3]. Arencon D., Velasco J.I., Realinho V., Antunes M., Maspoch M.L. - *Essential work of fracture analysis of glass microsphere-filled polypropylene and polypropylene/poly (ethylene terephthalate-co-isophthalate) blend-matrix composites*, Polymer Testing, 26, pp. 761-769, (2007).

[4]. Bai S.-L. - *The role of the interfacial strength in glass bead filled HDPE*, Journal of Materials Science Letters, 19, pp. 1587-158, (2000).

[5]. Banik K., Mennig G. - *Influence of the Injection Molding Process on the Creep Behavior of Semicrystalline PBT During Aging Below its Glass Transition Temperature*, Mechanics of Time-Dependent Materials, 9, pp. 247-257, 2006.

[6]. Bessmertnyi V.S., Krokhin V.P., Lyashko A.A., Drizhd N.A., Shekhovtsova Zh. E. - *Production of Glass Microspheres Using the Plasma-Spraying Method*, Glass and Ceramics, vol.58, nos.7-8, (2001).

[7]. Brandrup, J., Immergut, E.H. & Grulke E.A. - *Polymer Handbook*, 4th Edition, Wiley-Interscience, England, (2003).

[8]. Brown, R., - *Handbook of Polymer Testing - Short-Term Mechanical Tests*, Rapra Technology, U.K., (2002).

[9]. Brydson, J.A. - *Plastics Materials*, 7th Edition, Butterworth-Heinemann, Oxford, (1999).

[10]. Bula K., Jesionowski T., Krysztafkiewicz A., Janik J. - *The effect of filler surface modification and processing conditions on distribution behaviour of silica nanofillers in polyesters*, Colloid Polym Sci, 285, pp.1267-1273, (2007).

[11]. Crowson R.J., Arridge R. G. C. - *The elastic properties in bulk and shear of a glass bead-reinforced epoxy resin composite*, Journal of Materials Science, 12, pp. 2154-2164, (1977).

[12]. Dekkers M. E. J., Heikens D. - *Crazing and shear deformation in glass bead-filled glassy polymers*, Journal of Materials Science, 20, pp. 3873-3880, (1985).

[13]. Dekkers M. E. J., Heikens D. - *Shear band formation in polycarbonate-glass bead composites*, Journal of Materials Science, 19, pp. 3271-3275, (1984).

[14]. Deleanu L., Andrei G., Maftei L., Georgescu C., Cantaragiu A. - *Wear maps for a class of composites with polyamide matrix and micro glass spheres*, Journal of the Balkan Tribological Association, vol. 17, no 3, pp. 371-379, (2011).

[15]. Deshmukh G.S., Peshwe D.R., Pathak S.U., Ekhe J.D. - *A study on effect of mineral additions on the mechanical, thermal, and structural properties of poly (butylene terephthalate) (PBT) composites*, J Polym Res, 18, pp. 1081-1090, (2011).

[16]. Deshmukh G.S., Peshwe D.R., Pathak S.U., Ekhe J.D. - *Evaluation of mechanical and thermal properties of Poly (butylene terephthalate) (PBT) composites reinforced with wollastonite,* Transactions of The Indian Institute of Metals, vol. 64, issues 1 & 2, February-April, pp. 127-132, (2011).

[17]. Kolesov Yu. I., Kudryavtsev M. Yu., Mikhailenko N. Yu. - *Science for Glass Production Types and Compositions of Glass for Production of Continuous Glass Fiber (Review)*, Glass and Ceramics, vol. 58, nos. 5-6, (2001).

[18]. Lahiri J., Paul A. - *Effect of interface on the mechanical behaviour of glass bead-filled PVC*, Journal of Materials Science, 20, pp. 2253-2259, (1985).

[19]. Le Blanc J. - *Filled Polymers. Science and Industrial Applications*, Taylot & Francis Group, (2010).

[20]. Maftei L. - *Contribuţii la studiul comportării tribologice a compozitelor cu poliamidă şi microsfere de sticlă*, PhD, "Dunarea de Jos" University, Galati, (2010).

[21]. Meddad A., Fisa B. - *Filler–matrix debonding in glass bead-filled polystyrene*, Journal of Materials Science, 32 pp. 1177-1185, (1997).

[22]. Sánchez-Soto M., Gordillo A., Maspoch M. LL., Velasco J.I., Santana O.O., Martínez A.B. - *Glass bead filled polystyrene composites: morphology and fracture*, Polymer Bulletin, 47, 587-594, (2002).

[23]. Tsui C.P., Chen D.Z., Tang C.Y., Uskokovic P.S., Fan J.P., Xie X.L. - *Prediction for debonding damage process and effective elastic properties of glass-bead-filled modified polyphenylene oxide*, Composites Science and Technology, 66, pp. 1521-1531, (2006).

[24]. Vincent L., Connolly S. N., Dolan F., Willcocks P.H., Pendlebury R. - *Determination and Comparison of the Plane Stress Essential Work of Fracture of Three Polyesters PET, PPT and PBT*, Journal of Thermal Analysis and Calorimetry, Vol. 86, 1, pp. 147-154, (2006).

[25]. Yang W., Liu Z.-Y., Shan G.-F., Li Z.-M., Xie B.-H., Yang M.-B. - *Study on the melt flow behavior of glass bead filled polypropylene*, Polymer Testing, 24, pp. 490-497, (2005).

[26]. *** DuPont Engineering Polymers. *Blow Moulding of Technical Components*, Available from: http://www2.dupont.com/Plastics/en_US/assets/downloads/processing/BM_PM_e.pdf Accessed: 2012-01-12.

[27]. *** DuPont. Crastin® PBT. thermoplastic polyester resin Crastin® 6130 NC010, Available from: http://plastics.dupont.com/plastics/dsheets/crastin/CRASTIN6130NC010.pdf Accessed: 2012-01-12.

[28]. *** Polybutylene Terephthalate (PBT), on-line: http://www.rtpcompany.com/info/guide/descriptions/1000.htm Accessed: 2012-01-23.

[29]. *** SR EN ISO 527-2:2000 Materiale plastice. Determinarea proprietăţilor de tracţiune. Partea 2: Condiţii de încercare a materialelor plastice pentru injecţie şi extrudare.

THE ANNALS OF "DUNAREA DE JOS" UNIVERSITY OF GALATI.
FASCICLE IX. METALLURGY AND MATERIALS SCIENCE
N^0. 2 – 2012, ISSN 1453 – 083X

THE CORROSION BEHAVIOUR OF ALUMINUM ALLOY 2024 - T3 IN ACIDIC ENVIRONMENTS

Vasile HOTEA, Jozsef JUHASZ, Elena POP, Gheorghe IEPURE, Aurica POP
North University of Baia Mare,
email: vasilehotea50@yahoo.com

ABSTRACT

This research aimed at analysing the acidic corrosion behavior of aluminum alloy 2024-T3 commonly used in the aerospace. We study the variation of corrosion rate with immersion time at different values of H_2SO_4 concentration and corrosion rate variation depending on the concentration of the solution setting the group of corrosion of the alloy. Aluminum forms initially a few-nm-thick layer of aluminum oxide, γ-Al, which after prolonged exposure in humidified air is covered by aluminum oxyhydroxide, γ-AlOOH, and subsequently by various hydrated aluminum oxides and aluminum hydroxides. The exposed metal surfaces involved aspects of the corrosion process in 0.1M H_2SO_4, 0.01M H_2SO_4 and 0.001M H_2SO_4 solutions, to determine the type of corrosion and propagation mechanism in acidic environments.

KEYWORD: corrosion, aluminum alloy, corrosion rate, penetration index, pitting, sulfuric acid

1. Introduction

Aluminum is prone to pitting corrosion in the average pH near neutral, which covers virtually all natural environments, such as surface water, sea water and moist air.

Aluminum and its alloys has a natural corrosion protection from its oxide layer, but if exposed to aggressive environments it may corrode. But, if properly developed, alloys of aluminum may be reliable and have a long service life. In oxygen containing environment (air, water), aluminum is rapidly covered with a dense oxide layer. The aluminum oxide is essentially passivated, prevents corrosion, and the thickness of the layer may vary as a function of alloying elements, temperature and environment. There are many factors that may affect the stability of the aluminum oxide and thereby cause corrosion:

- the oxide is not stable in alkaline (pH > 9) or acidic (pH < 4) environments [1];
- some elements may become incorporated in the oxide and destabilize it; aggressive ions (chlorides, fluorides) may attack the oxide locally [2].

These factors lead to corrosion by pitting, which can propagate to the extent that conditions are favorable. Electrochemical corrosion mechanisms of the pitting are very complex and not fully understood. By pitting corrosion has two distinct phases: initiation and propagation.

Sulfur dioxide (SO_2) has long been considered as the most important gaseous agent in atmospheric corrosion. In the presence of atmospheric acidifying pollutants, such as SO_2, the anode reaction is facilitated and, consequently, the total corrosion rate as well. Upon deposition of SO_2, it interacts with the aqueous environment.

Pitting corrosion is observed commonly in aluminum and aluminum alloys exposed to aqueous environments. This type of corrosive attack can lead to premature failure of high-strength Al alloys used in aerospace structures. Traditionally, the fundamental cause of pitting corrosion has been attributed to local breakdown of the passive film that forms on a metal surface, resulting in subsequent dissolution of the substrate material [3, 4].

In the presence of SO_2, oxidizing agents such as O_3 and H_2O_2 may also play a role in the atmospheric corrosion of aluminum. Besides a strong humidity dependence, it is generally agreed that deposition of SO_2 has mainly been investigated through field studies and chlorides and the pH in rain are major factors that determine the corrosion rate of aluminum [5].

This work aimed at analysing the acidic environment behavior, such as of 2024 aluminum alloy commonly used in the aerospace. We investigated the variation of corrosion rate with immersion time at different values of the H_2SO_4 concentration, and corrosion rate versus the concentration of the solution and setting the group of corrosion of the alloy. Also, we studied the metal surfaces aspects exposed of the corrosion process in 0.1M H_2SO_4, 0.01M H_2SO_4, and 0.001M H_2SO_4, solutions to determine the type of corrosion and propagation mechanism in acidic environments.

2. Experimental procedure

Corrosion measurement involves the application of various techniques to determine the corrosiveness of the environment and the rate of metal loss. Corrosion measurement is usually a quantitative method of evaluating the performance and effectiveness of corrosion control and prevention techniques [6]. The corrosion penetration rate due to direct attack can usually be estimated from relatively simple laboratory test in which small samples of the related materials are exposed to a well simulated actual environment with a frequent weight change and dimensional measurements carefully taken.

The corrosion penetration rate (V_{cor}) is usually expressed in mm/yr and may be calculated as:

$$V_{cor} = \frac{\Delta m}{S \cdot t} \quad (1)$$

where V_{cor} is the rate of corrosion penetration in mm/yr, Δm is the weight loss in milligrams; S is the exposed specific area of the specimen in square centimeter, ρ is the density of the specimen in grams per cubic centimeter and t is the exposed time in hours [7, 8].

The use of this corrosion rate expression in predicting corrosion penetration is usually successful if the environment has been properly simulated in the laboratory, and the corrosion forms homogeneous [9]. Penetration index (P) is calculated taking into account the corrosion rate and the specific weight of aluminum [10]:

$$P = (24 \cdot 365 \cdot V_{cor}) / (1000\rho) \quad (2)$$

where ρ is the specific weight, g/cm^3.

2.1. Materials and method

The weight loss technique which is a destructive method has been applied in the corrosion characterization of aluminium alloy 2024 in diluate solution of sulfuric acid 0.1M, 0.01 M and 0.001 M at a temperature of 25^0 C. Exposure time was set at one day (24 hours) to 30 days. Alloy composition is shown in Table 1.

Table 1. *Chemical composition of aluminum alloy 2024, (% wt)*

Al	Mg	Si	Mn	Cu	Zn	V	Ni	Cr	Ti	Zr
rest	1.4294	0.0878	0.7845	4.4791	0.0422	0.0123	0.0116	0.0025	0.0289	0.1339

The materials used for this work were purchased from Universal Alloy Corporation Europe SRL. The strips of the materials were cut into coupon sizes of dimension of about 50×30×1 mm and initial surface area of about 0.0015 cm^2 followed by polishing with emery paper, degreasing with lime, washed with distilled water and dried by dabbing with filter paper.

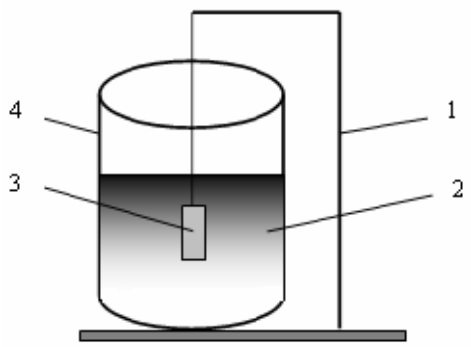

Fig. 1. *Device setup: 1 – support; 2 – dilute H_2SO_4; 3 – sample; 4 –Berzelius glass*

Weigh the sample to four decimal electronic analytical balance (m_1), is then suspended on the support (1) (Figure 1).

Samples of each type were removed at the same time intervals, which were examined visually and microscopically.

Removal of corrosion products was performed by wiping with cotton wool soaked in distilled water, followed by washing with water and drying with filter paper and reweighing.

In the corrosive vessel was poured sulfuric acid solution at concentrations of 0.1M, 0.01M and 0.001M to 2/3 of its height. The samples was immersed in the environment corrosive rectangular aluminum plate (50x30×1 mm) and held for 14 days. The sample removed, rinsed with tap water, was distilled water, dried by dabbing with filter paper and reweighed (m_2).

Sample weight loss $\Delta m = m_1 - m_2$, corrosion rate (V_{cor}) (equation 1), and penetration index P (equation 2) were calculated.

2. Results and Discussion

In table 2, the results of mass loss (Δ m) during corrosion tests, corrosion rate (V_{cor}) and penetration index (P) computed for the experimental samples are presented.

The curves corresponding to the variation in time of the corrosion rate (V_{cor}) for each of the solution concentration for the samples corrosion tested are presented in figure 2.

Table 2. *Values of mass losses, corrosion rate (V_{cor}) and penetration index (P)*

Conc. H_2SO_4	Temp. [^{0}C]	Time [h]	Δm [g]	V_{cor} [g/m^2·h]	P [mm/an]
0.1 M	25^{0}C	24	0.0015	0.000401	0.0012
		48	0.002	0.00107	0.0034
		96	0.0037	0.00396	0.0127
		168	0.0049	0.00918	0.0295
		336	0.0058	0.0217	0.0698
		672	0.0009	0.00675	0.0217
0.01 M	25^{0}C	24	0.0058	0.0015	0.0048
		48	0.0061	0.00326	0.0104
		96	0.0073	0.00782	0.0251
		168	0.0085	0.01593	0.0513
		336	0.0094	0.0352	0.1153
		672	0.00085	0.0037	0.0119
0.001 M	25^{0}C	24	0.0094	0.00251	0.0080
		48	0.01	0.00535	0.0172
		96	0.018	0.0192	0.0618
		168	0.024	0.045	0.1449
		336	0.032	0.067	0.2157
		672	0.00087	0.00652	0.0209

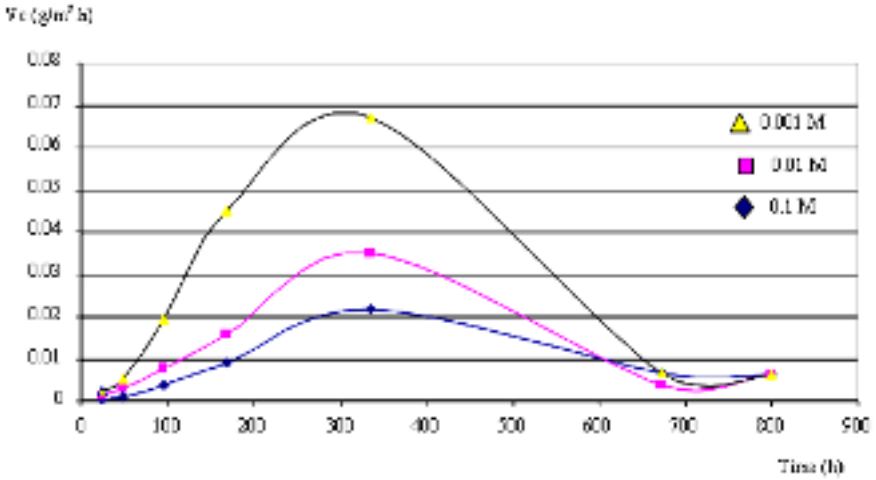

Fig. 2. *Variation of corrosion rate with immersion time at different values of concentration of H_2SO_4.*

According to Figure 2, the results indicate an increase in corrosion rate to 336hours, after which the corrosion rate decreases and stabilizes at 672hours, both for the solution of 0.1 M and 0.01M for 0.001M solution. The significant increase is recorded at 336h and 0.001M H_2SO_4 solution, the corrosion rate reaches the maximum value of 0.067g/m^2.h.

After the value of (V_{cor}) was established in the group of corrosion resistance alloy part studied and its degree of corrosion resistance (Table 3).

Table 3. *Corrosion resistance*

Group corrosion resistance	Corrosion rate	The degree of corrosion resistance
I. Perfectly stable	0.001	1
II. Very stable	0.001-0.005	2
III. Stable	0.01-0.05 0.05-0.1	3 4
IV. Relatively stable	0.1-0.5 0.5-1.0	5 6
V. Less stable	1.0-5.0 5.0-10.0	7 8
VI. Unstable	10.0	9

After the value of (V_{cor}) in Table 2 are observed for aluminum alloy 2024 is part of the corrosion resistance (Table 3).

At the same time, it may happen that the corrosion product, ($Al(OH)_3$), formed on the metal surface of aluminum hydroxide deposits that isolates Al from contact with corrosive agents, so that the curves showing variation of corrosion rate versus time have a tendency to flattening (Figure 2).

Following the change in the corrosion rate depending on the concentration of the solution, there is an increase of low corrosion rate in solutions of dilute H_2SO_4, appreciable growth rate of corrosion taking place in the 0.001M H_2SO_4 solution (Figure 3).

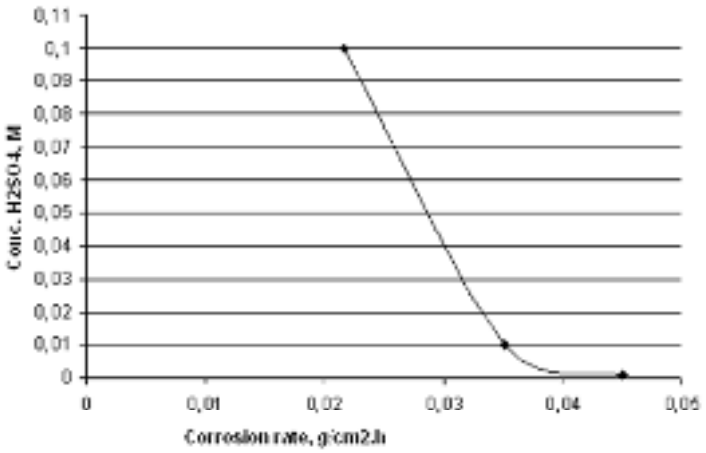

Fig. 3. *Dependence of corrosion rate vs. solution of H_2SO_4 concentration at: 0.1M, 0.01M and 0.001M*

Following penetration index variation versus on the concentration of sulfuric acid solution is found increasing penetration index in weak diluted solutions, increasing penetration index appreciable place with 0.001M H_2SO_4 solution (Figure 4), when its value is 0.2157 (mm/year).

From the study of metal surfaces aspects of the corrosion process in solutions of H_2SO_4, 0.1 M 0.01M and 0.001M, it is found that the corrosive process is not a generalized process, but one located. Increasing the concentration of the location of the process of corrosion, corrosion is the type pitting that is more pronounced as the solution is less diluted. Corroded samples were examined under an electron microscope type Leica metallographic M2500, determining their surface microstructure, after having been processed in this aim by grinding, polishing and chemical attack with 5% orthophosphoric acid for 5 minutes.

Examination and photography was performed at a magnification of 50 times.

Figures 6 - 8 show micrographs of samples exposed to the solution of H_2SO_4 (0.1 M, 0.01 M and 0.001M), after exposure of 672 hours, where there is a localized corrosion by pitting or points.

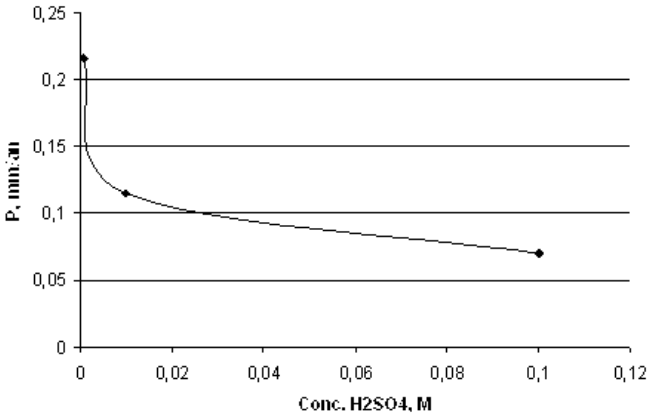

Fig. 4. *Penetration index variation of aluminum alloy 2024 in H_2SO_4 solution at different concentrations*

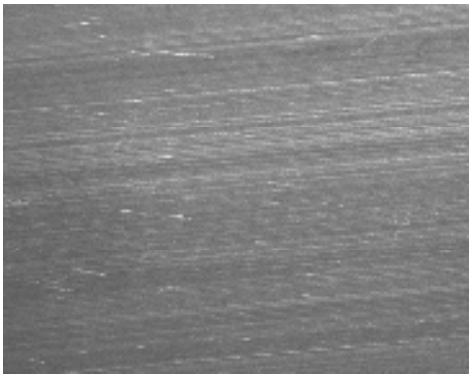

Fig. 5. *Initial sample (50×)*

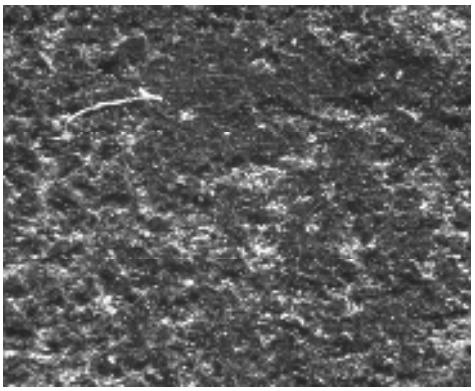

Fig. 6. *Corrosion in 0.1M H_2SO_4 solution (50×)*

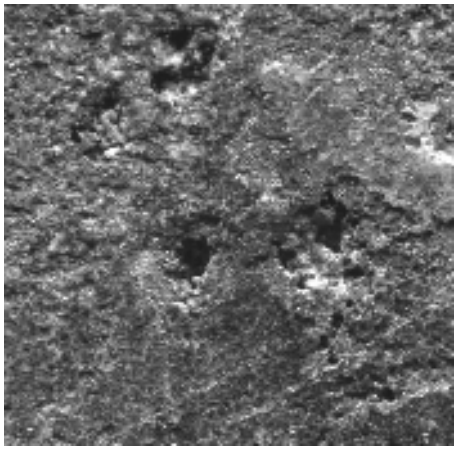

Fig. 7*. Corrosion in 0.01M H_2SO_4 solution (50×)*

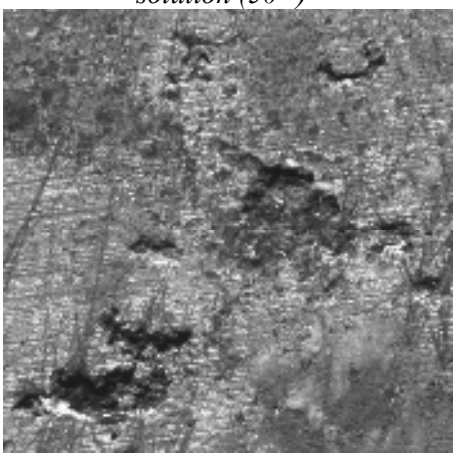

Fig. 8. *Corrosion in 0.01M H_2SO_4 solution (50×)*

According to data from Figures 6-8, aluminum dissolution by forming ions (Al^{3+}) in the bottom of pit as is observed more strongly, creates an electric field that directs ions (SO_4^{2-}) by the cavity, chemically solution neutralizing and forming aluminum sulfate. Ions (SO_4^{2-}) are the most mobile of all ions involved in these reactions.

Dissolution reaction of aluminum in dilute solutions of sulfuric acid based on the reaction (3):

$$2Al + 3H_2SO_4 \rightarrow Al_2(SO_4)_3 + 3H_2 \qquad (3)$$

Hydrolysis of aluminum sulfate was according to the reaction:

$$Al^{3+} + 3H_2O \rightarrow Al(OH)_3 + 3H^+ \qquad (4)$$

This will lead to the forming of pits acidification with pH <3.

The environment is very aggressive.

$Al(OH)_3$ will precipitate. Micro-bubbles of hydrogen to reduce H^+ ions will move to the surface of aluminum hydroxide where pits are formed which will form white aluminum hydroxide deposits, as it is illustrated in Figure 9, which accumulate on the bottom.

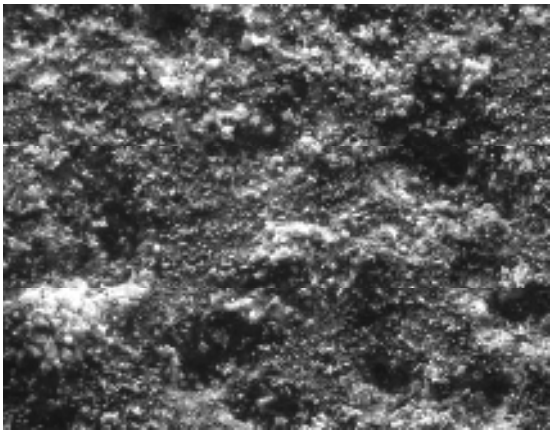

Fig. 9. *Deposits of white aluminum hydroxide (×20).*

Aluminum forms initially a few-nm-thick layer of aluminum oxide (γ-Al), which after prolonged exposure in acidic environments is covered by aluminum oxyhydroxide, (γ-AlOOH), and subsequently by various hydrated aluminum oxides and aluminum hydroxides. The stability of the compounds decreases with acidity and results in the dissolution of Al^{3+}.

Most pits stop after a few days. Polarization studies have shown that when pits stop growing, they will be repassivated.

If the alloy is polarized again, these points will not be restarted, but the pits will appear in new areas.

Conclusions

The main objective of this investigation was to study to acidic corrosion behavior of 2024 aluminum alloy. We study the variation of corrosion rate with immersion time at different values of H_2SO_4 concentration.

Corrosion rate variation depends on the concentration of the solution setting the group of corrosion of the alloy.

The exposed metal surfaces studied aspects of the corrosion process in solutions, to determine the type of corrosion and propagation mechanism in acidic environments. After the value of (V_{cor}) was established in the group of corrosion resistance alloy part studied and its degree of corrosion resistance.

Following the change in corrosion rate versus the concentration of the solution, there is an increase of low corrosion rate in solutions of dilute H_2SO_4, appreciable growth rate of corrosion taking place to the 0.001M H_2SO_4 solution. According to penetration index variation versus on the concentration of sulfuric acid solution, this is found increasing penetration index in weak diluted solutions, and increasing penetration index appreciable place with 0.001M H_2SO_4 solution, when its value is 0.2157 (mm / year).

The micrographs of samples exposed to the solution of H_2SO_4 at different concentrations and time show that there is a localized corrosion by pitting. Dissolution reaction of aluminum in dilute solutions reveals the presence of aluminum hydroxide precipitate. Micro-bubbles of hydrogen to reduce H^+ ions will move to the surface of aluminum hydroxide where pits are formed which will form white aluminum hydroxide deposits.

References

[1]. M. Pourbaix - *Atlas of electrochemical equilibria in aqueous solutions*, NACE Cebelcor, Huston, (1974).

[2]. K. Shimizu, R. C. Furneaux, G. E. Thompson, G. C. Wood, A. Gotoh, and K. Kobayashi - *On the nature of "easy paths" for the diffusion of oxygen in thermal oxide films on aluminium*, Oxidation of aluminium, 35 (5/6): pp. 427-439, (1991).

[3]. C. Leygraf - *Corrosion Mechanisms in Theory and Practice,* Second edition, New York, NY 10016, USA, chapter 15, pp. 529–582, (2002).

[4]. P. Marcus - *Corrosion Mechanisms in Theory and Practice,* Second edition, New York, NY 10016, USA, pp. 535-536, (2002).

[5]. S. Syed - *Atmospheric corrosion of materials*, Emirates Journal for Engineering Research, 11 (1), pp.1-24, (2006).

[6]. Y.I. Kuznetsov - *Protection of Metals*, Zashchita Metallov, 42(1), pp. 3, (2006).

[7]. R. D. Joseph - *Concise Metals Engineering Data Book*, ASM International USA, pp.156, (2007).

[8]. C.E. Ekuma, N. E. Idenyi, G. O. Avwiri, I.O. Owate - Proceedings of the Minerals, Metals and Materials (TMS) Annual Conference and Exhibition, California, USA (15 Feb.), pp. 51 – 58, (2009).

[9]. C. E. Ekuma, N. E. Idenyi, F. K. Onwu - Asian J. Sci. Res., Pakistan **1**(2), pp.113, (2008).

[10]. C. E. Ekuma, N. E. Idenyi - J. Appl. Sci., Pakistan 6(8), pp. 1751, (2006).

THE ANNALS OF "DUNAREA DE JOS" UNIVERSITY OF GALATI.
FASCICLE IX. METALLURGY AND MATERIALS SCIENCE
N^0. 2 – 2012, ISSN 1453 – 083X

ENVIRONMENTAL BENEFITS OF RAPESEED METHYL ESTER USE AS FUEL FOR DIESEL ENGINES

Raluca-Cristina BUTURCA, Dan SCARPETE, Daniela TASMA, Catalin Bogdan MOCANU
"Dunarea de Jos" University of Galati
email: raluca.buturca@ugal.ro

ABSTRACT

The continuously increasing number of auto vehicles that determine a substantial growth of greenhouse gas emissions, along with the decrease of fossil fuel supply and the increase of its price, make necessary the intensification of research for less polluting, alternative fuels for car engines. Through the laws adopted by governments around the world and the huge funds allocated, biofuels receive growing attention as they are considered the number one substitute for fossil fuels. This paper focuses on some aspects concerning the use of biodiesel with regard to its environmental benefits. Even if vegetable oils as fuel for diesel engines are principally considered to be CO_2 neutral, yet there are significant carbon dioxide emissions from the cultivation and conversion processes. The Life Cycle Assessment is used to evaluate and compare the environmental effects when using rapeseed oil (RO), rapeseed oil methyl ester (RME) or diesel fuel. The results show benefits first in favor of RO then RME compared to diesel fuel; this indicates the potential to reduce greenhouse gas emissions and finite energy consumption through the substitution of conventional petro diesel with RO and RME.

KEYWORDS: diesel engine, biofuel, vegetable oil, biodiesel, emissions, life cycle assessment

1. Introduction

The European transport sector is responsible for emitting more than 17.5% of the overall greenhouse gas emissions which increased by 23% between 1990 and 2009 [1]. It is also responsible for a large share of urban air pollution as well as noise nuisance. It also accounts for around a third of all final energy consumption in the EEA member countries and increasing.

Biofuels are important because they tackle two of the most difficult challenges we face in energy policy: the security of energy supply and the climate change [2]. For all these reasons, biofuels are a key part of our energy policy.

The increasing number of automobiles is an aspect worth mentioning. Among all types of engines used in the transportation sector, the diesel one receives growing attention (Table 1) because of its superiority in fuel efficiency (30-50% economy) and low emissions of greenhouse gases (CO2, CO, CH) [4]. Today diesel-powered vehicles represent about 50% of the vehicles sold in Europe; in the United States it is predicted that diesel run automotives will rise from 4% (2004) to 11% by 2012 [4], [5].

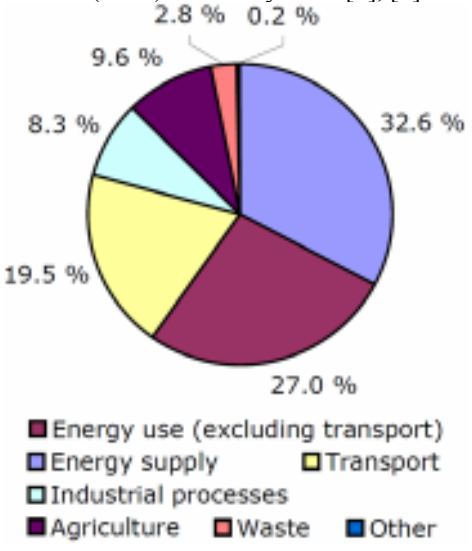

Fig. 1. *Share of GHG emissions by main source [3]*

***Table 1**. Percentage of new diesel vehicles in Europe and the United States [4]*

Year	Europe	U.S.
1997	21.7	<1
2001	35.9	<1
2004	47	4
2012	≈ 60	≈ 11

Being a substitute for fossil based diesel in the transportation sector, the use of biodiesel and vegetable oils is considered to be the easiest and most crucial solution for environmental problems as it requires no or very few engine modifications and reduces greenhouse gas (GHG) emissions substantially as well as improves lubricity. [5]. This makes rapeseed oil and rapeseed methyl ester more adaptable to the current energy scenario to ensure energy security, environmental sustainability, and boost rural development by shifting of power from petro to agro-industry, simultaneously.

In this paper we intend to compare the environmental benefits of using rapeseed methyl ester (RME) and fossil based diesel as fuel for diesel engines. One of the best methodologies to assess environmental impacts associated with all the stages of a product's life from-cradle-to-grave is the

Life Cycle Assessment, a technique regulated according to the international standard ISO 14044 [6]; moreover it also allows an identification of opportunities for environmental improvement [7] [8].

2. RME as fuels for diesel engines

The production of biodiesel from oil plants usually follows the route presented in Figure 2. The most widely used oil plant for the production of fuel based on vegetable oil is rape due to its high oil content (39–50%, varying genetic differences and climate conditions [9]).

Rape is cultivated in Europe as summer rape and winter rape. The production potential of winter rape is between 2.8 and 4.8 t/ha.

This corresponds to 1.1-2.0 t oil. For summer rape, the production potential is from 2.0 to 2.8 t/ha.

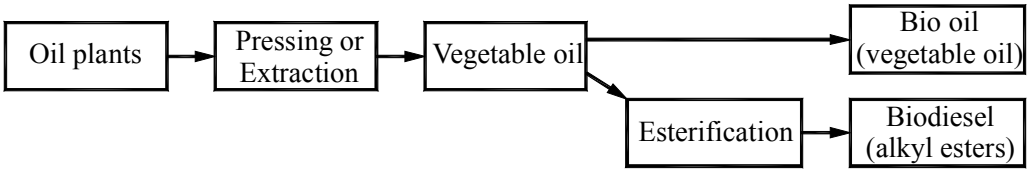

***Fig. 2.** Conversion route from oil plants to biofuels [9]*

Reports have shown that vegetable oils are possible alternative fuel for diesel engines [10]. Diesel engines with vegetable oils offer acceptable engine performance and emissions for short-term operation [11]. Long-term operation results in operational and durability problems. For these reasons it is preferable to transesterify the rapeseed oil with an alcohol to RME, reaction that takes place in the presence of an alcohol, in the presence of a catalyst, such as sodium or potassium hydroxide [12], [13].

The reaction is shown in Figure 3 [14]. Because the reaction is reversible, the excess alcohol is used to shift the equilibrium to the products side [14]. The by-products of this chemical reaction are glycerol and water [13].

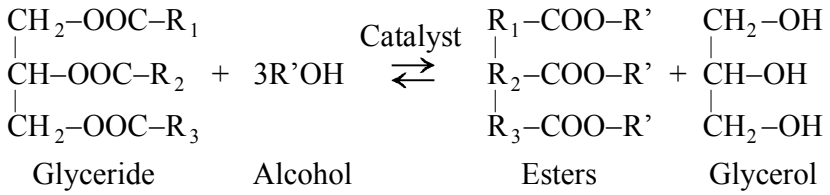

***Fig. 3.** Transesterification of triglycerides with alcohol [14]*

The specific fuel is called after the plant (or animal) source plus the alcohol [15]. Made from rapeseed oil and methanol, the biodiesel is called Rape Methyl Ester (RME), from canola oil and ethanol, Canola Ethyl Ester (CEE), and from used McDonald's cooking oil and ethanol or methanol ("McDiesel"). The base catalyzed reaction is also more economical than other production methods [16].

The reaction has a very high conversion rate (98%), generally requires only a single production step, and proceeds quickly at relatively low pressure (137.9 kPa) and temperature (65.5°C).

3. LCA of RME and Diesel used in diesel engines

As common liquid biofuels are produ-ced from biomass, i.e. energy crops, the fuels are principally considered to be CO_2 neutral [17]. Thus it can be assumed that during the combustion about the same amount of carbon dioxide is being set free as that has been bound from the atmosphere during the growing of the crops. Having the emission balance in mind, it can be said that the carbon circle is closed. Yet there are significant carbon dioxide emissions from the cultivation and conversion processes.

All these processes are connected with environmental effects, such as air pollution and waste disposal [18]. These effects have to be taken into account for a life cycle assessment of the fuel provision. To quantify all the environmental effects of the renew-able fuel provision, the whole provision chain has to be investigated including all the efforts for transport, infrastructure and all the preliminary products. The method to rea-lize this is the life cycle assessment (LCA).

Life cycle assessment is an established technique for quantifying the total environ-mental impacts of the provision of a product or service from original resources to final disposal, or so-called "cradle-to-grave" [19].

Amongst numerous reasons for conducting LCA studies is the possibility of comparing the total environmental impacts of alterna- tive products or services.

There are four phases in an LCA-study [20], according to ISO 14040: 1. Goal and scope definition; 2. Inventory analysis; 3. Impact assessment and 4. Interpretation. In [19], there are two more stages: 5. Reporting and 6. Critical reviewing.

The central feature of a life cycle assessment is the process chain which summarizes the main activities in the provision of a product or service [19]. For a product such as a liquid transport fuel, the process chain consists of a sequence of activities, starting with the provision of the basic raw material and ending with a suitable product, distributed and available for use in suitable road transport vehicles. It should be noted that the actual use of the fuel in a vehicle could be included in the process chain and subjected to the life cycle assessment. The main stages in the life-cycle of RME for use as a transport fuel are summarized below [21]:

- agriculture - production of oilseed rape;
- transport - rapeseed to crushing plant to produce oil;
- processing - oil extraction and refining;
- transport - rapeseed oil to processing plant;
- processing - rapeseed oil to rape methyl ester;
- distribution and storage - RME to filling station;
- end-use - in a RME fuelled vehicle.

To compare the environmental impacts of RME and diesel oil, the complete life cycles of both fuels are compared against each other (Fig. 4) [23].

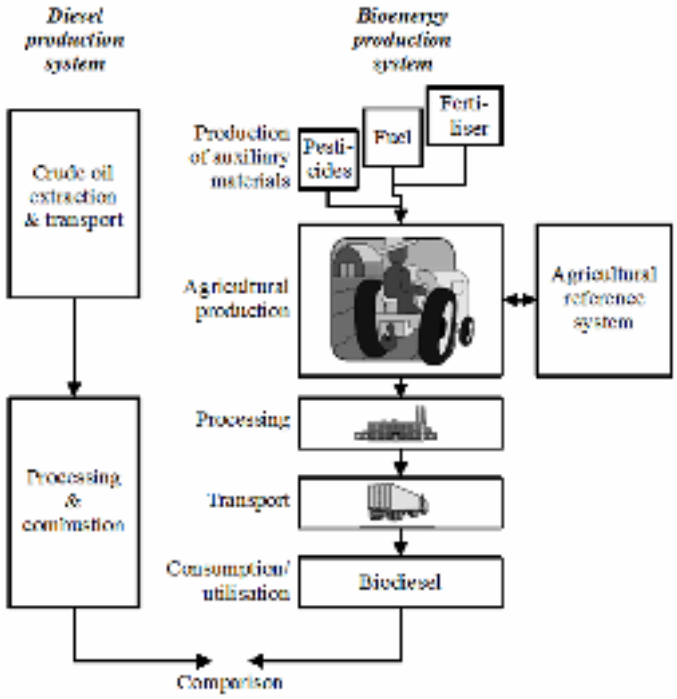

Fig. 4. *Comparative assessment of liquid biofuels versus fossil fuels [22]*

The detailed inven-tory of the life cycle assessment of RME and diesel oil for finite energy, CO_2 equivalents, NO_x emissions and SO_2 equivalents is pre-sented in [23]. Since the cycle for rapeseed oil (RO) is included in the RME cycle, the inventory was detailed in Table 2. Additionally, the credits for RME and RO (which account for the energy for producing cattle cake and/or using rape straw as fuel etc.).

Table 2. *Energetic expenditures and selected emissions for RME and diesel oil [22]*

Life cycle step	**Finite energy**	**CO_2 equiv.**	**NO_x**	**SO_2 equiv.**
	[MJ/kg]		[g/kg]	
Plant production	11.36	2319	4.474	17.441
Provision				
Oil	*5.56*	*347*	*0.800*	*1.005*
Esterification	*7.61*	*517*	*0.355*	*0.704*
Total Provision	13.17	864	1.155	1.709
Energetic use	0.22	233	10.348	7.437
Total RME	24.75	3415	15.977	26.587
Total RO	17.14	2898	15.622	25.883
Diesel oil	47.78	3766	10.839	9.925
RME minus Diesel oil	**-23.03**	**-351**	**5.138**	**16.662**

4. Conclusions

Biofuels have received a growing atten-tion as an alternative to fossil based fuels to reduce greenhouse gases, to create of new markets for agricultural products and to reduce dependence of imported oil.

Vegetable oils are attractive by their high biodegradability, high calorific value and reduced emission, particularly carbon dioxide, sulphur oxides, soot and aromatic compounds. The disadvantages of vegetable oils (high viscosity, lower volatility, a mediocre ignition quality, reactivity of unsa-turated hydrocarbon chains and the tendency of large molecules to crack) make them unu-sable as fuel for the modern diesel engines.

To reduce the high viscosity of vegetable oils and to improve their combustion quality, there are three possible solutions:

1) to modify the oil to methyl ester, i.e. to use biodiesel;

2) to blend the raw oil with diesel fuel;

3) To use conversion kits to adapt the fuel system or to modify the engine concept to run directly on vegetable oil.

The use of esters of vegetable oil as fuels for stationary and on vehicle diesel engines brings one to the conclusion that the emissions of HC are reduced in some studies as much as 50 percent; CO is reduced by as much as 10 percent; NO_x and PM are related and tend to change inversely with each other, differing from diesel by at most 10-15 percent. Generally, NO_x was found to be slightly higher than diesel and PM slightly lower than diesel, although this differs with particular conditions.

Even if vegetable oils as fuels are mainly considered to be CO_2 neutral, there are significant carbon dioxide emissions from the cultivation and conversion processes. To evaluate the environmental effects of all these processes and to compare biofuels with diesel fuel, the life cycle assessment is used. Individual results for rapeseed oil, RME and diesel oil signal benefits first in favor of RO and then of RME. The balance shows the potential to reduce finite energy consumption by the substitution of diesel oil with RO and RME and to reduce the greenhouse gas emissions.

Acknowledgments

The authors would like to acknowledge the Project SOP HRD - TOP ACADEMIC 76822 and SOP HRD – EFICIENT 61445 for supporting this research and the paper publishing.

References

[1]. *** - European Environment Angency. s.l. : www.eea.europa.eu, (2010).

[2]. Andris Piebalgs - *Biofuels – the green alternative for transport.* July (2007).

[3]. *** - European Environment Agency **-** *GHG trends and projections in the EU-27.* October 2010.

[4]. Huebner, T., Sáez, D.D. - *Diesel Vehicle Sales Discrepancies Between Europe and the United States* - For BIOWA Development Association, (2012).

[5]. Jayed, M.H. et al. - *Renewable and Sustainable Energy Reviews Environmental aspects and challen-ges of oilseed produced biodiesel in Southeast Asia, 13 2452–2462,* (2009).

[6]. *** - *Environmental management - Life cycle assessment,* Requirements and guidelines ISO 14044, (2006).

[7]. Consoli, F. et al. - *Guidelines for life-cycle assessment: a "Code of practice"* - Society of Environmental Toxicology and Chemistry (SETAC), (1993).

[8]. Lindfors, L.G. et al. - *Guidelines on Life-Cycle Assessment* - Nordic Council of Ministers, (1995).
[9]. Ammerer, A. et al. - *Rapeseed oil as a fuel for farm tractors,* IEA Bioenergy Task 39, (2003).
[10]. Alamu, O.J. et al. - *Power and Torque Characteristics of Diesel Engine Fuelled by Palm-Kernel Oil Biodiesel.* s.l. : Leonardo Journal of Sciences, Issue 14, (2009).
[11]. *** - www.biodiesel.org**.** *Straight Vegetable Oil as a Diesel Fuel? - Clean Cities, Fact sheet,* National Renewable Energy Laboratory (NREL).
[12]. Hamelinck, C.N. - *Outlook for advanced Biofuels, Universiteit Utrecht,* (2004).
[13]. Schmidt, L., - *Biodiesel vehicle fuel: GHG reductions, air Emissions, supply and economic overview,* (2004).
[14]. Ma, F. and Hanna, M.A. - *Biodiesel production: a review.* s.l. : Elsevier Science B.V., (1999).
[15]. *** - www.cogeneration.net. *Biofuel Industries, A Cogeneration Technologies Company (Cogeneration Technologies, Trigeneration Technologies, EcoGene-ration Solutions, LLC),* (2002).
[16]. Mixon, J. et al. - *The case for biodiesel, ENVIRON 55,* (2003).
[17]. Arnold, K. et al. - *Synopsis of German and European experience and state of the art of biofuels for transport, Wuppertal Institute for Climate,* Environment and Energy, (2005).
[18]. Mehlin, M. et al., Reichmuth, M. et al., Wacker, M. et al. - *Renewable Fuels for Cross Border Transportation*-Final Report to the European Commission, Directorate-General for Environment, for study contract ENV.C1/ETU/2001/0092, (2003).
[19]. Mortimer, N.D. et al. - *Evaluation of the comparative energy, global warming and socio-economic costs and benefits of biodiesel,* Contract Reference No. CSA 5982/NF0422, Report No. 20/1, Sheffield Hallam University, (2003).
[20]. Bernesson, S. - *Farm-scale Production of RME and Ethanol for Heavy Diesel Engines-with Emphasis on Environmental Assessment.* Doctoral thesis, (2004).
[21]. Lewis, C.A. - *Fuel and Energy Production Emission Factors,* MEET Project, Contract No. ST-96-SC.204, (1997).
[22]. Andersen, O. et al. - *Biodiesel in heavy-duty vehicles in Norway – Strategic plan and vehicle fleet experiments.* Final report from European Commission, ALTENER-project XVII/4.1030/Z/209/96/NOR, (1998).
[23]. Reinhardt, G.A., Jungk, N. - *Pros and cons of RME compared to conventional diesel fuel*, IFEU-Institut für Energie- und Umweltforschung Heidel-berg.

THE ANNALS OF "DUNAREA DE JOS" UNIVERSITY OF GALATI.
FASCICLE IX. METALLURGY AND MATERIALS SCIENCE
N^0. 2 – 2012, ISSN 1453 – 083X

STUDY FOR EVALUATION AND OPTIMIZATION OF MINERAL COMPOSITION AND STRUCTURE OF IRON ORE GRANULATION IN SINTERING PROCESS

Paul Petruș MOGOȘ, Nicolae CONSTANTIN, Sinziana ITTU, Denisa-Elena ANCA, Lavinia-Marilena HARCEA
"Polytechnic" University of Bucharest,
email: mogospaul@yahoo.com

ABSTRACT

The characterization of iron ore particles is of vital importance for the study of mineral composition. The specific surface area of iron ore particles can be measured by laser diffraction, and mathematical models (based on the size distribution). Particle size fractions and chemical composition were determined of several types of iron ore (symbolically marked A, B, C, D, E, F). These features have direct influence on the sintering process by particle size analysis, permeability, reducibility, porosity, CaO/SiO ratio, influence of MnO in sinter. The granulation experiment show that these minerals (more than 50% with diameters of <1mm) can be successfully used in the sintering process, or by alloying with other minerals in Europe. Large irregularly shaped and adhesive particles can get a higher efficiency of granulation easily. The usage of iron ore with big and rough particles can improve the permeability while the iron ore with smooth and sphere particles has poor ability of granulation.

KEYWORDS: iron ore, sinter, size distribution, chemical composition, mathematical model

1. Introduction

The performance of blast furnace depends, to a greater extent, on the physical and chemical characteristics of the burden materials and their consistency. Sinter constitutes 70–80% of the iron bearing burden material in the modern blast furnaces (**Figure 1**).

An important aspect of the sinter, as ferrous burden, is that it could be tailor made. Its physical & chemical properties depend on the properties of individual components and on its micro-structure, especially on the size, shape distribution and the mutual interaction of the individual components.

A thorough appreciation of the microstructure of sinter is a basic necessity and the first step towards establishing structure–property relationship.

Sinter is an agglomerate made of fine iron ore that is cheaper than pellets and lump iron ore and is superior in terms of reducibility and dropping characteristics. For the two reasons of better production, cost performance and stable operation of blast furnaces, sinter has been used in many countries as one of the main sources for blast furnace operation.

In order to satisfy the need to improve the productivity of sinter, a broad range of research and development efforts have been made from the viewpoints of the technology to pre-treat fine iron ore and the technology to control the charging structure on the entire spread of the sintering bed.

The characterization of the particle size and the surface features of iron ores is of vital importance for the study of mineral processing. The specific surface area of iron ore particles can be measured by laser diffraction, and mathematical models based on the size distribution. However, what is the difference among these methods and what is the indication of the results were less discussed on the iron ore granulation, which is the exactly topic of the present study.

With the progressive deterioration in the quality of iron ore in recent years, there has been an increase in the quantity of pisolite ore used in the raw material mix. It is known that the use of large quantities of these ores as sinter raw materials greatly reduces the granulation and air permeability of the raw material packed bed, resulting in reduced productivity.

This is thought to be because these ores are porous and the added moisture is absorbed into the ore particles, with the result that the volume of moisture is not sufficient for granulation. Accordingly, to ensure the stable use of large quantities of these ores, it is necessary to optimize the adding volume of moisture. Accordingly, it takes a certain period to stabilize the optimal moisture value, and this was one factor in producing instability in the operations.

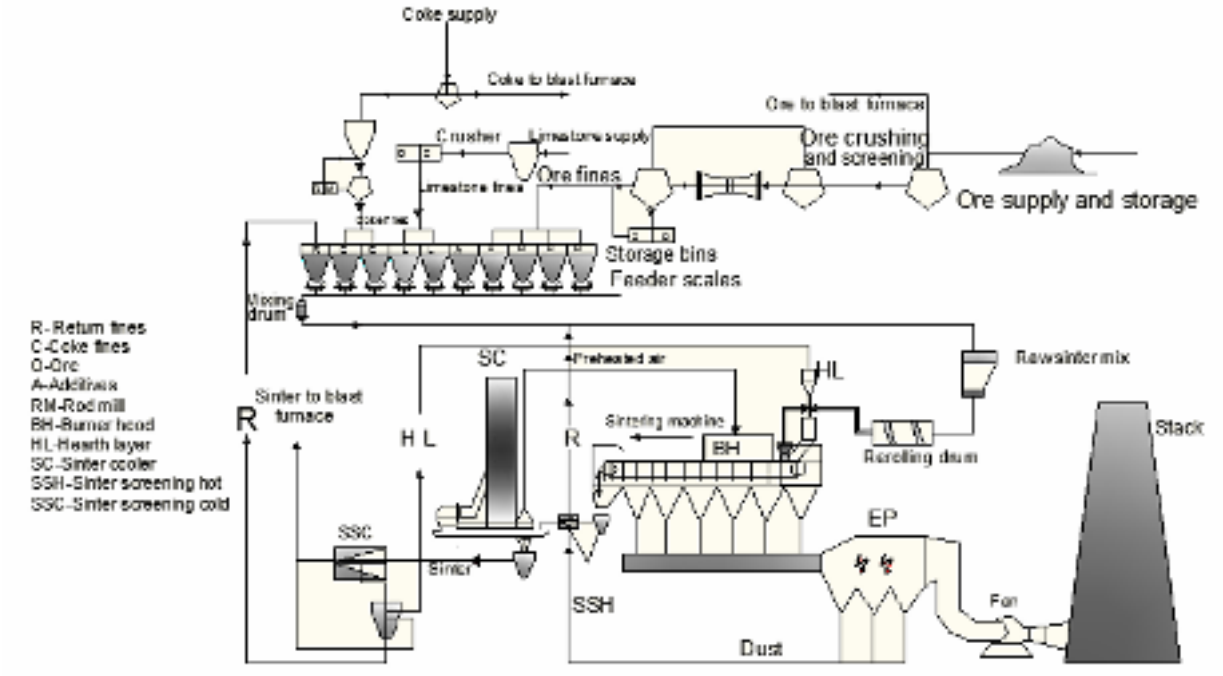

***Fig. 1**. Schematic diagram of the sintering process*

2. Materials and methods

The properties of iron ore sample related to granulation were measured from different locations: A, B, C, D, E, F. Diffraction shows that all are in compositions a significant amount of Fe (from 64.2% to 68.3%). Minerals present in raw materials are: goethite, hydrated iron oxide, hematite, kaolinite and quartz.

2.1 Particle size measurement

***Table 1**. Particles size analysis.*

Size (μ)	Ore A	Ore B	Ore C	Ore D	Ore E	Ore F
8mm	2	2	6	2	20	21
4mm	8	7	24	7	14	12
2mm	0	0	0	20	12	5
1mm	31	48	26	30	12	9
500μm	0	0	10	13	10	10
250 μm	0	0	8	11	0	0
180 μm	22	27	4	4	13	17
90 μm	12	4	6	5	4	7
63 μm	10	0	15	8	3	5
-63μm	15	12	0	0	11	11

Samples of iron ore properties related to grain are presented in **Table 1, Figure 2**, for each sample separately, using laser diffraction.

Parameters follow:
-mixture sintering;
-CaO/SiO_2 report.

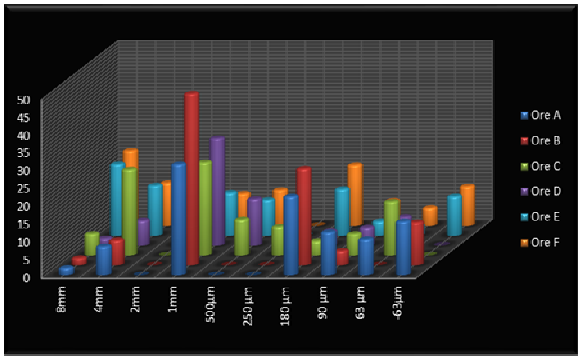

***Fig. 2**. Particle size distribution*

In the present study, six samples of iron ore were selected for the measurements. The samples were analyzed by particle size, analysis that was performed in a 0.5kg volume of each sample

determining the particle size classes between 63µm-8mm. Particle size distribution for each type of ore is presented in **Tables 2-7** and **Figure 3**.

In terms of grain, more than 50% of the particles are> 1mm, which contributes to the sintering process by high productivity and permeability. Also we observe a significant percentage of fine ore, but they may become adherent particles, increasing the diameter.

***Tables 2-7**. Particles size distribution*

Size (µ)	Ore A (%)	Size (µ)	Ore B (%)
4mm÷8mm	2	4mm÷8mm	2
2mm÷4mm	8	2mm÷4mm	7
1mm÷2mm	0	1mm÷2mm	0
500µm÷1mm	31	500µm÷1mm	48
250 µm÷500µm	0	250 µm÷500µm	0
180 µm÷250 µm	0	180 µm÷250 µm	0
90 µm÷180 µm	22	90 µm÷180 µm	27
63 µm÷90 µm	12	63 µm÷90 µm	4
-63µm÷63µm	10	-63µm÷63µm	0
<-63 µm	15	<-63 µm	12

Size (µ)	Ore C (%)	Size (µ)	Ore D (%)
4mm÷8mm	6	4mm÷8mm	2
2mm÷4mm	24	2mm÷4mm	7
1mm÷2mm	0	1mm÷2mm	20
500µm÷1mm	26	500µm÷1mm	30
250 µm÷500µm	10	250 µm÷500µm	13
180 µm÷250 µm	8	180 µm÷250 µm	11
90 µm÷180 µm	4	90 µm÷180 µm	4
63 µm÷90 µm	6	63 µm÷90 µm	5
-63µm÷63µm	15	-63µm÷63µm	8
<-63 µm	0	<-63 µm	0

Size (µ)	Ore E (%)	Size (µ)	Ore F (%)
4mm÷8mm	20	4mm÷8mm	21
2mm÷4mm	14	2mm÷4mm	12
1mm÷2mm	12	1mm÷2mm	5
500µm÷1mm	12	500µm÷1mm	9
250 µm÷500µm	10	250 µm÷500µm	10
180 µm÷250 µm	0	180 µm÷250 µm	0
90 µm÷180 µm	13	90 µm÷180 µm	17
63 µm÷90 µm	4	63 µm÷90 µm	7
-63µm÷63µm	3	-63µm÷63µm	5
<-63 µm	11	<-63 µm	11

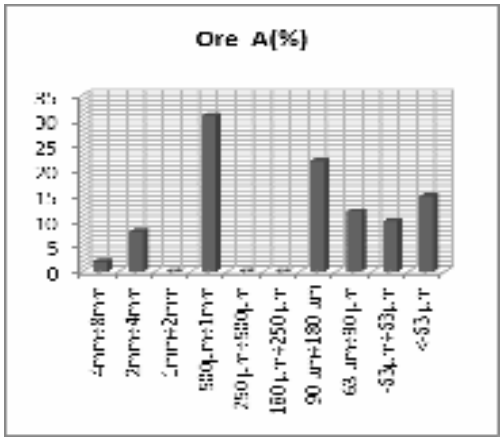

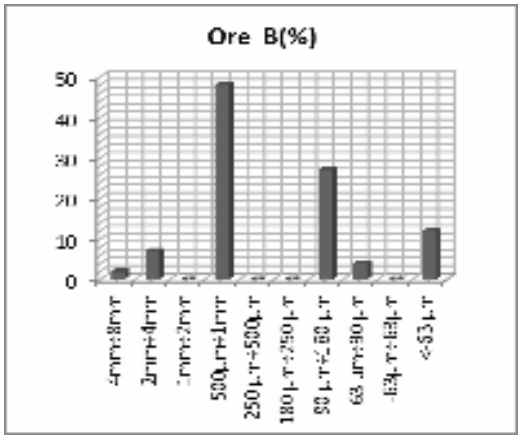

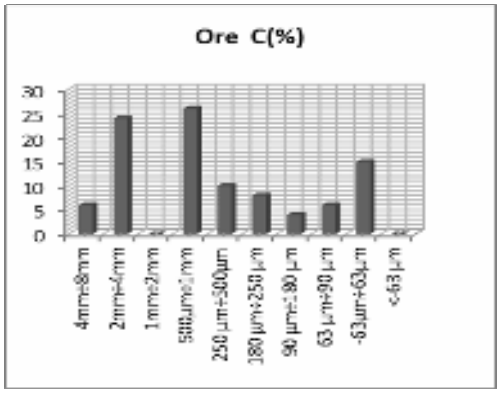

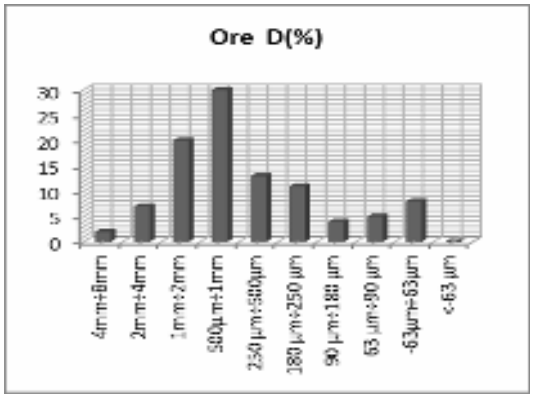

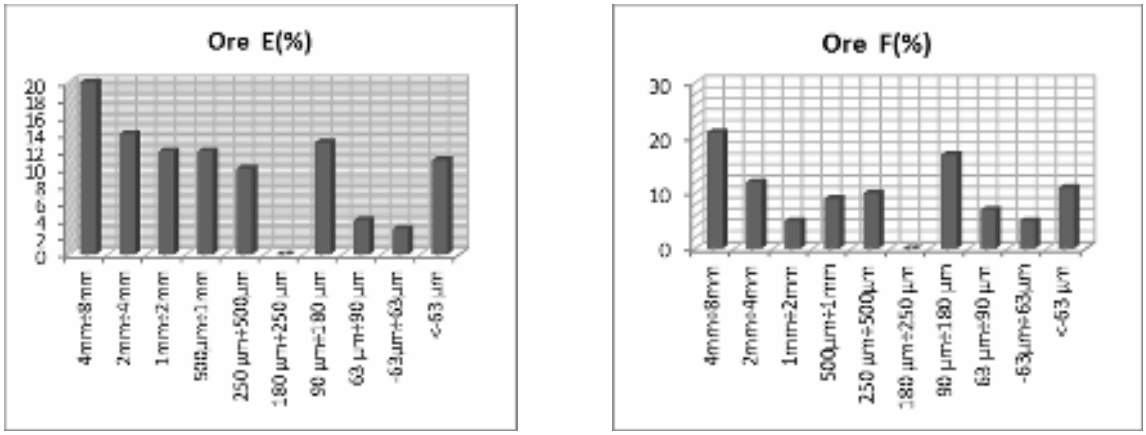

***Fig. 3**. Variation of particle size fraction for each component separately*

2.2. Mathematical analysis

According to Fig. 1, samples A, B, C, D, E, F are fine ore samples. Surfaces of ore samples can be mathematically calculated with formula (1), assuming that most of the sample particles are spheres, as follows:

$$S = 4\pi \cdot n \cdot r^2 \quad (1)$$

where: *S* is the total surface area of all particles of unit mass, *r* is the radius of the particles.

Assuming that in this experiment there will be *i* particles, our formula becomes:

$$S_1 = 4\pi \cdot n_1 \cdot r_1^2 \quad (2)$$

$$S_2 = 4\pi \cdot n_2 \cdot r_2^2 \quad (3)$$

$$S_i = 4\pi \cdot n_i \cdot r_i^2 \quad (4)$$

$$S_{1+2+3+...+i} = 4\pi \sum n_i \cdot r_i^2 \quad (5)$$

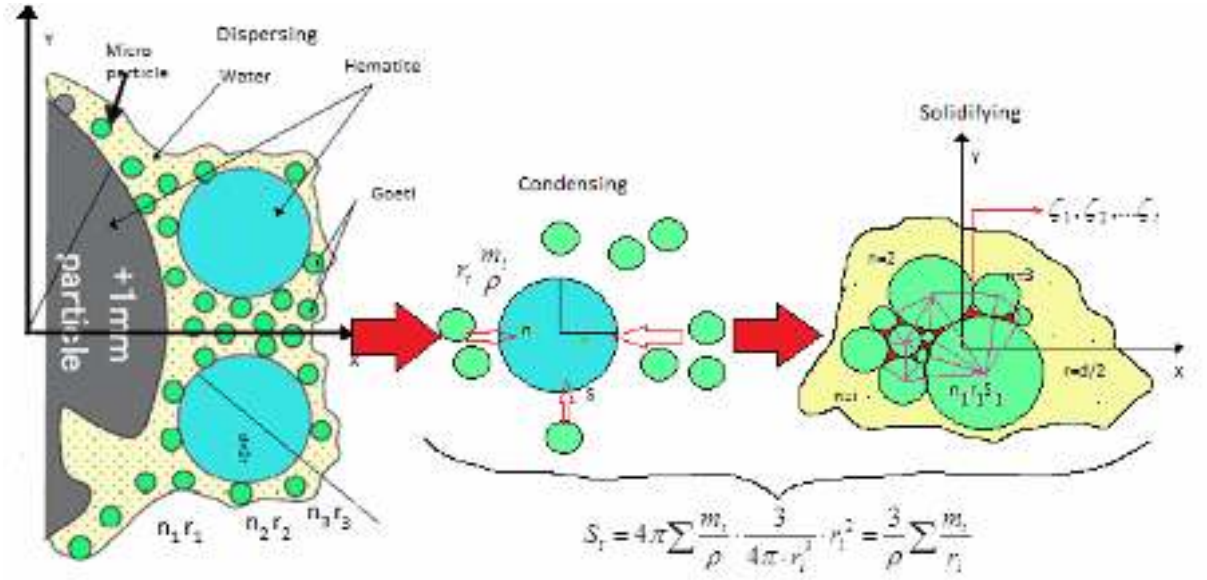

***Fig. 4**. Mathematical calculation of particle diameter*

The total number of particles n_i can be calculated by the relationship:

$$n_i = \frac{m_i}{\rho} \cdot \frac{3}{4\pi \cdot r_i^3}$$

$$S_t = 4\pi \sum \frac{m_i}{\rho} \cdot \frac{3}{4\pi \cdot r_i^3} \cdot r_i^2 = \frac{3}{\rho} \sum \frac{m_i}{r_i}$$

where *m* is the mass of particles of *r* radius compared to a mixture of 100g raw density ρ.

We can determine the diameters for each particle. At the same time, with the increase particle diameter, (a fundamental step in preparing sintering), we observe the emergence of a new size ξ-mathematical model imperfections (open spaces), as shown in **Figure 5**.

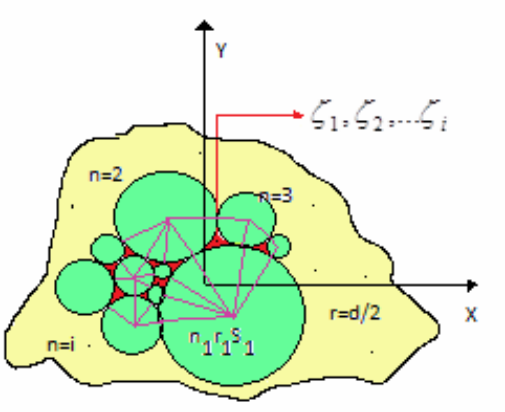

Fig. 5. *Increasing particle diameter*

Here follow relationships depending on particles diameters:

$$\sum r_i^2 = \frac{S_1}{4\pi \cdot n_1} + \frac{S_2}{4\pi \cdot n_2} + \ldots + \frac{S_i}{4\pi \cdot n_i}$$

$$\sum r_i^2 = \frac{1}{4\pi} \sum \frac{S_i}{n_i}$$

$$\sum 4r_i^2 = \frac{1}{\pi} \sum \frac{S_i}{n_i}$$

$$\sum 2r_i = \frac{\sqrt{\pi}}{\pi} \sqrt{\sum \frac{S_i}{n_i}}$$

If we note $d = 2r$, $r \geq 0$, the diameter of each particle; S_ξ-surface imperfections, S_s-sintering surface, the relationship becomes:

$$\sum d_i = \frac{\sqrt{\pi}}{\pi} \sqrt{\sum \frac{S_i}{n_i}}$$

$$S_s = S_i - S_\zeta$$

Note that with the migration of particles, $\xi \to 0$ (reducing the distances between particles). This is necessary because small diameter spherical particles have a low grip and the sintering process is difficult. This is necessary to obtain particles with large diameters and high porosity mathematical method.

2.3. Chemical composition analysis

The chemical composition of the 6 types of ore is given in **Table 8** and **Figure 6**. In all 6 samples over 50% of the chemical composition is owned by Fe, dominated by raw materials with a low basicity and MgO content between 0.02% -0.05%.

Table 8. *Chemical composition of ores*

Ch. Composition	Ore A	Ore B	Ore C	Ore D	Ore E	Ore F
Fe	64.2	67.2	68.3	64.7	64.5	65.2
SiO_2	5.1	0.6	1.3	4	4.2	4.2
Al_2O_3	1	0.94	0.9	1.1	0.7	0.8
TiO_2	0.08	0.03	0.04	0.03	0.07	0.09
CaO	0.02	0.01	0.03	0.05	0.02	0.03
MgO	0.03	0.02	0.04	0.05	0.04	0.05
Na_2O	0.005	0.01	0.006	0.02	0.006	0.006
K_2O	0.008	0.01	0.004	0.01	0.006	0.007
Mn	0.2	0.45	0.229	0.2	0.07	0.07
P	0.045	0.037	0.03	0.04	0.057	0.04
S	0.007	0.01	0.005	0.005	0.006	0.006
V	0	0	0.006	0	0	0
LOI	1.5	1.4	0.61	0.05	2.3	1.5

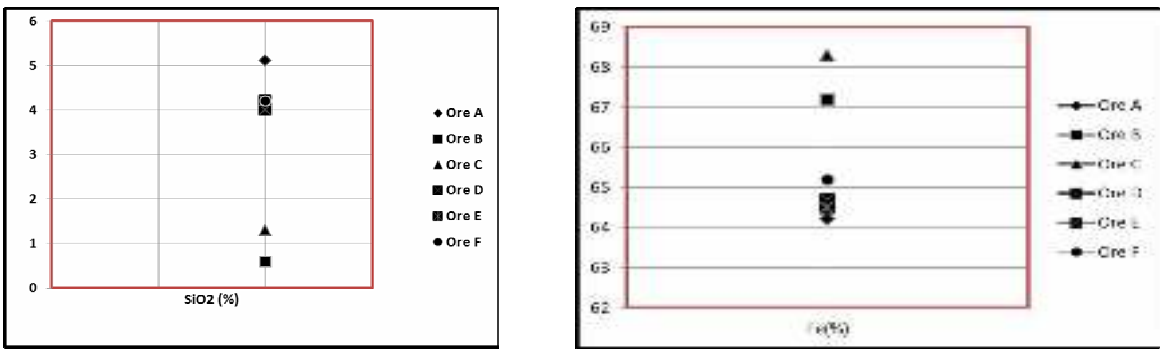

Fig. 6. *Fe and SiO_2 distribution in the samples analysed*

Ore C holds a significant amount of iron and ore A, is a low one. We see an inverse distribution in the amount of Fe and SiO_2 in that ore, with a high quantity of Fe correspond a small amount of SiO_2, ore C with 1.3% SiO_2 and 68.3% Fe, respectively ore A with 5.1% SiO2 and 64.2% Fe.

The chemical composition shows that these types of ores can be successfully used in the sintering process. Meet one ore with a SiO_2 content <1%, as-Al_2O_3 can be used to reduce ores containing SiO_2 or in combination with Australian ore, where it prevails, and can be successfully used in Europe and the Far East. P and Mn levels are moderate, and the basic oxides level is very low for these types of ores (MgO and CaO).

The S, V, and other impurities level is very low. The alkalinity level is low, mainly due to the high amount of SiO_2 in ores A, D, E and F.

Table 9 and Figure 7 shows the distribution of alkalinity in the type of ore. Minimum values <0.01 are typical for ore A, E and F, and the maximum for ores C at a rate of CaO/SiO2 = 0.023.

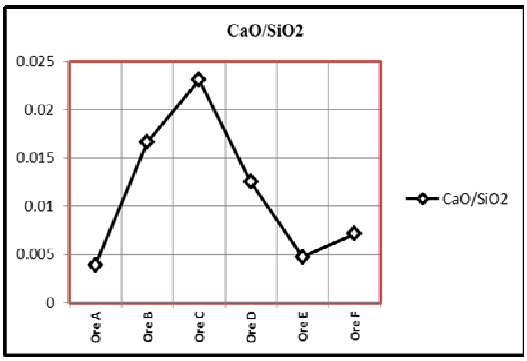

Fig. 7. Alkalinity evolution depending on the type of ore

Table 9. Alkalinity variation

Ch. Comp.	Ore A	Ore B	Ore C	Ore D	Ore E	Ore F
CaO/SiO2	0.004	0.017	0.0231	0.013	0.0048	0.007
ΣOa	5.18	0.63	1.34	4.03	4.27	4.29
ΣOb	1.063	0.99	0.98	1.23	0.772	0.893
ΣEd	0.007	0.01	0.011	0.005	0.006	0.006
ΣOb/ΣOa	0.205	1.571	0.7313	0.305	0.1808	0.208

3. Conclusions

The preparation for sintering requires a particle size analysis for quality and high efficiency of processes. Particles with a small diameter can be used for the sintering process after previous training, their measurement can be done by diffraction into developing comparative simulation models needed later to develop the first fusion iron.

The difference between the 2 measurements is that if the mathematical model size $\xi \to 0$ (the spaces between particles shrinks iron ore with small and spherical diameter have low grain capacity), in practical measurements $\xi \neq 0$ because the efficiency of grain increases with the increase of water saturation and iron ore. Size ξ depends on the homogeneity of the particle size, shape, total and initial surface sintering bed.

References

[1]. S. N. Ahsan, T. Mukherjee and J. A. Whiteman - Ironmaking Steelmaking, 10 (1983), 54.
[2]. N. J. Bristow and C. E. Loo - ISIJ Int., 32 (1992), 819.
[3]. T. Maeda and Y. Ono - Tetsu-to-Hagané, 77 (1991), 1569.
[4]. Y. H. Yang and N. Standis - ISIJ Int., 31 (1991), 468.
[5]. S. C. Panigrahy, P. Verstraeten and J. Dilewinjns - Metall. Trans. B, 15B (1984), 23.
[6]. Yu. S. Karabasov, A. N. Pokhvishev, E. F. Shkurko and V. S. Valvin - Steel USSR, 5 (1975), 583.
[7]. N. K. Kornilova, E. F. Vegman and S. E. Lazutkin - Steel USSR, 3 (1973), 1.
[8]. T. Hamada, T. Koitabashi and K. Okabe - Tetsu-to-Hagané, 60 (1974), 465.
[9]. H. Toda and K. Kato - Trans. Iron Steel Inst. Jpn., 24 (1984), 178.
[10]. Y. Hosotani, N. Konno, K. Yamaguchi, T. Orimoto and T. Inazumi - ISIJ Int., 36 (1996), 1439.
[11]. N. Matsuo, T. Maeda and Y. Ono - CAMP-ISIJ, 4 (1991), 1081.
[12]. S. Sato, M. Ichidate, K. Kato and T. Kawaguchi - Tetsu-to-Hagané, 69 (1983), S744.
[13]. D. Jeulin, J. L. Latailleur, A. M. Schneider - Proc. Int. Symp. on Agglomeration (Agg. 77), ed. by K. V. S. Sastry, Amer. Inst.of Mining, Metallurgical & Petroleum Engineers, NY, (1977), 526.
[14]. Ram Pravesh Bhagat, Uday Shankar Chattoraj - ISIJ Int., 46 (2006), 1728.
[15]. Takeshi Maki and Isao Sekiguchi - ISIJ Int., 49 (2009), 631.
[16]. Shinji Kawachi and Shunji Kasama - ISIJ Int., 51 (2011), 1057.
[17]. Xuewei LV, Xiaobo HUANG, Jaqing YIN and **Chenguang BAI** - ISIJ Int., 51 (2011), 1432.

THE ANNALS OF "DUNAREA DE JOS" UNIVERSITY OF GALATI.
FASCICLE IX. METALLURGY AND MATERIALS SCIENCE
N^0. 2 – 2012, ISSN 1453 – 083X

INVESTIGATION OF CORROSION PROTECTION BY CHEMICALLY APPLIED PATINA ON ARTISTIC BRONZES

J.D. SABĂU (CHELARU)[1], L. M. MUREŞAN[2], V.F. SOPORAN[1], O. NEMEŞ[1], T KOLOZSI[3]

[1]Technical University of Cluj-Napoca, Faculty of Materials and Enviromental Engineering, Department of Environmental Engineering,
[2]Babes-Bolyai University, Physical Chemistry Department,
[3]University of Art and Design, Cluj Napoca
email: julieta_dana@yahoo.com

ABSTRACT

Increase of pollution in recent years, requires monitoring of the corrosion behavior of artistic bronzes coated with syntetic patina, in urban atmosphere.

This present work aims to investigate the corrosion rezistance of various artificial patina currently used in bronze sculpture. Electrochemical and microscopic methods were used to investigate the protective effect of several chemically produced patinas on artistic bronze.

KEYWORDS: bronze, corrosion, patina, polarization curves

1. Introduction

On a bronze sculpture, the color of the surface has the ability to enrich the aesthetic.

The art of patination can be defined as a slip coloring metal surface oxidation, caused by prolonged exposure in the surrounding atmosphere. This definition is actually describing the two patina categories used in the case of bronzes: natural and artificial.

Natural patina is the result of compounds formation after corrosive chemical reactions that occur on the surface of bronze. There is no way to achieve a true natural patina except with time itself. This is very important to natural patina but very impossible for the sculptor, because it requires years to accomplish an end result. Artificial patinas, on the other hand, have the advantage not only of creating similar results of natural patina, they also have the ability to incorporate a wider range of color hue and depth not found in natural patinas, and this is accomplished almost immediately [1].

Making a special color on the surface of bronze art objects requires a mastery of the artist. This work is almost unknown until recently, the secrets being kept by each artist.

The importance of producing artificial patinas on bronze comes from the well known ability of this alloy to react against atmospheric agents by forming different coloured corrosion products of pleasant aspect, which protect the bronze objects from further corrosion [2].

Many factors influence the initial development of the patina, some of them being active throughout the life of a work of art.

The final quality of the patina depends on the alloy composition and on environmental conditions it develops in. From a chemical point of view the patina layer can be described as a hydrated copper oxide stabilized on a copper oxide substrate [2, 7 - 9]. However, the poluants present in urban atmosphere gives birth to various corrosion products on bronze surface. The most damaging are chlorides (especially sodium chloride, which encourages the development of copper chloride), sulfates and oxides, particularly sulfur dioxide [9 - 13].

Increase of pollution in recent years requires monitoring of the patination process that was formerly left to the action of nature.

Artificially produced patina gives to the surface protection against corrosion and aesthetic value and can be formed on bronze surfaces by using chemical reagents or by electrochemical methods [14, 15]. For this reason, finding new artificial patinas to protect works of art cast in bronze is a current concern.

In this context, the main objective of this paper is to study the protective effect of various artificial patinas deliberately produced by sculptors on bronze. The study was conducted under conditions that simulate acid rain.

2. Experimental data

The bronze used in the experiments was chosen to be similar to the bronze monument of Matthias Corvinus in Cluj Napoca which dates back to 1902. The statues of this monument were made of bronze on a metal frame and according to the chemical analysis, the composition of the alloy varies in different parts of the sculptural group; there are variations in the percentage of tin, zinc, lead, but the content of copper exceeds 90% of the alloy in most cases (Table 1).

Table 1. *The chemical composition of the alloy used in the casting of the King Matthias the Ist sculptural group*

	Sn	**Pb**	**Zn**	**Cu**
	[%]			
Sample 1	7.17	0.08	0.36	rest
Sample 2	8.00	0.52	1.30	rest
Sample 3	7.72	0.41	0.21	rest

Consequently the alloy used in electrochemical studies, according to current standards, was chosen CuSn8, whose chemical composition is displayed in Table 2.

Table 2. *The chemical composition of the used alloy*

Alloy	**Cu**	**Sn**	**Impurities,** [%] max										
	[%]		Zn	Pb	Sb	Fe	Al	S	Bi	Mg	As	Mn	Ni
CuSn8	rest	7-9	0.8	1.0	0.1	0.2	0.02	0.1	0.01	0.01	0.15	0.2	1.0

For microscopic study, the electrodes were polished on the polishing machine with alumina paste, after which the surface was washed with ammoniacal cupric chloride. The study of the surface was conducted through optical microscopy (OLIMPUS GS 51).

The metallographic analysis revealed the existence of a homogeneous structure, the crystals having polyhedral appearance with macles (Fig 1).

Crystalline grain size is between 50-200 μm, which gives the alloy a high resistance to corrosion [16].

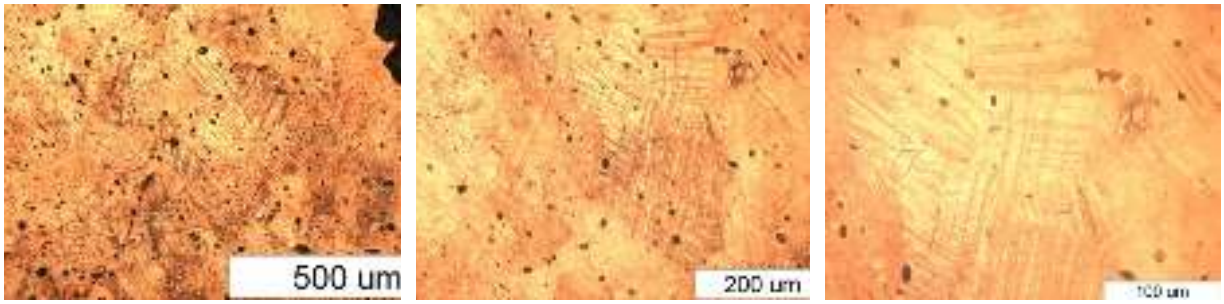

a) b) c)

Fig. 1. *Microscopic structure of alloy use in the casting of King Matthias I sculptural group: a – x100; b – x200; c – x500*

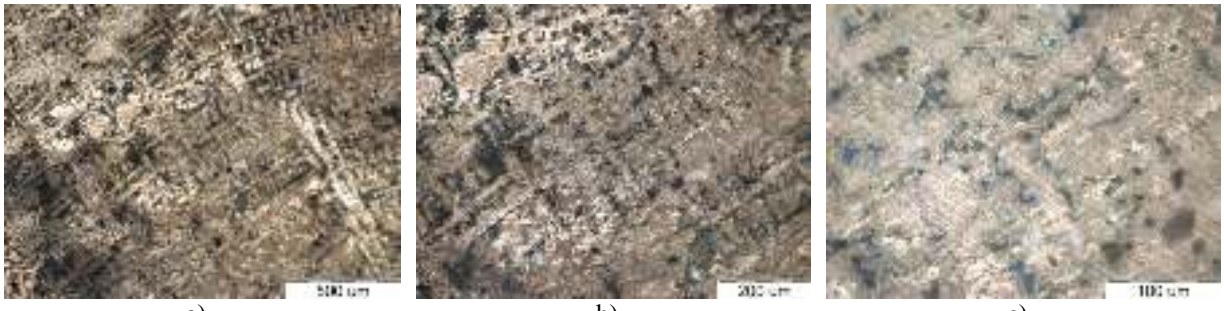

a) b) c)

Fig. 2. *Microscopic structure of bronze used for electrochemical studies: a – x100; b – x200; c – x500*

Figure 2 presents the microscopic structures of electrodes, magnified at x100, x200, x500, which were subjected to accelerated corrosion in an environment that simulated acid rain.

The images in Figure 2 display the dendritic segregation of the α solid solution and interdendritic segregations of eutectoid α + δ in small quantities. The eutectoid α + δ is formed in a Cu - Sn alloy and results from the decomposition of phase γ at a temperature of 520 ° C (see the equilibrium diagram Cu - Sn). According to the picture displayed in the Metallurgic Atlas, the structure is the specific one for a cast bronze. The electrochemical corrosion measurements were performed on a PC – controlled electrochemical analyzer AUTOLAB – PGSTAT 10 (Eco Chemie BV, Utrecht, The Netherlands) using a three electrodes cell containing a working electrode, a saturated calomel electrode (ECS) as reference electrode and a platinum counter electrode.

The working electrodes made of bronze CuSn8, cylindrical shaped, were placed in a PVC tube, while the sealing was assured with epoxy resin. In this way, the surface of the electrode exposed to the solution was disk - shaped, with a surface S = 1.76cm^2. For electrical contact a metal rod was attached (Figure 3).

The electrolyte solution for corrosion measurements contained 0.2g/L Na_2SO_4 + 0.2g/L $NaHCO_3$ (pH = 5) and simulate acid rain.

Fig. 3. *The electrodes used during the experiments*

The study was conducted on three electrodes covered with an artificial patina: electrode (1) was treated with flowers of sulfur; electrode (2) was treated with a solution containing copper sulfate and potassium permanganate and electrode (3), with sodium thiosulfate and ferric nitrate.

3. Results and discussion

The experiments started with measuring the potential of the working electrode in an open circuit for a period of 3600s, the records being presented in Figure 4.

As shown in figure 4, for all studied electrodes, in the first minutes of immersion in the corrosive solution, the potential in open circuit evolves towards more positive values, reaching a stationary value after approx. 35 minutes. This behavior can be attributed to the chemisorption of oxygen on the surface of the dissolved bronze, along with the formation of surface oxide layers, hydroxisulfate and/or hydroxycarbonate [19].

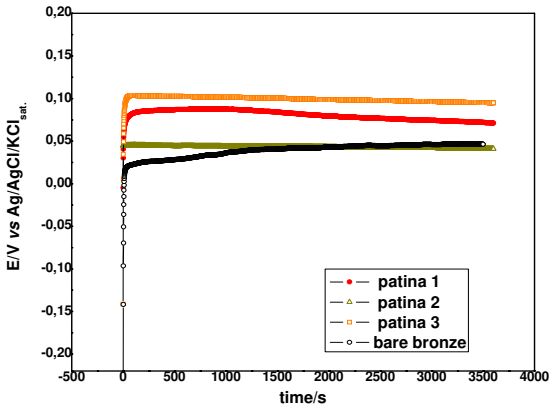

Fig. 4*. Time variations of the open circuit potential of the bronze electrodes immersed in 0.2g/L Na_2SO_4 + 0.2g/L $NaHCO_3$ (pH = 5)*

It can be noticed that the open circuit potentials of the coated electrodes 1 and 3 are more positive than that of bare bronze, suggesting an interaction of the patina with the anodic process (metal dissolution), while the open circuit potential of electrode 2 is the same with that of bare bronze suggesting a weak protection effect of the corresponding patina.

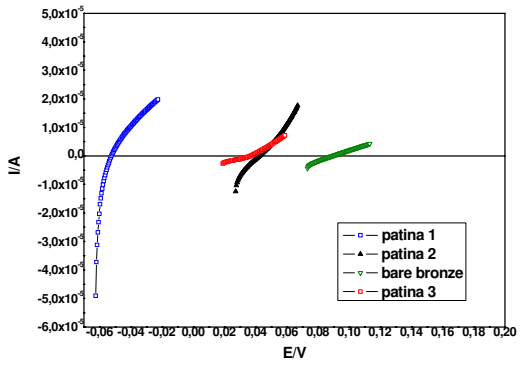

Fig. 5. *Linear polarization curves (± 20 mV vs. ocp) for the studied electrodes immersed in 0.2g/ L Na_2SO_4 + 0.2 g/L $NaHCO_3$ (pH = 5)*

To determine the polarization resistance of the electrodes, linear polarization curves were recorded, in the potential domain of ± 20 mV around the value

of the open circuit potential (ocp) (Figure 5). The polarization resistance values for each electrode, calculated as the inverse of the slope of each curve, are shown in Table 3.

Tabel 3. *The value of polarization resistance (R_p = 1/p, p is the slope of the curve)*

Electrode	**Slope** (p)	**R_p=1/p** [Ω]
Patina 1	$7.25x10^{-4}$	1380
Patina 2	$2.25x10^{-4}$	4444
Patina 3	$1.87x10^{-4}$	5348
Bare bronze	$3.24x10^{-4}$	2060

As can be seen from Table 3, the highest value for R_p was noticed in the case of the electrode (3), treated with a solution containing sodium thiosulfate and ferric nitrate.

To determine the kinetic parameters of the corrosion process, polarization curves were recorded in the potential range of ± 200mV *vs.* ocp (Figure 6).

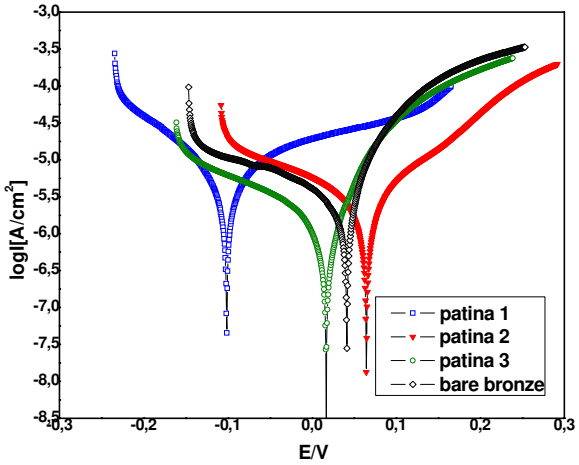

Fig. 6. *The polarization curves (± 200 mV vs. ocp) for the studied electrodes immersed in 0.2g/L Na_2SO_4 + 0.2g/L $NaHCO_3$ (pH = 5)*

The kinetic parameters of the corrosion process were determined from the Tafel interpretation of the polarization curves and the results are presented in Table 4.

Table 4. *Corrosion process parameters for the examined samples*

Electrode	**Ocp**	**E_{cor}**	**i_{cor}**	**β_a**	**β_c**
	[mV *vs* SCE]		[μA/cm^2]	[mV]	
Patina 1	-48	-101	3.25	91	77
Patina 2(brown)	95	65	1.87	85	134
Patina 3(green)	41	17	1.33	55	164
Bare bronze	51	46	5.36	46	284

β_a and β_c are the Tafel coefficients

As shown in Table 4, all the patinas determine a decrease of corrosion current density of the bronze sample. Among them the coated electrode 1 is the less resistant to corrosion and it presents accelerated corrosion in comparison with the other two synthetic patinas. Treatment 3 seems to be the best among the treatments tested; however, the amelioration of corrosion rate is not significant. Moreover, no definite

trend was observed in the shift of β_a and β_c values in the case of different patinas. A comparison between the corrosion current density and of the polarization resistance values of investigated electrodes is shown in Figure 7. The electrodes surfaces after the accelerated corrosion tests are presented in Figure 8.

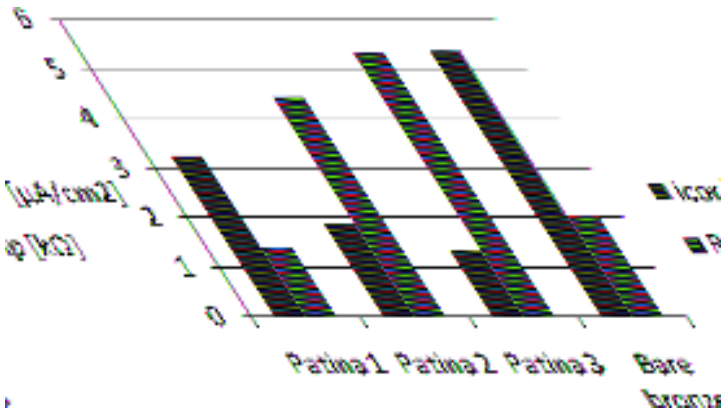

Fig. 7. *Variation of corrosion current density and of polarization resistance for the investigated electrodes*

a) b) c)

Fig. 8*. The electrode surfaces after the corrosion test performed in a solution containing 0.2g/L Na_2SO_4 + 0.2g/L $NaHCO_3$ (pH = 5), a) patina 1, b) patina 2, c) patina 3*

4. Conclusions

In this paper we compare the corrosion resistance of the patina obtained by using traditional flowers of sulfur with new synthetic, chemically obtained patinas on bronze. Corrosion tests were conducted in an environment that simulates acid rain.

Bronze coated with new synthetic patinas have a higher corrosion resistance than the traditional one prepared with sulfur.

In future we intend to investigate some new recipes and new methods of corrosion protection of artistic bronzes.

Acknowledgments

The "PRODOC" POSDRU/6/1.5/S/5, ID 7676 project is acknowledged for financial support of this work.

References

[1]. **P. Kipper -** *Patina for Silicon Bronze*, Regal Printing, Hong Kong, 2003.

[2]. **B. Rosales, R. Vera, G. Moriena -** *Evaluation of the protective properties of natural and artificial patinas on copper. Part I. Patinas formed by immersion*, Corrosion Science, vol. 41, 1999, pg. 625-651

[3]. **R. Picciochi**, **A.C. Ramos s.a** - *Influence of the environment on the atmospheric corrosion of bronze*, Journal of Applied Electrochemistry, vol. 34, 2004, pg. 989-995.

[4]. **L. Robbiola**, **J.M. Blengino** - C. Fiaud, *Morphology and mechanisms of formation of natural patinas on archaeological Cu-Sn alloys*, Corrosion Science, vol. 40, 1998, pg. 2083 – 2111.

[5]. **L. Robbiola**, **R. Portier** - *A global approach to the authentication of ancient bronzes based on the characterization of the alloy – patina – environment system*, Journal of Cultural Heritage, vol. 7, 2006, pg. 1-12.

[6]. **K.P. FitzGerald**, **J. Nairn**, s.a. - *Atmospheric corrosion of cooper and the colour,structure and composition of natural patinas on copper*, Corrosion Science, Vol. 48, pg. 2480-2509, 2006

[7]. **F.J.R. De Oliveira**, **D.C.B. Lago**, s.a. - *Study of patina formation on bronze specimens*, Materials Chemistry and Physics,vol. 115, 2009, pg. 761–770.

[8]. **C. Chiavari**, **A. Colledan**, s.a. - *Corrosion evaluation of traditional and new bronzes for artistic castings*, Materials Chemistry and Physics, vol.95, 2006, pg. 252-259.

[9]. **G.M. Ingo**, **T. De Caro**, **Riccucci C., Khosroff S. -** *Uncommon corrosion phenomena of archaeological bronze alloys*, Applied Physics A, Material Science & Processing, Vol. 83. 2006, pg. 581-588.

[10]. **A. Domenic-Carbo, M.T. Domenic-Carbo, I. Martinez-Lazaro** - *Electrochemical identification of corrosion products in archaeological artefacts. A case study*, Microchimica Acta, Vol.162, 2007, pg. 351-359.

[11]. **J.D. Chelaru, V.F. Soporan, O. Nemeş -** *Time analysis of King Matthias The I Sculptural Group*, International journal of conservation science, Vol.1, 2010, pg. 69-74.

[12]. **M.P. Casaletto, G.M. Ingo, M. Albini, A. Lapenna, I. Pierige, C. Riccucci, F. Faraldi -** *An integrated analytical characterization of corrosion products on ornamental objects from the necropolis of Colle Badetta-Tortoreto (Teramo, Italy)*, Applied physics a: materials science & processing, Vol 100, 2010, pg. 801-808.

[13]. **I. Sandu, A. Dima, I.-G. Sandu -** *Restauration and conservation of metal objects*, Corson Publishing House, Iaşi, 2002.

[14]. **I. Sandu -** *Deterioration and degradation of the cultural patrimony treasures. Supply of inorganic materials,* vol. I, „Alexandru Ioan Cuza" University Publishing House, Iaşi, 2008.

[15]. **L. Mureşan, S. Varvara**, **s.a**. - *Protection of bronze covered with patina by innoxiouus organic substances*, Electrochimica Acta, vol.52, 2007, pg. 7770-7779.

[16]. **V., Cândea, C. Popa**, *Iniţiere în ştiinţa metalelor,* Editura Vega, ISBN 973-951-70-3-0, Bucureşti, 1995

[17]. **A.Vlasa, S. Varvara, L. Mureşan -** *Electrochemical investigation of the influence of two thiadiazole derivatives on the patina of an artchaeological bronze artefact using a carbon paste electrode*, Studia Universitatis BABEŞ – BOLYAI, vol.2, 2007, pg. 63 -71.

[18]. **J.D. Chelaru, V.F. Soporan, O. Nemes, T. Koloszi, V. Duca -** *The influence of the enviromental factors on the King Matthias Sculptural Group*, „International Conference 16th Building Services, Mechanical and Building Industry Days", 2010, pg. 265-272.

[19]. **N. Souissi, L. Bousselmi, s.a. -** *Electrochemical behavior of an archaeological bronze alloy in various aqueous media: New method for understanding artifacts preservation*, Material and Corrsion, vol. 54, 2003, pg. 318-325.

[20]. **T. Koloszi, A. Pasat, R. Moraru, O.M. Gui, J.D. Chelaru -** *Digital techniques in reinforcement and conservation of a large sculptural group. Case study: the sculptural group of Mathias I in Cluj Napoca, Romania, 5th International Conference on Interdisciplinarity in Education - ICIE'10*, Tallinn, 2010, Estonia.

MANUSCRISELE, CARŢILE ŞI REVISTELE PENTRU SCHIMB, PRECUM SI ORICE CORESPONDENTE SE VOR TRIMITE PE ADRESA:

MANUSCRIPTS, REVIEWS AND BOOKS FOR EXCHANGE COOPERATION, AS WELL AS ANY CORRESPONDANCE WILL BE MAILED TO:

LES MANUSCRIPTS, LES REVUES ET LES LIVRES POUR L'ECHANGE, TOUT AUSSI QUE LA CORRESPONDANCE SERONT ENVOYES A L'ADRESSE:

MANUSCKRIPTEN, ZIETSCHRITFTEN UND BUCHER FUR AUSTAUCH SOWIE DIE KORRESPONDENZ SID AN FOLGENDE ANSCHRIFT ZU SEDEN:

After the latest evaluation of the journals achieved by National Center for the Science and Scientometry Politics (**CENAPOSS**), as recognition of its quality and impact at national level, the journal is included in B^+ category, 215 code (http://www.cncsis.ro/2006_evaluare_rev.php).

The journal is indexed in:
CSA: http://www.csa.com/ids70/serials_source_list.php?db=mechtrans-set-c
EBSCO: http://www.ebscohost.com/titleLists/a9h-journals.pdf
Copernicus: http://journals.indexcopernicus.com/karta.php

The papers published in this journal can be visualized on the "Dunarea de Jos" University of Galati site, the Faculty of Metallurgy, Material Science and Environment, page: www.fimm.ugal.ro.

Publisher's Name and Address:
Contact person: Antoaneta Căpraru
Galati University Press - GUP
47 Domneasca St., 800008 - Galati, Romania
Phone:+40 336 130139, Fax: +40 236 461353
Email: gup@ugal.ro

Editor's Name and Address:
Prof. Dr. Eng. Marian BORDEI
Dunarea de Jos University of Galati, Faculty of Metallurgy, Materials Science and Environment
111 Domneasca St., 800201 - Galati, Romania
Phone: +40 336 130223, Phone/Fax: +40 236 460750
Email: mbordei@ugal.ro

AFFILIATED WITH:

- *ROMANIAN SOCIETY FOR METALLURGY*
- *ROMANIAN SOCIETY FOR CHEMISTRY*
- *ROMANIAN SOCIETY FOR BIOMATERIALS*
- *ROMANIAN TECHNICAL FOUNDRY SOCIETY*
- *THE MATERIALS INFORMATION SOCIETY (ASM INTERNATIONAL)*

Annual subscription (4 issues per year)

Edited under the care of
Faculty of
METALLURGY, MATERIALS SCIENCE AND ENVIRONMENT

Edited date: 30.06.2012
Issues number: 200
Printed by
Galati University Press
accredited CNCSIS
47 Domnească Street, 800036
Galati, Romania